
White Rose Research Online

eprints@whiterose.ac.uk
https://eprints.whiterose.ac.uk
Universities of Leeds, Sheffield and York

Deposited via The University of Leeds.

White Rose Research Online URL for this paper:
https://eprints.whiterose.ac.uk/id/eprint/92079/

Version: Accepted Version

Article:
Colombera, L, Mountney, NP, Howell, JA et al. (2016) A test of analog-based tools for quantitative prediction of large-scale fluvial architecture. AAPG Bulletin, 100 (2). pp. 237-267. ISSN: 0149-1423

https://doi.org/10.1306/11181514227

Reuse
Items deposited in White Rose Research Online are protected by copyright, with all rights reserved unless indicated otherwise. They may be downloaded and/or printed for private study, or other acts as permitted by national copyright laws. The publisher or other rights holders may allow further reproduction and re-use of the full text version. This is indicated by the licence information on the White Rose Research Online record for the item.

Takedown
If you consider content in White Rose Research Online to be in breach of UK law, please notify us by emailing eprints@whiterose.ac.uk including the URL of the record and the reason for the withdrawal request.



A test of analog-based tools for quantitative prediction of large-scale fluvial architecture

Luca Colombera[1], Nigel P. Mountney[1], John A. Howell[2], Andreas Rittersbacher[3], Fabrizio Felletti[4], William D. McCaffrey[1]

1) Fluvial & Eolian Research Group, School of Earth &Environment, University of Leeds, LS2 9JT, Leeds, UK
2) School of Geosciences, University of Aberdeen, Meston Building, AB24 3UE, Aberdeen, UK
3) Statoil ASA, Sandsliveien 90, 5254 Bergen, Norway
4) Dipartimento di Scienze della Terra 'Ardito Desio', Università degli Studi di Milano, Via Mangiagalli 34, 20133, Milano, Italy

Acknowledgements

The FRG-ERG sponsors (Areva, BHP Billiton, ConocoPhillips, Murphy Oil Corporation, Nexen, Saudi Aramco, Shell, Tullow Oil, Woodside, and YPF) are thanked for their financial support of this project. Collection of the 3D virtual outcrop was funded by the SAFARI consortium and the Norwegian Research Council's Petromax program. Michael Sweet, Janok Bhattacharya, Gary Hampson, and an anonymous reviewer are gratefully acknowledged for their constructive comments.

Abstract

Outcrop analogs are routinely used to constrain models of subsurface fluvial sedimentary architecture built through stochastic modeling or inter-well sandbody correlations. Correlability models are analog-based quantitative templates for guiding the well-to-well correlation of sand-bodies, whereas indicator variograms used as input to reservoir models can be parameterized from data collected from analogs,

using existing empirical relationships. This study tests the value and limitations of adopting analog-informed correlability models and indicator-variogram models, and assesses the impact and significance of analog choice in subsurface workflows for characterizing fluvial reservoirs.

A 3.2 km long architectural panel based on a Virtual Outcrop from the Cretaceous Blackhawk Formation (Wasatch Plateau, Utah, USA) has been used to test the methodologies: vertical 'dummy' wells have been constructed across the panel, and the intervening fluvial architecture has been predicted using correlability models and sequential indicator simulations. The correlability and indicator-variogram models employed to predict the outcrop architecture have been compiled using information drawn from an architectural database. These models relate to: (i) analogs that partially match with the Blackhawk Formation in terms of depositional setting, and (ii) empirical relationships relating statistics on depositional-element geometries and spatial relations to net-to-gross ratio, based on data from multiple fluvial systems of a variety of forms.

The forecasting methods are assessed by quantifying the mismatch between predicted architecture and outcrop observations in terms of the correlability of channel complexes and static connectivity of channel deposits. Results highlight the effectiveness of correlability models as a check for the geologic realism of correlation panels, and the value of analog-informed indicator variograms as a valid alternative to variogram-model parameterization through geostatistical analysis of well data.

This work has application in the definition of best-practice use of analogs in subsurface workflows; it provides insight into the typical degree of realism of analog-based predictions of reservoir architecture, as well as on the impact of analog choice, and draws attention to associated pitfalls.

1. INTRODUCTION

Outcrop analogs have long been used to guide predictions of large-scale lithologic heterogeneity in subsurface fluvial successions of economic importance (e.g. Bridge et al. 2000; Bridge & Tye 2000; Bridge 2001; Miall 2006; Al-Ajmi et al. 2011; Keogh et al. 2014). Outcrop analogs can be used, with provisos, to predict the likely distribution of channel and overbank deposits, themselves a first-order control on petrophysical heterogeneity. The value of outcrop analogs is widely recognized, but so are the problems associated with their use (Alexander 1993; Geehan 1993; Bridge & Tye 2000; Bridge 2001; Martinius and Næss 2005; Miall 2006; Howell et al. 2014). The most important issue is related to the uncertainty as to whether the chosen outcrops are appropriate analogs for the subsurface successions being characterized. Despite their known limitations, outcrop analogs are routinely employed as a means for achieving geologic realism in static models of fluvial hydrocarbon reservoirs and aquifers. In effect, outcrop-derived experience is often transferred to the subsurface through both stochastic modeling and as a guide in inter-well correlation.

The well-to-well correlation of fluvial sandstones can be guided by reference to 'correlability' models; these probabilistic models have recently been proposed as a means to quantify the likelihood of correlation of discrete channel bodies between equally spaced wells, based on analog sandstone-body width distributions (Colombera et al. 2014). Through their use, a subsurface practitioner can assess the geologic likelihood of a well-to-well correlation panel being a valid representation by

contrasting correlations against on one or more analogs. Then, the geologist can revise correlations to obtain a better match with the analog-derived model, if deemed appropriate.

Sequential indicator simulation (SIS) is a stochastic technique for constructing multiple, equiprobable geocellular realizations of categorical variables (Journel & Alabert 1990; Deutsch & Journel 1998), such as facies, which control reservoir architecture. Despite its limitations (cf. Seifert & Jensen 1999; Emery 2005; Deutsch 2006) and the emergence of new techniques such as multi-point statistical and event-based approaches, SIS is still widely used in the hydrocarbon industry and in hydrogeology.

Object-based stochastic methods are the preferred alternative for modeling the architecture of channelized reservoirs, because of (i) their ability to reproduce predefined and potentially complex three-dimensional (3D) shape types, and because (ii) these models can be readily constrained using analog data on the geometric parameters of the modeled units (e.g. distributions of thickness, width-to-thickness aspect ratio, sinuosity). However, object-based models are not always optimal, mostly in relation to the challenges of conditioning to large numbers of wells or modeling systems with a very high proportion of channel deposits. Therefore it is at times desirable to consider other approaches such as SIS as extra tools in the fluvial modelling tool box. However, while the analog-derived information used to constrain object-based models of fluvial reservoirs is intuitive, the application of the same type of analog information for building reservoir models through SIS is not straightforward. Indicator variograms employed to condition SIS models can be parameterized using geologic knowledge through the application of existing empirical relationships proposed by Ritzi (2000). These relationships permit conditioning SIS

models without the need for traditional geostatistical analysis (e.g. applications in Proce et al. 2004; Venteris 2007), and can themselves be constrained by information derived from analogs because they relate indicator-variogram parameters to geologically meaningful quantities (Colombera et al. 2012a).

This study demonstrates the application of a technique to test the value and limitations of these tools, and to assess the impact of analog choice in workflows involving their use. In particular, this study demonstrates how data from a variety of analogs can be employed to model the large-scale sedimentary architecture of a fluvial succession by following a typical subsurface workflow. Stochastic methods have previously been employed to simulate outcrop architecture in order to test output sensitivity to the chosen modeling technique or approach (Falivene et al. 2006; Comunian et al. 2011; dell'Arciprete et al. 2012). In contrast, this work demonstrates the predictive value of transferring analog information to the subsurface, and introduces a technique to quantify how well this is achieved by means of correlability models and SIS models based on geologic experience.

The overall aim of this work is to provide a test of the outcrop-analog approach in the guidance of subsurface predictions of large-scale fluvial architecture. If the approaches used to model subsurface architecture are appropriate, they should satisfactorily model outcrop architecture as well. Based on this premise, this study assesses the value and limitations of the forecasting tools, and demonstrates potential problems associated with their use. Specific objectives of this work are as follows:

(i) to determine the grade of confidence associated with correlability models; this is achieved by assessing the amount of discrepancy exhibited by the correlation panel

under evaluation as compared to the correlability model, below which the panel can be considered as effectively matching the model;

(ii) to demonstrate the importance of well-array sampling in the application of correlability models, by assessing how the number of sandstone bodies sampled by well penetration affect the quality of the predictions made by the models;

(iii) to determine the reliability of indicator variograms based on analog data, with particular reference to their use in modeling large-scale fluvial architecture through SIS methods;

(iv) to assess the likely impact of well spacing on the uncertainty (variability) associated with SIS models;

(v) to quantify the impact of the choice of inappropriate analogs or, more generally, analogs that display architecture with variable degree of match with a target subsurface succession, on resulting correlability models and SIS realizations.

2. CASE STUDY AND ANALOG SELECTION

Given that this work aims to assess the proposed predictive tools through their employment in modeling outcropping fluvial architecture using subsurface methods, it is essential that the fluvial successions considered as real-world tests are extensively exposed both vertically and laterally. For this study, an extensive cliff-forming outcrop exposing the continental interval of the Upper Cretaceous (Campanian) Blackhawk Formation in the central part of the Wasatch Plateau (Utah, USA) has been used (Figure 1).This outcrop is part of the dataset discussed by Rittersbacher et al. (2014), to which the reader is referred for a more detailed sedimentological description of the studied section.

The non-marine Blackhawk Formation in the Wasatch Plateau area consists of a ca. 200 to 300 m-thick succession of mudstone, sandstone and coal that is interpreted to have accumulated in an alluvial to coastal plain setting (cf. Flores et al. 1984; Adams & Bhattacharya 2005; Hampson et al. 2012) as part of a clastic wedge that prograded eastward from the Sevier Orogen into a retroarc foreland basin on the western margin of the Western Interior Seaway. The study interval is interpreted as representing the preserved expression of a highstand systems tract of a low-frequency sequence (Howell & Flint 2003).

Architecturally, the non-marine Blackhawk Formation consists of isolated channelized sandstone bodies encased in fine-grained mudstones and thin sandstones of overbank origin that are themselves locally interbedded with coal bodies. The mud-prone character of much of the Blackhawk Formation makes the current study particularly relevant to low net-to-gross subsurface fluvial depositional systems, in which predictions regarding sandbody distribution are typically very important (cf. Jones et al. 1995).

The dataset used in this work takes the form of an architectural panel that depicts a section that is 3.2 km wide and 200 m high. The panel has been constructed via the interpretation of a ‘virtual outcrop model’ (*sensu* Pringle et al. 2006) which was derived from a LiDAR acquisition system, obliquely mounted on to a helicopter (Rittersbacher et al. 2014). Interpretation of the virtual outcrop resulted in the generation of a ‘map’ of the distribution of the sand-prone channel-bodies in a background of dominantly fine-grained floodplain deposits. The outcrop is oriented close to orthogonal to the mean drainage direction of the Blackhawk Formation paleo-river systems, as based on regional geologic constraints and inferred from a number of paleocurrent indicators from measured sections, which return an average

paleoflow direction of ca. 070° (Rittersbacher et al. 2014). The interpreted architecture has been projected onto a vertical plane oriented parallel to the average cliff-face azimuth, and a series of 65 vertical logs, each spaced 50 m apart, have been constructed to serve as 'dummy' wells across the panel (Figure 2). These dummy wells consist of a vertical sample of the outcrop panel: they are therefore based on the same interpretation and do not represent measured sedimentological sections.

Given that the aim of this work is to predict the intervening architecture by means of correlability and SIS models based on other outcrop analogs, analog data have been drawn from the Fluvial Architecture Knowledge Transfer System (FAKTS), a database storing hard and soft data on the sedimentary architecture of a range of fluvial depositional systems (Colombera et al. 2012b). The FAKTS database quantifies geometries, internal organization and spatial relationships of genetic units belonging to three hierarchical orders and assigned to depositional systems that are classified on the basis of several parameters and characterized in terms of their spatial and temporal evolution. The database stores architectural data drawn from multiple sources, much of which has been collated from peer-reviewed publications. The inclusion within the database of different datasets is enabled by a process of standardization of sedimentary architecture, which enforces consistency in the attribution of units to a hierarchical order and in their classification. The highest order of sedimentary unit included in FAKTS is the so-called ‘depositional element’; these units are classified as *channel-complex* or *floodplain* elements, and represent the large-scale features that are of relevance in this analysis.

Channel complexes represent discrete bodies of channel deposits, rather than genetically defined units: when complexly juxtaposed or interfingered with floodplain

deposits, channel complexes are distinguished in part on the basis of flexible but unambiguous geometric criteria (Colombera et al. 2012b). Floodplain elements are defined geometrically after channel-complex definition (i.e., they make up the background in which the channel complexes occur). At the scale of the depositional element, the FAKTS database does not consider the genetic relationships between a channel-complex and neighboring floodplain deposits for stratigraphic subdivision. Rather, stratigraphic volumes are subdivided into floodplain packages that neighbor channel complexes laterally and vertically, through a geometric segmentation of the floodplain deposits (Colombera et al. 2012b; 2013). Thus, depositional elements in FAKTS do not correspond to a single genetically defined hierarchical order of sedimentary units. Accordingly, channel complexes in FAKTS include a range of unit types at multiple scales, such as channel fills, channel belts, or parts of incised valley fills, for example. As of December 2014 (version of the database used in this analysis), FAKTS incorporated data on 12103 classified depositional elements, 6266 of which are channel complexes. The same definition of depositional elements has been applied to the Blackhawk Formation by subdividing the panel into channel-complex and floodplain units, to enable comparison with the analogs chosen from the FAKTS database.

The geometry of the genetic units is characterized by data describing their thickness, cross-gradient width and dip length; genetic-unit width and length are classified into categories that describe the nature of observations (real, apparent, partial and unlimited; cf. Geehan & Underwood 1993).

Since the FAKTS database quantifies sedimentary architecture and classifies depositional systems and stratigraphic volumes, it is possible to filter the database to query for analogs that match a particular succession (usually in the subsurface) in

terms of architectural features (e.g. net-to-gross ratio, lithofacies thicknesses) or depositional-system parameters (e.g. basin type, climatic regime, interpreted channel pattern). Additionally, datasets can be filtered on metadata, such as descriptors of the quality of datasets and attributes, which are rated according to a threefold ranking system (data quality index, DQI). In effect, the capability of the database to synthesize information from a variety of analogs into a composite quantitative analog enables a facies-model approach (Colombera et al. 2013).

For this study, the FAKTS database has been queried to derive filtered depositional-element data with which to model the Blackhawk Formation architecture. The utilization of filtered datasets to define analogs classified on system parameters has not been carried out assuming that it necessarily ensures a close match with the target succession (in this case the outcrop panel). Rather, this approach has been used because the filtering process likely helps narrow down variability (i.e. uncertainty) by discarding depositional systems that are obviously not relevant.

Two types of analogy to the Blackhawk Formation have been considered for this work:

(i) a synthetic analog, which has been compiled by merging data from a range of FAKTS analogs that partially match with the Blackhawk Formation in terms of system classification, by considering datasets scoring highest (i.e. A) in DQI, and relating to successions that have accumulated under the influence of humid to sub-humid climatic settings in foreland basins;

(ii) empirical relationships (Figure 3) relating depositional-element width statistics (mean, standard deviation) to channel-deposit proportion, which is simply referred to as net-to-gross ratio hereafter. These relationships

result from analysis of several different stratigraphic volumes digitized in FAKTS, and permit prediction of depositional-element geometries from knowledge of the net-to-gross ratio. A net-to-gross ratio of 18% is computed for the overall outcrop area represented on the architectural panel of the studied part of the Blackhawk Formation.

To ensure a fair test of the analog approach, all data relating to the Blackhawk Formation and included in FAKTS were excluded from the pool of chosen analogs. The choice of system classification for the synthetic analog has not been driven by the belief that those parameters represent the dominant controls on sedimentary architecture. Rather, a balance has been sought between the detail in system classification and size of query output (i.e., the number of analog depositional elements returned), which may significantly decrease with the consideration of additional or alternative conditions due to data filtering.

A summary of analog depositional-element width descriptive statistics (inclusive of data from classes of width corresponding to apparent measurement and incomplete measurement, i.e. partial and unlimited widths) is given in Tables 1 and 2, for channel-complex and floodplain elements respectively, together with the corresponding statistics derived from the Blackhawk Formation panel to be modeled. Comparing values for the Blackhawk Formation with its supposed analogs, it is evident how the average width of the channel complexes is overestimated by the synthetic analog based on the A-DQI (data quality index) data and underestimated by the corresponding net-to-gross-based empirical relationship. In contrast, the average width of the floodplain elements is underestimated by the A-DQI synthetic analog and overestimated by the corresponding net-to-gross-based empirical relationship. Thus the A-DQI synthetic analog is slightly optimistic, and the net-to-

gross-based empirical relationships overly pessimistic with respect to lateral continuity and separation of the channel sandstone bodies.

As we lack data on the orientation of each individual channel complex in the Blackhawk panel, their true width remains uncertain. The inability to account for variability in channel-complex orientation for the Blackhawk panel is a source of error in the assessment of the degree to which one analog matches the outcrop panel. The mean and standard deviation of channel-complex width for the Blackhawk panel would almost certainly be lower if the panel was oriented at exactly 90° with the mean drainage direction, because measures of channel-complex 'apparent' widths would be closer to the 'real' values. This would make the net-to-gross based analogy a better fit to the outcrop, and the A-DQI analogy a worse fit.

Analog information concerning depositional-element thickness and vertical stacking has also been considered for the part of work on geostatistical modeling, as explained later.

3. BENCHMARKING CORRELABILITY MODELS

3.1 Methods

The first part of this work deals with an outcrop test of correlability models that are based on the aforementioned analogs. Distributions of channel-complex width are typically well described by log-normal probability density functions (Colombera et al. 2014); from these functions and knowledge of well-array spacing – under the assumption of constant spacing – it is possible to derive curves that quantify the total probability of well penetration and well-to-well correlation of a channel-complex as a function of well spacing and correlation distance (Colombera et al. 2014). It is then

possible to obtain values from these curves corresponding to (i) the total probability of penetration for the well-array spacing and to (ii) the total probability of correlation for each integer multiple of the well-spacing. By computing the ratio between the values of total probability of correlation and the total probability of penetration it is then possible to derive the correlability model, i.e. a curve describing the proportion of penetrated channel bodies that are likely to be correlatable as a function of correlation distance – see Colombera et al. (2014) for details of the implementation of the correlability-model method.

The architectural panel of the Blackhawk Formation outcrop has been treated as a correlation panel, by considering as ‘correlations’ the traceability of channel complexes across the array of dummy wells. In this way, it has been possible to quantify the proportions of channel complexes penetrated by different well-arrays and ‘correlated’ across different values of well spacing (3200 m, 1600 m, 800 m, 400 m, 200 m, 100 m, 50 m). These proportions correspond exactly to what is meant to be predicted by the curves of total probability of penetration and correlation.

Next, total-probability curves have been compiled based on the following: (i) channel-complex width statistics (inclusive of partial widths due to outcrop termination) derived from the Blackhawk Formation panel itself, which can be used to test the assumption of log-normally distributed channel-complex widths; (ii) channel-complex width statistics associated with the two types of analogs selected.

This allows for evaluation of the total-probability curves that underpin the correlability models, through observation of the deviation between the curves and the proportion of penetrated or ‘correlated’ channel complexes expressed as a function of well spacing and correlation distance (Figure 4).

Both sets of total-probability curves have then been employed in the construction of correlability models, which can be used to determine the error inherent in a typical application of the method. Four different sets of correlability models have been constructed for four different values of well-array spacing (Figure 5), corresponding to values of well spacing typical of developed hydrocarbon fields (North & Prosser 1993). Appraisal of the correlability models can therefore be undertaken by quantifying the deviation between the curves and the ratios between proportions of 'correlated' channel complexes for variable correlation distances (multiples of the well-array spacing), and the proportion of channel complexes penetrated by the well array (i.e. the architectural-panel correlability). This deviation is measured by a value called *cumulative discrepancy*, which is the sum of the absolute values of the panel-model difference in correlability at each correlation distance; this represents a measure of how well the correlation panel matches the model. In this case, the same quantity is used as a measure of how well the model matches the outcrop architectural panel.

3.2 Results

All the analog-based functions of total probability of channel-complex penetration and correlation are based on the assumption of log-normally distributed widths. This assumption is valid for the Blackhawk Formation architectural panel: a lognormal probability density function provides a good fit to the distribution of channel-complex width in the panel (Figure 6), attaining a p-value of 0.235 (if partial observations due to outcrop termination are included) for a significance level alpha of 0.05. The distribution of channel-complex widths in Figure 6 represents apparent and partial widths, and this fact is likely to partly control the emergence of a lognormal

distribution (cf. Lorenz et al. 1985). The fact that thicknesses are also log-normally distributed suggests that the true-width distribution is probably well described by a lognormal curve as well. As expected, the fact that a lognormal distribution provides a good fit to the lateral extent of the channel complexes on the Blackhawk outcrop is reflected in the corresponding curves of total probability of channel-complex penetration and correlation: the curves based on channel-complex width statistics from the Blackhawk Formation outcrop itself attain a good fit to the proportions of channel complexes penetrated and ‘correlated’ for different values of well spacing (Figure 4).

The correlability model generated from the total-probability curves based on Blackhawk Formation channel-complex width statistics provides a useful indication of the confidence level of panel-to-analog discrepancy over which correlability is meaningful and operated correlations can be sensibly considered as requiring revisions to match the analog. In other words, if the value of panel-model cumulative discrepancy is below a threshold, the panel correlations can be considered to effectively match the correlability model. The cumulative discrepancy used to rank a correlation panel as a whole is not normalized to take into account variable well arrays and the number of different correlation distances on which it is evaluated: it is therefore not possible to provide an exact value of cumulative discrepancy that works as a universal reference of method confidence. Instead, values of panel-model difference in correlability at each correlation distance provide useful references.

For the four different sets of correlability models constructed, values of their cumulative discrepancy from the architectural-panel correlability are reported and compared in Figure 7. Over the four sets, the correlability models generated on the basis of A-DQI synthetic analog data are consistently over-optimistic, whereas

correlability models based on the net-to-gross-defined analogy are over-pessimistic (Figure 5). Of the two types of analogy considered, the A-DQI synthetic analog represents the best approximation of the actual architectural-panel correlability. This is consistent with the corresponding channel-complex width statistics (Table 1). It is evident that, for the sparsest sampling (well spacing = 400 m), the cumulative discrepancy shown by the correlability model based on the A-DQI synthetic analog is even lower than the cumulative discrepancy shown by the correlability model based on width statistics from the outcrop itself. In practical terms, this means that choosing the better analog would not result in a better correlation panel. This problem is not a limitation of the correlability models. Instead, it relates to the outcrop-derived proportions, and shows the importance of sampling a statistically significant number of bodies for the method to be most valuable: only six channel complexes are 'correlated' for the scenario based on a well array with spacing of 400 m. For all the denser well-array scenarios, the values of cumulative discrepancy are all consistent with how closely channel-complex width descriptive statistics on which the models are based approximate the architectural panel.

Additionally, results presented in Figure 5 suggest the significance of considering alternative analogs as a way to handle uncertainty connected with analog selection, whereby correlation panels are compared with an envelope of correlability models, rather than a single model.

4. ASSESSING SEQUENTIAL INDICATOR SIMULATIONS CONDITIONED ON ANALOG-BASED INPUT

4.1 Methods

4.1.1 Analog attributes and indicator variogram models

When using binary indicator geostatistics to model the distribution of geologic heterogeneities in a reservoir, it is ideal to employ realistic indicator-variogram models and ranges, although this may not necessarily translate in a realistic model. To favor the use of geologically sound analog data in SIS, there exist empirical relationships (Ritzi 2000) that relate geologic attributes (deposit-type proportion, size and spatial relationships) to indicator-variogram parameters. These relationships have been used here for conditioning SIS models of the distribution of channel and overbank deposits. The range and curvature of the indicator variograms are related to the mean and variance in the size of the heterogeneities they represent. As the coefficient of variation (C_v; i.e. the ratio of standard deviation to mean) of the length of each type of heterogeneity increases toward unity, the effective range of the variogram increases, whereas the correlation structure (i.e. the type of indicator-variogram model required as input by SIS) has been shown to evolve in a way that it is best described by different models for different values of C_v. In particular, an increase in C_v corresponds to a progressive transition from a spherical to exponential variogram structure (Ritzi 2000).

On the basis of the findings by Ritzi (2000), a value of 0.8 in the coefficient of variation of the spatial extent of a category (channel or overbank deposits) in a given direction (i.e. width or thickness, in this case) has been taken as a threshold for the choice of a spherical (if $C_v < 0.8$) or exponential (if $C_v > 0.8$) indicator-variogram model. Indicator-variogram sills can be calculated from channel- or floodplain-deposit proportions (p_k, where k is the type of deposit, i.e. ‘channel’ or ‘floodplain’) as: $p_k(1-p_k)$. The range ($a_{k,x}$) of the indicator variogram of a category k (e.g. channel or floodplain deposit) in a given direction x is instead estimated as:

$a_{k,x} = \Phi(1 - p_k)\bar{l}_{k,x}\chi_{k,x}^{-1}$ (Ritzi 2000), [Equation 1]

where Φ is equal to 1.5 or 3 for a spherical or exponential model respectively, p_k is the proportion of k, $\bar{l}_{k,x}$ is its mean size along direction x, and $\chi_{k,x}$ is called 'embedding coefficient' and is defined as:

$$\chi_{k,x} = \frac{\text{number of contacts defining a change from category k to category j along x}}{\text{number of occurrences of category k}}$$ (Ritzi 2000). [Equation 2]

These empirical relationships have been employed to constrain model indicator variograms for channel and floodplain deposits for the two types of analogs to the Blackhawk Formation architectural panel. Two complementary categories – as channel and overbank deposits are in this case study – have identical indicator variograms. However, in most of the current work, sequential indicator simulations of channel and floodplain deposits are run using a 'full indicator kriging' conditioned on two different indicator-variogram models. This was done to force simulations to reproduce different spatial continuities for the two types of deposits, because it would result in a more realistic distribution of channel and overbank deposits.

Before applying this approach to modeling the Blackhawk Formation outcrop, a generic test was made of SIS conditioned on indicator variograms based on a combination of the empirical relationships by Ritzi (2000; i.e. C_v threshold and Equation 1) with the empirical relationships that relate depositional-element characteristics to the net-to-gross ratio on the basis of FAKTS output (i.e. the second type of outcrop analog; Figure 3). The empirical relationships reported in Figure 3a-h relate mean and standard deviation of depositional-element (channel-complex and floodplain) width and thickness as a function of the proportions of channel or floodplain deposits. The empirical relationships in Figure 3i-j relate channel-complex

and floodplain vertical embedding coefficients (based on FAKTS depositional-element vertical transition statistics; cf. Equation 2) to channel- or floodplain-deposit proportions. Horizontal embedding coefficients can be taken as equal to 1 for both types of depositional elements for any value of net-to-gross ratio, because of the way the depositional elements are defined in FAKTS. To better understand why this is done, consider Equation 2 together with the fact that a floodplain depositional element is a geometrically defined unit that will always be laterally transitional to a channel-complex depositional element and never to another floodplain element. Applying the relationships reported in Figure 3 to Equation 1, it has been possible to synthesize curves that describe vertical and horizontal (cross-gradient) indicator variogram ranges as functions of net-to-gross ratio for channel and floodplain deposits (Figure 8). The values of indicator-variogram ranges predicted by the curves in Figure 8 refer to spherical and exponential models, for vertical and horizontal directions respectively. This is a result of the fact that the coefficient of variation (C_v) of depositional-element width is predicted to be higher than the 0.8 threshold for every value of net-to-gross ratio, whereas the C_v of depositional-element thickness is invariably lower than that. The curve in Figure 8b permits using knowledge of the net-to-gross ratio of the stratigraphic interval that needs to be modeled for the derivation of a value of indicator-variogram range for the horizontal direction. This is significant given that, typically, horizontal ranges cannot be obtained by means of geostatistical analysis of sparse well data.

4.1.2 Testing net-to-gross-based indicator variogram models: unconditional simulations

A generic test of the value of SIS predictions made on the basis of the net-to-gross-based relationships is necessary. This test has been undertaken here by evaluating unconditional (i.e. not conditioned on well data) SIS realizations, constrained on indicator-variogram ranges from Figure 8, and assuming exponential variogram models for both channel and floodplain deposits. However, because Figure 3 predicts depositional-element widths being more variable ($C_v > 0.8$) than depositional-element thicknesses ($C_v < 0.8$), the relationship that relates horizontal indicator-variogram range and net-to-gross is based on the assumption of an exponential model, whereas the relationship that relates vertical indicator-variogram range and net-to-gross is based on the assumption of a spherical model. In spite of the choice for exponential models in the simulations, values of vertical range as derived from Figure 8a – which refers to a spherical model – have not been corrected upward to account for the difference in variogram model, as there is currently no empirical knowledge that tell us what that correction would need to be (although a tentative correction is applied later in this work). Simulations of a 4 km-wide, 200 m-high (horizontal resolution: 4 m; vertical resolution 1 m) fluvial stratigraphy have been run for a 10% net-to-gross scenario, which, being mud-prone, is relevant to the case study treated in this work, and favors distinction of channel deposits as discrete channel complexes, therefore enabling a comparison with FAKTS analog data for equivalent net-to-gross. All realizations have been modeled using the code SISIM (Deutsch & Journel 1998), as implemented in SGeMS (Remy et al. 2009). To force the realizations to exactly honor the channel-deposit proportion (10%) and to clean them from noise, smoothing has been applied using a 5 x 3 moving window in TRANSCAT (Journel & Xu 1994; Remy et al. 2009). The realizations were visually inspected to qualitatively assess their geologic realism

and the variability across the set. Then, a quantitative comparison was made between a randomly chosen realization (Figure 9a) and FAKTS output from case studies with corresponding net-to-gross ratio (10% ±1.5%), in terms of channel-complex geometries (Figure 9b, c and d).

4.1.3 Sequential indicator simulations of the Blackhawk Formation outcrop

Application of the technique has then focused on simulating the Blackhawk Formation outcrop architecture by means of SIS constrained on the selected analogs. The outcrop has been modeled adopting a resolution of 0.2 m x 1 m. A value of indicator variogram range (10 m) for the vertical direction has been computed from geostatistical analysis of dummy-well lithologic data (Figure 10a), as would normally be done in subsurface studies. Geostatistical analysis is, however, inapplicable to the horizontal direction even in case of tightly spaced wells (Figure 10b). Thus, SIS input values of horizontal indicator-variogram range are based on the relationship), in Equation 1 (Ritzi 2000), applied making use of depositional-element attributes from the two types of analogs (A-DQI synthetic analog and analogy based on net-to-gross relationship). Additionally, a third set of simulations has been constrained on indicator-variogram parameters based on weighted depositional-element width statistics for the A-DQI synthetic analog, by taking into account the variable thickness of the depositional elements in a way that thicker depositional elements contribute more to the statistics. This is sensible in a pixel-based framework, in which descriptive statistics of the size of heterogeneities in a given direction would be drawn from sampling the extent of units across adjacent cells in that particular direction at multiple rows. Sets of 20 SIS runs were performed for each of 15 scenarios (Figure 11), given by a combination of the three analog

types (A-DQI synthetic analog, A-DQI synthetic analog with weighted depositional-element width statistics, and analogy based on net-to-gross relationship) with five different well arrays (spacing: 1000 m, 500 m, 250 m, 100 m, 50 m; based on a vertical sample of the outcrop) used for hard-data conditioning.

Although a vertical trend in the distribution of channel deposits across the outcrop is evident, this has not been accounted for by means of a vertical proportion curve, and no attempt has been made to separately model different stratigraphic intervals.

In addition, three different sets of 20 control simulations have been run as constrained by the following:

(i) indicator-variogram parameters entirely based on variography of a geocellular model (see below) of the Blackhawk Formation outcrop (Figure 10), i.e. conditioning SIS using 'mean indicator kriging' on a single indicator variogram that expresses the two-point statistics derived directly from the outcrop panel;

(ii) well-derived vertical variogram range combined with horizontal variogram range based on the relationship of Ritzi (2000), i.e. Equation 1, making use of depositional-element width statistics from the Blackhawk Formation outcrop; the outcrop is therefore considered as an analog to itself, as in the earlier part of the paper dealing with correlability models;

(iii) indicator-variogram parameters entirely based on the relationship by Ritzi (2000), i.e. Equation 1, applied to depositional-element attributes from the A-DQI synthetic analog, so that the values of the vertical variogram range are based on corresponding FAKTS output (i.e. depositional-element thicknesses and embedding coefficients for the A-DQI synthetic analog). An exponential variogram model was chosen for both channel and

overbank deposits and the corresponding value of Φ (Φ = 3) used for deriving both vertical and horizontal ranges, as based on the coefficients of variation in depositional-element width (C_v = 1.90 for channel complexes, C_v = 1.00 for floodplain elements), in spite of a spherical model being indicated by the coefficients of variation in depositional-element thickness (C_v = 0.70 for channel complexes, C_v = 0.42 for floodplain elements). The choice of setting value Φ = 3 for both directions was based on results from the unconditional simulations (see below).

The three sets of control simulations were conditioned on a single well-array (1000 m spacing), and their function is to contribute to a further assessment of model sensitivity to input parameters.

A summary of variogram parameters used as input for the six different families of SIS realizations is given in Table 3.

4.1.4 Model evaluation through 2D connectivity measures

The test of the forecasting method involves the quantification of the mismatch between the predicted inter-well architecture and the observed outcrop architecture. The degree of similarity between the outcrop and the realizations is evaluated in terms of two-dimensional static connectivity metrics of channel deposits, employing a geocellular model of the outcrop (Figure 12) as a reference. Two types of connectivity metrics have been considered:

(i) size (cross-sectional area) distribution of the connected geobodies (also termed ‘connected components’, or simply ‘geobodies’; cf. Deutsch 1998; Renard & Allard 2013) of channel deposits, i.e. clusters of cells modeled

as channel deposit and connected in two dimensions, computed considering edge connectivity using GEO_OBJ (Deutsch 1998);

(ii) vertical and horizontal connectivity functions of channel deposits, whose estimation is computed using CONNEC3D (Pardo-Igúzquiza & Dowd 2003); the connectivity function is defined as the probability that two points belonging to a given phase (here, channel deposits) are connected (i.e. belong to the same connected geobody), expressed as a function of their separation in a direction (Allard and HERESIM Group 1993; Renard & Allard 2013); connectivity functions have been calculated for a rectangular subset of the grid (2 km wide, 192 m high; see Figure 12), considering edge connectivity (Pardo-Igúzquiza & Dowd 2003).

The reference realization representing the outcrop geocellular model is characterized by a size distribution of the connected geobodies and vertical and horizontal connectivity functions as given in Figure 13 and 14.

Through quantification of the model-outcrop similarity by means of the same connectivity metrics, the impact of well-array spacing on the realism of the simulated architecture is also assessed.

4.2 Results

4.2.1 Simulations constrained on net-to-gross-based indicator-variogram models

Firstly, we assess the geometry of channel complexes modeled in the unconditional SIS realization (Figure 9). The unconditional realization is characterized by:

(i) average channel-complex thickness (2.58 m) that is significantly underestimated in comparison with both the empirical relationship on

which the channel-deposit indicator-variogram range was based (4.44 m) and the FAKTS stratigraphic volumes displaying corresponding net-to-gross ratio (4.54 m);

(ii) average channel-complex width (107.5 m) that is overestimated in comparison with the empirical relationship on which the channel-deposit indicator-variogram range was based (62.5 m), but underestimated as compared with the FAKTS stratigraphic volumes displaying corresponding net-to-gross ratio (140.1 m);

(iii) lognormally distributed channel-complex thicknesses and widths, in agreement with FAKTS output (Figure 9c and 9d).

It is particularly noteworthy that channel-complex width and thickness are respectively under- and over-estimated in comparison with what is predicted by the empirical relationships on which the variograms were based. These discrepancies may be due to the use of indicator-variogram vertical ranges drawn from the corresponding curve (Figure 8a), without application of a correction to account for the choice of an exponential, rather than spherical model (i.e. different value of Φ). No correction was applied because the same range value was expected to be broadly applicable to both model types. Instead, in view of these results, a tentative Φ correction was later applied when running some of the control simulations of the Blackhawk Formation panel. These control simulations were constrained using indicator-variogram ranges based on application of the A-DQI synthetic analog to Equation 1 for both the horizontal and vertical directions (‘control 3’ in Table 3). The tentative correction was made by taking $\Phi = 3$ for both directions. Generally, it is evident that there is limited precision in transferring analog experience to sequential

indicator simulations through empirical relationships linking indicator variogram model parameters to analog information.

4.2.2 Blackhawk Formation outcrop simulations

The cumulative distributions of the size of channel-deposit connected geobodies in the SIS realizations generated on the basis of the three sets of indicator-variogram models (A-DQI synthetic analog, A-DQI synthetic analog with weighted width statistics, analogy based on net-to-gross ratio) are compared with the equivalent curve for the outcrop-matching geocellular model (Figure 15a and b). The connected-geobody analysis reveals the following:

(i) the mean size of the channel-deposit connected geobodies tend to be largest for the sets of simulations constrained by the highest value of channel indicator-variogram horizontal range (A-DQI analog with weighted depositional-element width statistics) and to be smallest for the sets of simulations constrained by the lowest value of horizontal range (net-to-gross-based analogy);

(ii) SIS realizations based on the A-DQI analog tend to match best with the outcrop when variogram horizontal ranges are not derived from weighted width statistics;

(iii) SIS realizations based on the A-DQI analog with weighted depositional-element width statistics are more consistently over-optimistic (as compared with the outcrop) than the realizations associated with non-weighted width statistics, since they tend to distribute channel deposits across fewer and larger connected geobodies; thus, as the A-DQI analog is known to overestimate mean channel-complex widths and underestimate mean floodplain-element widths, the

simulations based on thickness-weighted width statistics return results that better match expectations in terms of connected-geobody size distributions;

(iv) SIS realizations constrained on the net-to-gross-based analogy are apparently over-pessimistic, as compared with the outcrop, as they display a distribution of channel deposits across more and smaller connected geobodies, if tens of connected geobodies are considered; however, this may not be so if the size of the largest connected geobody is solely taken into account (see below);

(v) noise, which is expressed as randomly distributed cells of channel deposits, and which has not been cleaned in these realizations, is evident by the tail of the cumulative distributions, especially for the simulations based on net-to-gross analogy. Application of a realization-cleaning algorithm would probably result in more optimistic styles of channel-deposit clustering, though further analysis of this is beyond the scope of this study;

(vi) all three groups of realizations show an overall tendency to a better match with the outcrop connected-geobody distributions with decreasing well-array spacing.

Channel-deposit vertical and horizontal connectivity functions for the SIS realizations generated on the basis of the three sets of indicator-variogram models (A-DQI synthetic analog, A-DQI synthetic analog with weighted width statistics, analogy based on net-to-gross) are also compared with the equivalent curves for the outcrop-matching geocellular model (Figures 16 and 17). This comparison permits the following observations and inferences:

(i) considering mean vertical and horizontal connectivity functions for groups of realizations conditioned on the most widely spaced well array (4 wells, 1000 m), we can quantify their deviation from the outcrop connectivity functions as the sum (computed according to the grid resolution) of the squared differences

$(\sum_{i=1}^{h}(f_{outcrop}(i) - f_{realization}(i))^2$; where *h* is the number of cells in a direction and *f* denotes the connectivity function). This shows that realizations associated with the A-DQI analog with non-weighted width statistics return the closest match with the outcrop (vertical $\Sigma(\Delta^2)$ =0.202, horizontal $\Sigma(\Delta^2)$ =0.525), whereas realizations constrained on the net-to-gross-based analogy return the worst match in terms of vertical connectivity function (vertical $\Sigma(\Delta^2)$ =0.316), and realizations based on the A-DQI analog with weighted width statistics return the worst match in terms of horizontal connectivity function (horizontal $\Sigma(\Delta^2)$ =8.296);

(ii) considering the median of the horizontal connectivity functions for groups of realizations conditioned on the most widely spaced well array (4 wells, each spaced 1000 m apart), it is significant to observe that realizations based on the A-DQI synthetic analog attain a worse match in channel-deposit connectivity than the simulations based on net-to-gross analogy; this apparently contrasts with the A-DQI synthetic analog being the better analog in terms of depositional-element geometries;

(iii) in terms of vertical channel-deposit connectivity function, there is a tendency for underestimation of shorter-range (ca. below 10 m) vertical connectivity coupled with overestimation of longer-range (ca. above 13 m) vertical connectivity, evident in all three groups for well-array spacings varying from 1000 m to 100 m, if mean and median connectivity functions for groups of realizations are considered;

(iv) there is a tendency for overestimation of horizontal channel-deposit connectivity function, evident in all three groups for well-array spacings varying from 1000 m to 100 m, if mean connectivity functions for groups of realizations are considered. This is particularly important in consideration of the fact that channel-complex

and floodplain-element mean widths were respectively under- and overestimated by the empirical relationships relating mean widths to net-to-gross, relative to the outcrop panel (Tables 1 and 2);

(v) if the standard deviation in vertical and horizontal connectivity function exhibited by each group of 20 simulations (i.e. for each analog type and well-array configuration) is plotted against distance (Figure 18), the area under the resulting curves will provide a measure of the total stochastic variability for each group. It is apparent that a decrease in well spacing does not necessarily result in a decrease in realization variability, which is particularly evident for simulations conditioned on 4 and 7 wells. It can also been noted that, thanks to the large size of the section considered, the realizations do not appear to suffer from a problem of 'volume support' (cf. Larue & Hovadik 2006; Hovadik & Larue 2007), whereby an increase in horizontal indicator variogram range of the channel deposits determines an increase in variability in connectivity due to the more variable size of the heterogeneities relative to their container.

The third point above needs further examination in consideration of what has been observed in Figure 15: channel-deposit vertical and horizontal connectivity functions of the SIS realizations constrained by the net-to-gross-based analogy are too optimistic despite connected-geobody analysis revealing a pessimistic style of channel-deposit clustering, whereby, as compared with the outcrop, channel deposits are distributed across a larger number of on average smaller connected geobodies. However, if the group of realizations conditioned on four wells is considered, for example, it is possible to observe how the largest and second largest channel connected geobodies in these realizations are on average larger (1.28 times and 1.05 times, respectively) than the same connected geobodies from the outcrop

geocellular model, and long-range horizontal connectivity functions seem to be controlled especially by these largest geobodies (Figure 19). It is important to note the following: (i) whereas horizontal indicator-variogram ranges differed, the input value of vertical range used to condition these realizations was the same (10 m) for all groups of simulations and for both channel and overbank deposits, as it was derived from geostatistical analysis of the dummy-well data; (ii) the group of simulations constrained by the net-to-gross analogy displayed the highest degree of noise (Figures 11 and 15). This has likely resulted in vertical paths of connected channel-deposit cells that controlled the size of the largest geobodies. Thus, the application of two alternative analogs that are respectively optimistic and pessimistic in terms of both channel-complex and floodplain-element lateral extent did not return corresponding simulation results in terms of connectivity functions and size of the largest geobodies. The important practical implication is that consideration of alternative outcrop analogs as a way to encompass architectural variability may not result in variations in mean connectivity functions and mean size of the largest connected geobody that directly reflect variations in the geometry of net-quality reservoir units seen across the different analogs.

The same analysis of channel-deposit connected-geobody size distributions and connectivity functions has been applied to the three groups of control simulations, with the scope to better test the sensitivity of sequential indicator simulations to their input (Figures 20 and 21). Results can be summarized as follows:

(i) the two sets of simulations based on application of analog-informed indicator-variogram models result in better estimations of distributions of channel-deposit connected-geobody size than SIS runs conditioned on indicator-variogram

parameters based on curve fitting of data from geostatistical analysis of the outcrop (Figure 20), emphasizing the value of this type of analog application;

(ii) SIS realizations constrained on variograms based on the Blackhawk Formation outcrop depositional-element statistics return, on average, slightly pessimistic channel-deposit geobody-size distributions;

(iii) realizations conditioned on indicator-variogram models based on the Blackhawk depositional-element width statistics return the closest match with the outcrop in terms of mean horizontal connectivity function (vertical $\Sigma(\Delta^2)$ =0.264, horizontal $\Sigma(\Delta^2)$ =0.401; Figure 21), whereas realizations conditioned on the A-DQI analog with definition of indicator-variogram vertical ranges based on depositional-element thickness statistics return the closest match with the outcrop in terms of mean vertical connectivity function (vertical $\Sigma(\Delta^2)$ =0.154, horizontal $\Sigma(\Delta^2)$ =1.373; Figure 21); realizations based on variogram parameters derived from outcrop geostatistical analysis return: vertical $\Sigma(\Delta^2)$ =0.267, horizontal $\Sigma(\Delta^2)$ =0.567. Thus, the application of a better 'analog' (i.e. the outcrop itself) for width statistics has determined improved reproduction of the horizontal connectivity function, whereas consideration of different values of vertical variogram range for channel and floodplain deposits (as based on analog thickness statistics) has determined improved reproduction of the vertical connectivity function;

(iv) in terms of mean vertical channel-deposit connectivity function, there is a tendency for underestimation of shorter-range (ca. below 10 m) vertical connectivity coupled with overestimation of longer-range (ca. above 13 m) vertical connectivity, evident in all three groups (Figure 21);

(v) there is a consistent overestimation of mean horizontal channel-deposit connectivity function for values of separation above ca. 1000 m (Figure 21).

5. DISCUSSION

As applied to the prediction of the Blackhawk Formation outcrop panel, results demonstrate the utility of correlability models (Colombera et al. 2014) as tools for checking the geologic realism of sandbody well-correlation panels against the large-scale fluvial architecture of outcrop analogs. The confidence in method application is strongly related to the degree of sandbody sampling, as is to be expected. With reference to this particular case study and to correlability-model applications where the approach works best (i.e. cases that allow for sufficient sand-body sampling), revisions of well correlations are advisable when values of panel-model discrepancy for each correlation distance are above 0.05. If a statistically significant number of bodies are sampled, consistency is achieved between the predictions made and the degree of panel-model match in sandstone width descriptive statistics, in terms of both magnitude and direction of panel-model deviation. This also suggests the value of simultaneously considering multiple analogs as a way to treat uncertainty associated with analog choice (Shepherd 2009), by checking subsurface correlation panels against alternative scenarios based on equally suitable analogs.

Both unconditional sequential indicator simulations and SIS models of the Blackhawk Formation outcrop architecture have been constrained by indicator-variogram parameters derived from empirical relationships (Ritzi 2000; Equations 1 and 2) that express such parameters as functions of geologic attributes. There is evidently imprecision inherent in the process of transferring outcrop-analog knowledge to pixel-based reservoir models through indicator-variogram models informed by these relationships, as shown by generic unconditional simulations. In particular, it seems that the empirical relationships proposed by Ritzi (2000) for the estimation of the

indicator variogram range could be improved, possibly by rendering the Φ parameter expressed as a continuous function of the coefficient of variation of the size of the heterogeneity. Nonetheless, it has been shown that in effect employing values of horizontal indicator-variogram range based on outcrop-analog data resulted in subsurface reconstructions that are as good as – if not better than – realizations simulated on the basis of indicator-variogram models based on curve fitting of experimental variogram values, if the quality of the prediction is assessed by static-connectivity metrics. Although this observation supports our approach in transferring outcrop-analog experience to the geostatistical modeling practice, it is important to note that different groups of SIS models display styles of channel-deposit clustering and connectivity that do not match with what is expected from descriptive statistics for the different analogs considered. As an increase in horizontal range is in effect anticipated to correspond to an increase in connectivity (Larue & Hovadik 2006), it should be expected that the choice of two alternative analogs that are known to be respectively rather optimistic and pessimistic (in terms of lateral continuity of sand-prone channel complexes versus mud-prone floodplain elements) would result in subsurface realizations that – on average – will predict corresponding characteristics of channel-deposit horizontal static connectivity. The fact that mean and median horizontal connectivity functions do not reflect analog depositional-element width data may be indicative of (i) problems connected with the SIS technique that seem to be overriding (e.g. noise, also evidenced by visual inspection and connected-geobody analysis), or of (ii) the fact that for a fixed net-to-gross ratio smaller channel bodies effectively determine a distribution of channel deposits that is more favorable for horizontal connectivity (cf. Hovadik & Larue 2007). These considerations should

be borne in mind when applying multiple analogs to SIS as a way to account for uncertainty in analog selection.

It has also been observed that an increase in the number of conditioning wells, which are therefore more closely spaced, does not necessarily result in a reduction in the variability in connectivity functions seen within each group of equiprobable realizations, and this is especially evident for the realizations conditioned to the most widely spaced well arrays; this is counter to the expectation that an increase in the number of wells should necessarily result in a decrease in model variability (Matheron et al. 1987; Felletti 2004), and so uncertainty.

Whereas object- or training-image-based approaches are advisable over variogram-based ones in application to the modeling of channelized units, SIS is still applied to modeling fluvial reservoirs (Ringrose and Bentley 2015), and there may be situations when particular features of a fluvial reservoir are preferably modeled using SIS. As pixel-based methods return realizations that perfectly honor all the well data, their application is particularly suitable for densely drilled reservoirs. SIS models invariably display unstructured geometries: this makes SIS inappropriate for the simulation of channelized units, but does not compromise the application of SIS to the simulation of rock units of unknown shape.

Although SIS does not particularly lend itself to the simulation of channelized reservoirs, in relation to its inability to reproduce complex curvilinear geometries, this specific application is still meant to be a generic test of the approach of analog-based SIS conditioning. This test has been carried out against a fluvial succession in relation to the type of analog data being available. In a real-world practice of subsurface characterization, the tested workflow for variogram parameterization described here could still be applied to (i) the simulation of sedimentary

heterogeneities within reservoirs of a different nature, possibly also through application of truncated Gaussian approaches, or (ii) to the generation of a number of equiprobable 2D well correlation panels through SIS.

Two elements of uncertainty need to be considered concerning the value of the results of this work for 3D reservoir-model building. The relationship between the indicator-variogram range of a channelized unit along a given direction is not a simple function of its continuity in that direction, if the channelized unit is characterized by a complex shape (e.g. wavelength and amplitude of a sinuous channel belt; cf. Caers & Zhang 2004). Thus, the tested empirical approach cannot be readily applied to the estimation of indicator-variogram ranges that relate the downstream physical continuity of 3D channelized units (downstream-oriented indicator-variogram range for channel deposits), in view of uncertainty on the 3D shape of these units. Additionally, because of the inability of indicator variograms to capture 3D shapes, and thus the inappropriateness of SIS as a tool for the reproduction of curvilinear features, all the results expressed as connectivity metrics cannot be directly extrapolated to a 3D scenario. However, in consideration of the unstructured nature of rock domains modeled with SIS, it is conceivable that the down-dip static connectivity of channel deposits would be significantly underestimated, even if realistic values of indicator-variogram ranges for the down-system direction were derived.

6. CONCLUSIONS

The current study has demonstrated the two-fold application of outcrop analogs as a basis for both informing and testing predictive tools for forecasting the architecture of subsurface fluvial successions.

Correlability models have been shown to serve as realistic templates for comparing the geologic realism of sandbody well correlations against outcrop analogs. Results also demonstrate that, if well arrays offer sufficient sampling of the sandbodies, different correlability models can be usefully applied to the same panel to account for uncertainty associated with analog suitability.

Although there is imprecision inherent in the process of transferring outcrop-analog knowledge to variogram-based reservoir models, and results suggest that existing empirical relationships are improvable, the use of analog information in the compilation of indicator-variogram models for channel and overbank deposits has been demonstrated to be effective. Sequential indicator simulations conditioned to such variogram models display a comparable degree of realism relative to equivalent simulations conditioned to variograms based on the outcrop two-point statistics. However, there may not be a straightforward correspondence between the degree of channel-deposit connectivity in a set of models and the analog dimensional parameters used for building them, when considering multiple analogs as representative of pessimistic or optimistic scenarios on the basis of their geometric properties.

These results support the use of outcrop-analog experience to build subsurface models of large-scale fluvial architecture, and stress the continuing need for analog studies and the utility of databases of outcrop-analog architecture. However, guidelines are necessary for ensuring best practice in the application of analogs to subsurface modeling problems, which can be drawn from studies of this type.

References

Adams, M. M., and Bhattacharya, J. P., 2005, No change in fluvial style across a sequence boundary, Cretaceous Blackhawk and Castlegate Formations of central Utah, USA: Journal of Sedimentary Research, v. 75, p. 1038-1051, doi: 10.2110/jsr.2005.080.

Al-Ajmi, H., Hinderer, M., Keller, M., Rausch, R., Blum, P., and Bohnsack, D., 2011, The Role of Outcrop Analogue Studies for the Characterization of Aquifer Properties: International Journal of Water Resources and Arid Environments, v. 1, p. 48-54.

Alexander, J., 1993, A discussion on the use of analogues for reservoir geology, *in* M. Ashton, ed., Advances in Reservoir Geology: Geological Society, London, Special Publications, v. 69, p. 175-194, doi: 10.1144/GSL.SP.1993.069.01.08.

Allard, D., and HERESIM Group, 1993, On the connectivity of two random set models: the truncated Gaussian and the Boolean, *in* A. Soares, ed., Geostatistics Tróia'92, 467-478: Springer Netherlands, doi: 10.1007/978-94-011-1739-5_37.

Bridge, J. S, 2001, Characterization of fluvial hydrocarbon reservoirs and aquifers: Problems and solutions: Asociación Argentina de Sedimentología Revista, v. 8, p. 87-114.

Bridge, J. S., Jalfin, G. A., and Georgieff, S. M., 2000, Geometry, lithofacies, and spatial distribution of Cretaceous fluvial sandstone bodies, San Jorge Basin, Argentina: outcrop analog for the hydrocarbon-bearing Chubut Group: Journal

of Sedimentary Research, v. 70, p. 341-359, doi: 10.1306/2DC40915-0E47-11D7-8643000102C1865D.

Bridge, J. S., and Tye, R. S., 2000, Interpreting the dimensions of ancient fluvial channel bars, channels, and channel belts from wireline-logs and cores: AAPG Bulletin, v. 84, p. 1205-1228, doi:10.1306/A9673C84-1738-11D7-8645000102C1865D.

Caers, J., and T. Zhang, 2004, Multiple-point geostatistics: A quantitative vehicle for integrating geologic analogs into multiple reservoir models, in M. Grammer, P. M. Harris, and G. P. Eberli, eds., Integration of outcrop and modern analogs in reservoir modeling: AAPG Memoir 80, p. 383-394.

Colombera, L., Felletti, F., Mountney, N. P., and McCaffrey, W. D., 2012a, A database approach for constraining stochastic simulations of the sedimentary heterogeneity of fluvial reservoirs: AAPG Bulletin, v. 96, p. 2143-2166, doi:10.1306/04211211179.

Colombera, L., Mountney, N. P., and McCaffrey, W. D., 2012b, A relational database for the digitization of fluvial architecture concepts and example applications: Petroleum Geoscience, v. 18, p. 129-140, doi:10.1144/1354-079311-021.

Colombera, L., Mountney, N. P., and McCaffrey, W. D., 2013, A quantitative approach to fluvial facies models: Methods and example results: Sedimentology, v. 60, p. 1526-1558, doi:10.1111/sed.12050.

Colombera, L., Mountney, N. P., Felletti, F., and McCaffrey W. D., 2014, Models for guiding and ranking well-to-well correlations of channel bodies in fluvial reservoirs: AAPG Bulletin, v. 98, p. 1943-1965., doi:10.1306/05061413153.

Comunian, A., Renard, P., Straubhaar, J., and Bayer, P., 2011, Three-dimensional high resolution fluvio-glacial aquifer analog–Part 2: Geostatistical modelling: Journal of Hydrology, v. 405, p. 10-23, doi:10.1016/j.jhydrol.2011.03.037.

dell'Arciprete, D., Bersezio, R., Felletti, F., Giudici, M., Comunian, A., and Renard, P., 2012, Comparison of three geostatistical methods for hydrofacies simulation: a test on alluvial sediments: Hydrogeology Journal, v. 20, p. 299-311, doi: 10.1007/s10040-011-0808-0.

Deutsch, C. V., 1998, Fortran programs for calculating connectivity of three-dimensional numerical models and for ranking multiple realizations: Computers & Geosciences, v. 24, p. 69-76, doi:10.1016/S0098-3004(97)00085-X.

Deutsch, C. V., 2006, A sequential indicator simulation program for categorical variables with point and block data: BlockSIS: Computers & Geosciences, v. 32, p. 1669-1681, doi:10.1016/j.cageo.2006.03.005.

Deutsch, C. V., and Journel, A. G., 1998, Geostatistical software library and user's guide (GSLIB): Oxford University Press, New York, 369 pp.

Emery, X., 2004, Properties and limitations of sequential indicator simulation: Stochastic Environmental Research and Risk Assessment, v. 18, p. 414-424, doi: 10.1007/s00477-004-0213-5.

Falivene, O., Arbués, P., Gardiner, A., Pickup, G., Muñoz, J. A., and Cabrera, L., 2006, Best practice stochastic facies modeling from a channel-fill turbidite sandstone analog (the Quarry outcrop, Eocene Ainsa basin, northeast Spain): AAPG Bulletin, v. 90, p. 1003-1029, doi: 10.1306/02070605112.

Felletti, F., 2004, Statistical modelling and validation of correlation in turbidites: an example from the Tertiary Piedmont Basin (Castagnola Fm., Northern Italy): Marine and Petroleum Geology, v. 21, p. 23-39, doi:10.1016/j.marpetgeo.2003.11.006.

Flores, R. M., Blanchard, L. F., Sanchez, J. D., Marley, W. E., and Muldoon, W. J., 1984, Paleogeographic controls of coal accumulation, Cretaceous Blackhawk Formation and Star Point Sandstone, Wasatch Plateau, Utah: Geological Society of America Bulletin, v. 95, p. 540-550, doi: 10.1130/0016-606(1984)95<540:PCOCAC>2.0.CO;2.

Geehan, G., 1993, The use of outcrop data and heterogeneity modelling in development planning, *in* R. Eschard, and B. Doligez, eds., Subsurface reservoir characterization from outcrop observations: Institut Français du Pétrole: Paris, Éditions Technip, p. 53-64.

Geehan, G., and Underwood, J., 1993, The use of length distributions in geological modelling, *in* S. S. Flint, and I. D. Bryant, eds., The geological modelling of hydrocarbon reservoirs and outcrop analogues: International Association of Sedimentologists Special Publication, v. 15, p. 205-212, doi: 10.1002/9781444303957.ch13

Hampson, G. J., Royhan Gani, M., Sahoo, H., Rittersbacher, A., Irfan, N., Ranson, A., Jewell, T. O., Gani, N. D. S., Howell, J. A., Buckley, S. J., and Bracken, B., 2012, Controls on large-scale patterns of fluvial sandbody distribution in alluvial to coastal plain strata: Upper Cretaceous Blackhawk Formation, Wasatch Plateau, Central Utah, USA: Sedimentology, v. 59, p. 2226-2258, doi: 10.1111/j.1365-3091.2012.01342.x.

Hovadik, J. M., and Larue, D. K., 2007, Static characterizations of reservoirs: refining the concepts of connectivity and continuity: Petroleum Geoscience, v. 13, p. 195-211, doi: 10.1144/1354-079305-697.

Howell, J. A., and S. S. Flint, 2003, Sequences and systems tracts in the Book Cliffs, *in* A. Coe, ed., The sedimentary record of sea level change: Cambridge, United Kingdom, Cambridge University Press, p. 179-197.

Howell, J. A., Martinius, A. W., and Good, T. R., 2014, The application of outcrop analogues in geological modelling: a review, present status and future outlook, *in* A. W. Martinius, J. A. Howell, and T. R. Good, eds., Sediment-body geometry and heterogeneity: Analogue studies for modelling the subsurface: Geological Society, London, Special Publications, v. 387, p. 1-25, doi: 10.1144/SP387.12.

Jones, A., Doyle, J., Jacobsen, T., and Kjønsvik, D., 1995, Which sub-seismic heterogeneities influence waterflood performance? A case study of a low net-to-gross fluvial reservoir, *in* H. J. deHaan, ed., New developments in improved oil recovery: Geological Society, London, Special Publications, v. 84, p. 5-18.

Journel, A. G., and Alabert, F. G., 1990, New method for reservoir mapping: Journal of Petroleum Technology, v. 42, p. 212-218, doi: 10.2118/18324-PA.

Journel, A. G., and Xu, W., 1994, Posterior identification of histograms conditional to local data: Mathematical Geology, v. 26, p. 323-359, doi: 10.1007/BF02089228.

Keogh, K. J., Leary, S., Martinius, A. W., Scott, A. S., Riordan, S., Viste, I., Gowland, S., Taylor, A., and Howell, J., 2014, Data capture for multiscale modelling of the Lourinhã Formation, Lusitanian Basin, Portugal: an outcrop analogue for

the Statfjord Group, Norwegian North Sea, *in* A. W. Martinius, J. A. Howell, and T. R. Good, eds., Sediment-body geometry and heterogeneity: Analogue studies for modelling the subsurface: Geological Society, London, Special Publications, v. 387, p. 27-56, doi: 10.1144/SP387.11.

Larue, D. K., and Hovadik, J., 2006, Connectivity of channelized reservoirs: a modelling approach: Petroleum Geoscience, v. 12, p. 291-308, doi: 10.1144/1354-079306-699.

Lorenz, J. C., Heinze, D. M., Clark, J. A., and Searls, C. A., 1985, Determination of widths of meander-belt sandstone reservoirs from vertical downhole data, Mesaverde Group, Piceance Creek Basin, Colorado: AAPG Bulletin, v. 69, p. 710-721.

Martinius, A. W., and Næss, A., 2005, Uncertainty analysis of fluvial outcrop data for stochastic reservoir modeling: Petroleum Geoscience, v. 11, p. 203–214, doi:10.1144/1354-079303-615.

Matheron, G., Beucher, H., De Fouquet, C., Galli, A., Guerillot, D., and Ravenne, C., 1987, Conditional simulation of the geometry of fluvio-deltaic reservoirs: Paper SPE 16753, presented at Annual Technical Conference and Exhibition, Society of Petroleum Engineers, p. 591-599, doi: 10.2118/16753-MS.

Miall, A. D., 2006, Reconstructing the architecture and sequence stratigraphy of the preserved fluvial record as a tool for reservoir development: A reality check: AAPG Bulletin, v. 90, p. 989-1002, doi: 10.1306/02220605065.

North, C. P., and Prosser, D. J., 1993, Characterization of fluvial and aeolian reservoirs: problems and approaches, *in* C. P. North, and D. J. Prosser, eds.,

Characterization of fluvial and aeolian reservoirs: Geological Society, London, Special Publications, v. 73, p. 1-6, doi: 10.1144/GSL.SP.1993.073.01.01.

Pardo-Igúzquiza, E., and Dowd, P. A., 2003, CONNEC3D: a computer program for connectivity analysis of 3D random set models: Computers & Geosciences, v. 29, p. 775-785, doi:10.1016/S0098-3004(03)00028-1.

Pringle, J. K., Howell, J. A., Hodgetts, D., Westerman, A. R., and Hodgson, D. M., 2006, Virtual outcrop models of petroleum reservoir analogues: a review of the current state-of-the-art: First break, v. 24, p. 33-42, doi: 10.3997/1365-2397.2006005.

Proce, C. J., Ritzi, R. W., Dominic, D. F., and Dai, Z., 2004, Modeling multiscale heterogeneity and aquifer interconnectivity: Ground Water, v. 42, p. 658-670, doi: 10.1111/j.1745-6584.2004.tb02720.x.

Remy, N., Boucher, A., and Wu, J., 2009, Applied geostatistics with SGeMS: A user's guide: Cambridge University Press, 259 pp., doi: 10.1017/CBO9781139150019.

Renard, P., and Allard, D., 2013, Connectivity metrics for subsurface flow and transport: Advances in Water Resources, v. 51, p. 168-196, doi:10.1016/j.advwatres.2011.12.001.

Ringrose, P., and Bentley, M., 2015, Reservoir model design, Springer, 249 pp. doi: 10.1007/978-94-007-5497-3

Rittersbacher, A., Howell, J. A., and Buckley, S. J., 2014, Analysis of fluvial architecture In the Blackhawk Formation, Wasatch Plateau, Utah, USA, using large 3D photorealistic models: Journal of Sedimentary Research, v. 84, p. 72-87, doi: 10.2110/jsr.2014.12.

Ritzi, R. W., 2000, Behavior of indicator variograms and transition probabilities in relation to the variance in lengths of hydrofacies: Water Resources Research, v. 36, p. 3375-3381, doi: 10.1029/2000WR900139.

Seifert, D., and Jensen, J. L., 1999, Using sequential indicator simulation as a tool in reservoir description: Issues and uncertainties: Mathematical Geology, v. 31, p. 527-550, doi: 10.1023/A:1007563907124.

Shepherd, M., 2009, Reservoir uncertainty, *in* Shepherd, M., Oil field production geology: AAPG Memoir, v. 91, p. 195-200.

Venteris, E. R., 2007, Three-dimensional modeling of glacial sediments using public water-well data records: An integration of interpretive and geostatistical approaches: Geosphere, v. 3, p. 456-468, doi: 10.1130/GES00090.1.

TABLE CAPTIONS

Table 1: summary of channel-complex (CC) width descriptive statistics (inclusive of partial- and unlimited-width data, associated with outcrop termination, *sensu* Geehan and Underwood, 1993), for both the architectural panel in Figure 2 and the chosen analogs. A-DQI means highest score in *data quality index*. N refers to the number of observations (depositional elements).

Table 2: summary of floodplain depositional element width descriptive statistics (inclusive of partial-width data, associated with outcrop termination), for both the architectural panel in Figure 2 and the chosen analogs. A-DQI means highest score in *data quality index*. N refers to the number of observations (depositional elements).

Table 3: summary of variogram parameters used as input for the six different groups of SIS realizations, as based on data from both the Blackhawk panel (geostatistical analysis of the outcrop geocellular model, depositional-element width statistics) and the FAKTS analogs. A-DQI means highest score in *data quality index*.

FIGURE CAPTIONS

Figure 1: location map showing the position of the outcropping study succession in the central Wasatch Plateau area (Utah, USA).

Figure 2: architectural panel of part of the Blackhawk Formation depicting the distribution of channel and overbank deposits based on interpretation of the chosen outcrop. The grid overlain on the panel represents an array of 65 'dummy' wells (see text for explanation).

Figure 3: scatter plots of different depositional-element architectural features against element proportions, as computed for suitable FAKTS stratigraphic volumes associated with high-quality datasets. Each data point represents a stratigraphic volume. Best-fit regression curves fitted to the data are graphed and reported as equations with associated R^2 values. These curves permit prediction of depositional-

element thickness mean (A, B) and standard deviation (C, D), width mean (E, F) and standard deviation (G, H), and vertical embedding coefficient (I, K). See text for definitions.

Figure 4: comparison between curves of the total probability of penetration (above) and correlation (below) of channel complexes as a function of distance, and proportions of channel complexes penetrated or 'correlated' for variable dummy-well separation. The total-probability curves are based on: (i) the outcrop itself, (ii) the A-DQI analog, (iii) channel-complex width descriptive statistics predicted for the observed net-to-gross ratio.

Figure 5: comparison between channel-complex correlability models (lines) and values of proportion-based outcrop channel-complex correlability (data points). The correlability models are based on: (i) the outcrop itself, (ii) the A-DQI analog, (iii) channel-complex width descriptive statistics predicted for the observed net-to-gross ratio. The four different sets of models and outcrop data relate to different well arrays (well spacing S reported in upper right corner of plots).

Figure 6: histogram of channel-complex apparent widths (as projected into the plane of the panel) from the Blackhawk Formation outcrop; a lognormal probability density function has been fitted to the width distribution.

Figure 7: bar chart of the values of outcrop versus model cumulative discrepancy shown by models for different well-array configurations, as given in Figure 5; Np =

number of penetrated channel complexes, Nc = number of ‘correlated’ channel complexes.

Figure 8: curves for the prediction of indicator variogram vertical (A) and horizontal (B) ranges as functions of net-to-gross ratio for channel and floodplain deposits; these curves are based on empirical relationships (see text for explanation); the two sets of curves refer to spherical (A) and exponential (B) indicator-variogram models.

Figure 9: unconditional SIS realization (A) constrained on indicator-variogram parameters derived from net-to-gross-based relationships and chosen for model evaluation, carried out as comparison against FAKTS stratigraphic volume with corresponding net-to-gross, in terms of channel complex thickness (B, C) and width (B, D).

Figure 10: experimental indicator variograms of the outcrop fluvial architecture, computed for vertical (A) and horizontal (B) directions from geostatistical analysis of dummy-well data, for well arrays with variable spacing; the actual horizontal indicator variogram of the outcrop, calculated from the outcrop geocellular model, is represented as a continuous line.

Figure 11: example SIS realizations for each of the 15 scenarios (5 well array configurations, 3 sets of analog-based SIS input) of modeled outcrop architecture; the shown examples were all generated from the same seed number (which generates the random path through the grid; Deutsch & Journel 1998).

Figure 12: realization matching the observed outcrop architecture, used as a reference against which to compare SIS modeling results; the rectangular frame delineates the outcrop section employed for the analysis of connectivity functions.

Figure 13: cumulative size distribution of the connected geobodies of channel deposits of the reference realization matching the outcrop architecture; the cumulative number of geobodies is ordered by decreasing connected-geobody size.

Figure 14: vertical and horizontal connectivity functions of channel deposits of a selected portion (see Figure 12) of the reference realization matching the outcrop architecture.

Figure 15: comparison between the outcrop distribution of channel-deposit connected-geobody sizes and the same distributions for the different sets of SIS realizations constrained by analog-based indicator variograms.

Figure 16: comparison between the vertical connectivity function for channel deposits for the outcrop and the same functions for the different sets of SIS realizations constrained by analog-based indicator variograms.

Figure 17: comparison between the horizontal connectivity function for channel deposits for the outcrop and the same functions for the different sets of SIS realizations constrained by analog-based indicator variograms.

Figure 18: plots of the standard deviation in vertical (left) and horizontal (right) channel-deposit connectivity function exhibited by the different groups of 20 realizations, presented for the different sets of analog-based SIS input and for the different well-array configurations used for SIS conditioning.

Figure 19: plots of the size of each of the five largest channel-deposit connected geobodies against the channel-deposit horizontal connectivity function at 1000 m (above) and 300 m (below), for the 20 realizations generated on the basis of the net-to-gross analogy and most widely spaced (1000 m) well array; results are compared with the outcrop-matching reference realization.

Figure 20: comparison between the outcrop distribution of channel-deposit connected-geobody sizes and the same distributions for the three sets of sequential indicator simulations used as controls.

Figure 21: comparison between the vertical and horizontal connectivity function for channel deposits for the outcrop and the same functions for the three sets of sequential indicator simulations used as controls.

TABLES

Table 1: summary of channel-complex (CC) width descriptive statistics (inclusive of partial- and unlimited-width data, associated with outcrop termination, *sensu* Greehan and Underwood, 1993), for both the architectural panel in Fig. 2 and the chosen analogs. A-DQI means highest score in *data quality index*. N refers to the number of observations (depositional elements).

Dataset	**Mean CC width (m)**	**CC width standard deviation**	**N**
All Blackhawk Fm. panel	160	171	99
Net:gross relationships	**Predicted mean CC width (m)**	**Predicted CC width standard deviation**	
0.18 net:gross ratio (all panel)	85	81	
Synthetic analog	**Mean CC width (m)**	**CC width standard deviation**	**N**
A-DQI humid/subhumid system in foreland basin	198	284	191
A-DQI humid/subhumid system in foreland basin - thickness weighted statistics -	314	431	111

Table 2: summary of floodplain depositional element width descriptive statistics (inclusive of partial-width data, associated with outcrop termination), for both the architectural panel in Fig. 2 and the chosen analogs. A-DQI means highest score in *data quality index*. N refers to the number of observations (depositional elements).

Dataset	**Mean floodplain width (m)**	**Floodplain width standard deviation**	**N**
All Blackhawk Fm. panel	661	686	187
Net:gross relationships	**Predicted mean floodplain width (m)**	**Predicted floodplain width standard deviation**	
0.18 net:gross ratio (all panel)	1177	1037	
Synthetic analog	**Mean floodplain width (m)**	**Floodplain width standard deviation**	**N**
A-DQI humid/subhumid system in foreland basin	575	496	116
A-DQI humid/subhumid system in foreland basin - thickness weighted statistics -	634	611	116

Table 3: summary of variogram parameters used as input for the six different groups of SIS realizations, as based on data from both the Blackhawk Fm. panel (geostatistical analysis of the outcrop geocellular model, depositional-element width statistics) and the FAKTS analogs. A-DQI means highest score in *data quality index*.

Geostatistical analysis	**Variogram model**	**Vertical range (m)**		**Horizontal range (m)**	
Architectural-panel indicator variogram (Control 1)	Exponential	10		320	
Analog-based SIS input	**Variogram model**	**Channel-deposit vertical range (m)**	**Floodplain-deposit vertical range (m)**	**Channel-deposit horizontal range (m)**	**Floodplain-deposit horizontal range (m)**
0.18 net:gross ratio (all panel)	Exponential	10 (curve fitting)	10 (curve fitting)	210	633
A-DQI humid/subhumid system in foreland basin	Exponential	10 (curve fitting)	10 (curve fitting)	488	310
A- DQI humid/subhumid system in foreland basin – thickness-weighted width statistics	Exponential	10 (curve fitting)	10 (curve fitting)	774	342
Control 2: Panel width statistics	Exponential	10 (curve fitting)	10 (curve fitting)	395	357
Control 3: *A- DQI* humid/subhumid system in foreland basin – thickness statistics included	Exponential	13	5	488	310

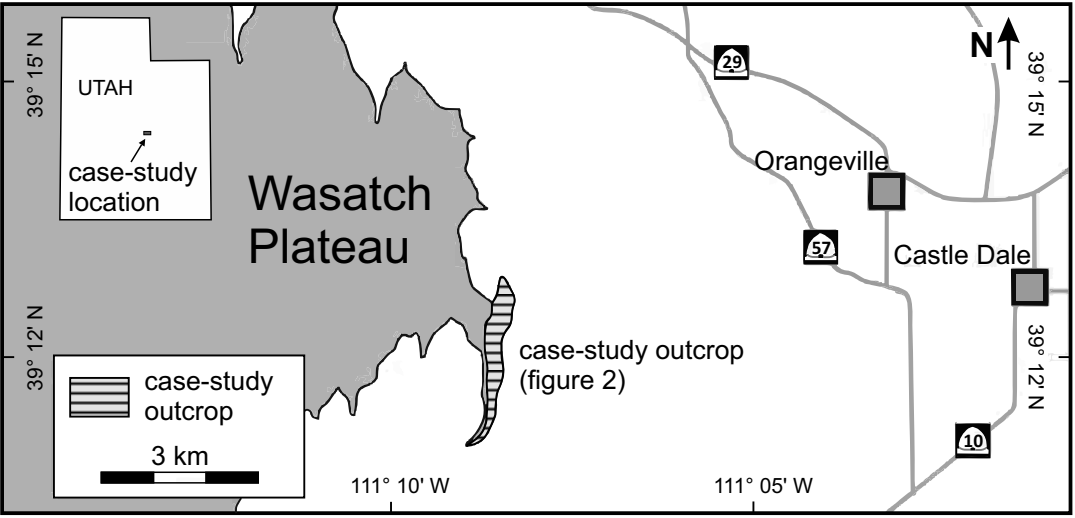
UTAH
case-study location
Wasatch Plateau
case-study outcrop
3 km
case-study outcrop (figure 2)
Orangeville
Castle Dale
29
57
10
N
39° 15' N
39° 12' N
111° 10' W
111° 05' W

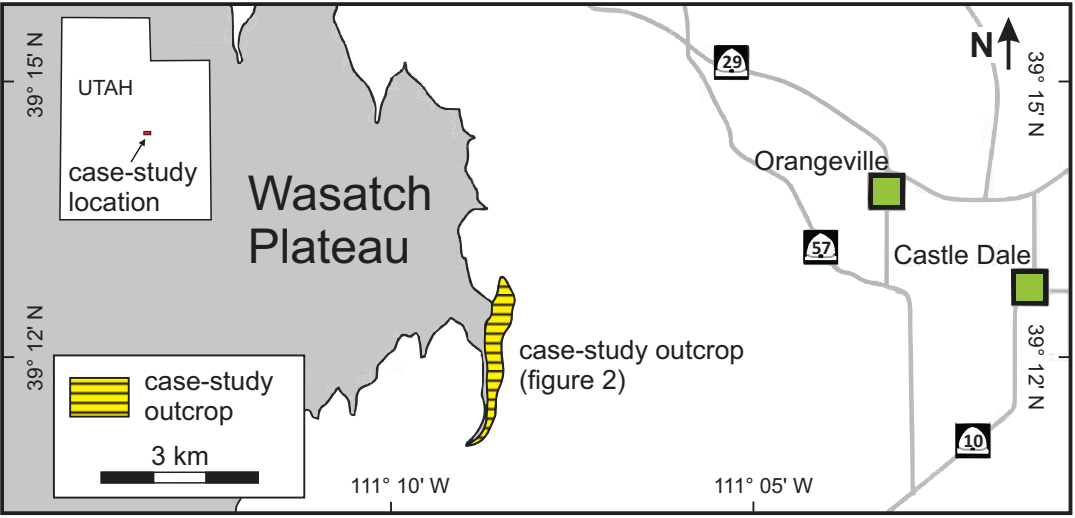
UTAH
case-study location
Wasatch Plateau
case-study outcrop (figure 2)
case-study outcrop
3 km
39° 15' N
39° 12' N
111° 10' W
111° 05' W
N
29
57
10
Orangeville
Castle Dale

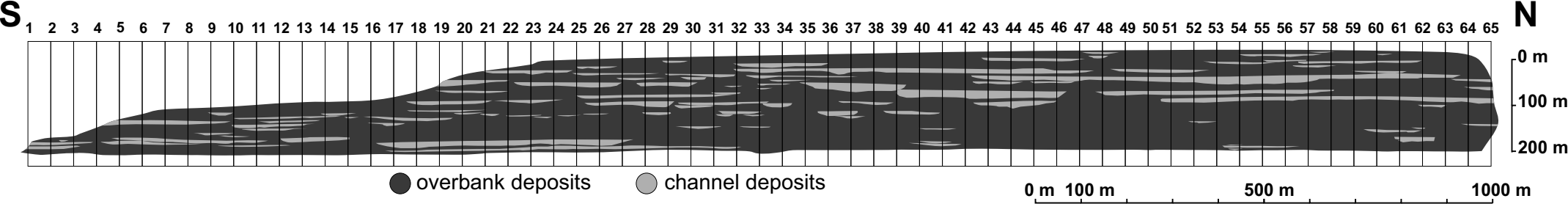
S
1 2 3 4 5 6 7 8 9 10 11 12 13 14 15 16 17 18 19 20 21 22 23 24 25 26 27 28 29 30 31 32 33 34 35 36 37 38 39 40 41 42 43 44 45 46 47 48 49 50 51 52 53 54 55 56 57 58 59 60 61 62 63 64 65
N
0 m
100 m
200 m
overbank deposits
channel deposits
0 m 100 m
500 m
1000 m

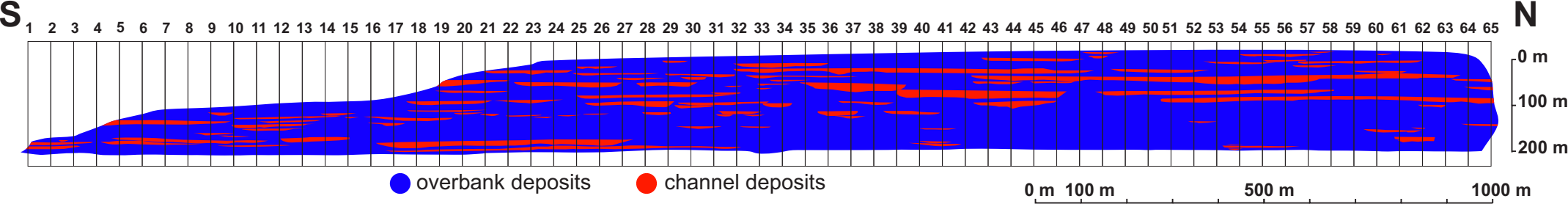
S
1 2 3 4 5 6 7 8 9 10 11 12 13 14 15 16 17 18 19 20 21 22 23 24 25 26 27 28 29 30 31 32 33 34 35 36 37 38 39 40 41 42 43 44 45 46 47 48 49 50 51 52 53 54 55 56 57 58 59 60 61 62 63 64 65
N
0 m
100 m
200 m
overbank deposits
channel deposits
0 m 100 m
500 m
1000 m

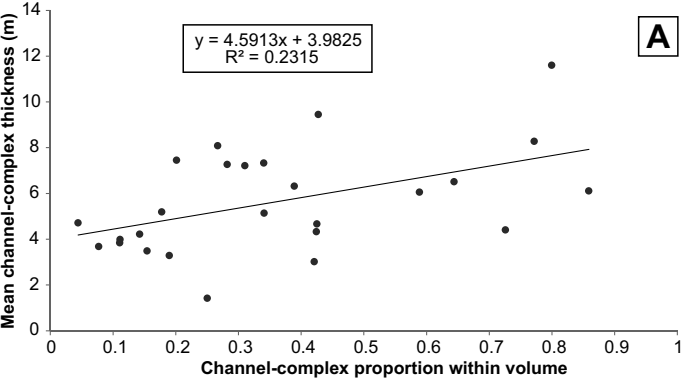
A
y = 4.5913x + 3.9825
R² = 0.2315
Mean channel-complex thickness (m)
Channel-complex proportion within volume

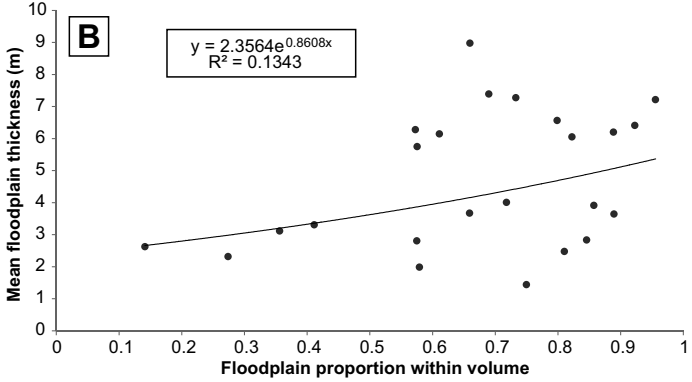
B
y = 2.3564e^0.8608x
R² = 0.1343
Mean floodplain thickness (m)
Floodplain proportion within volume

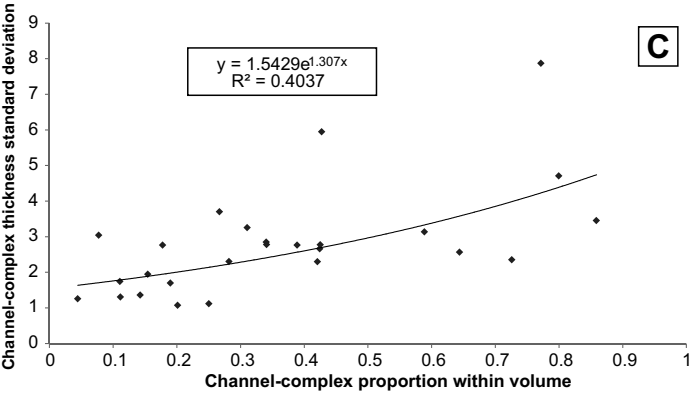
C
y = 1.5429e^1.307x
R² = 0.4037
Channel-complex thickness standard deviation
Channel-complex proportion within volume

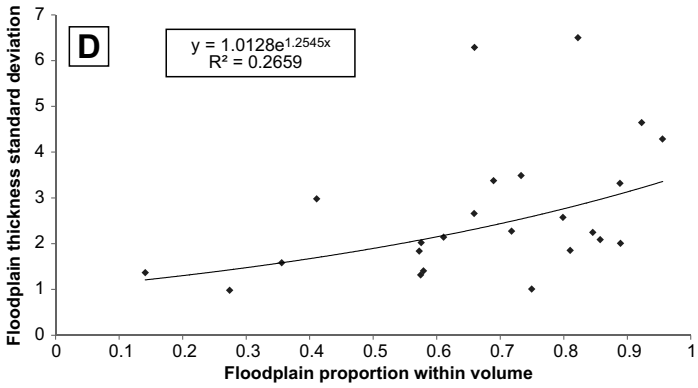
D
y = 1.0128e^1.2545x
R² = 0.2659
Floodplain thickness standard deviation
Floodplain proportion within volume

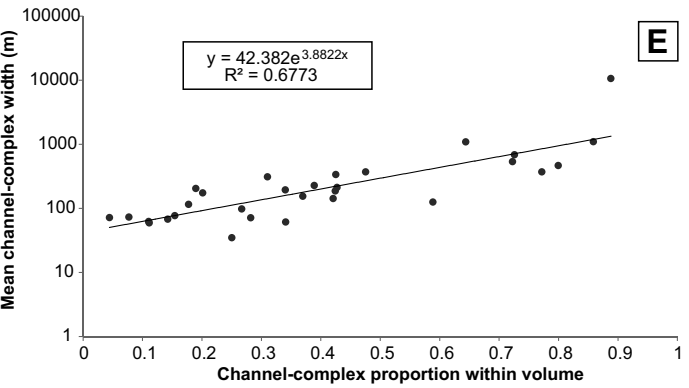
E
y = 42.382e^3.8822x
R² = 0.6773
Mean channel-complex width (m)
Channel-complex proportion within volume

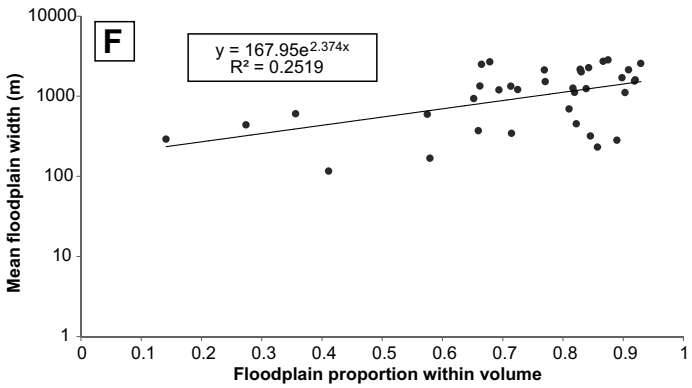
F
y = 167.95e^2.374x
R² = 0.2519
Mean floodplain width (m)
Floodplain proportion within volume

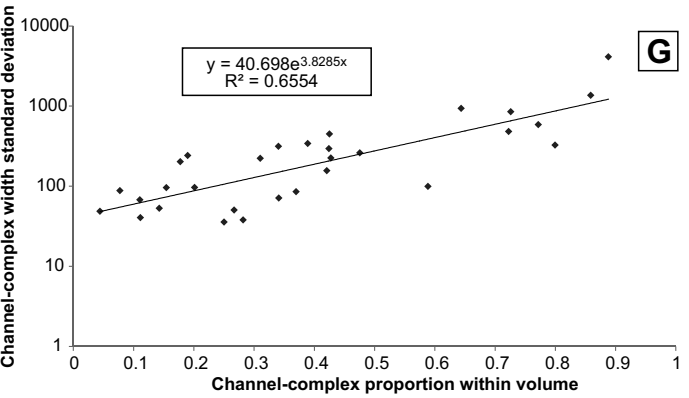
G
y = 40.698e^3.8285x
R² = 0.6554
Channel-complex width standard deviation
Channel-complex proportion within volume

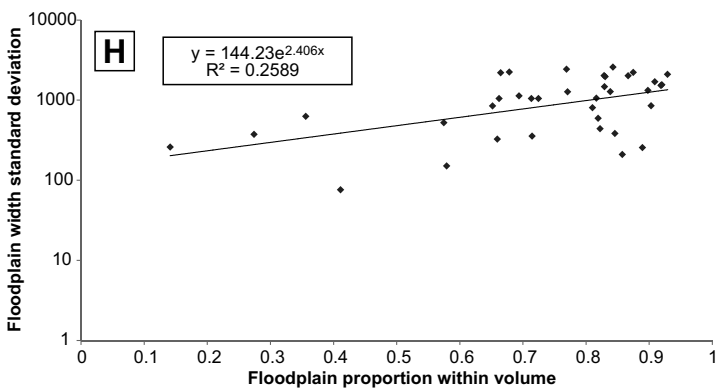
H
y = 144.23e^2.406x
R² = 0.2589
Floodplain width standard deviation
Floodplain proportion within volume

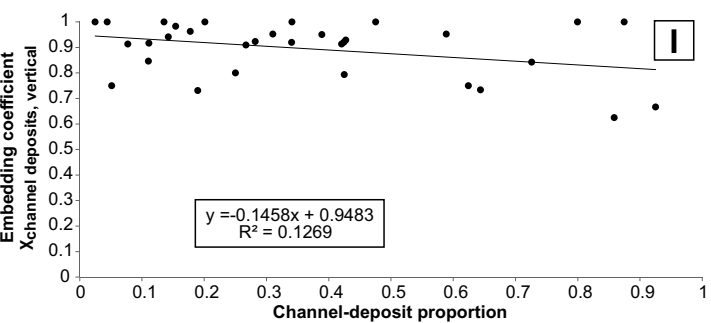
I
y =-0.1458x + 0.9483
R² = 0.1269
Embedding coefficient
Xchannel deposits, vertical
Channel-deposit proportion

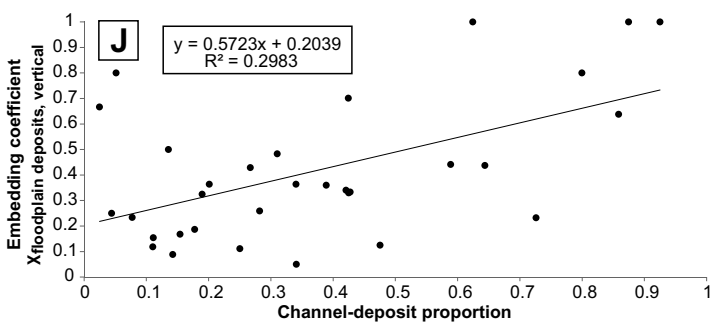
J
y = 0.5723x + 0.2039
R² = 0.2983
Embedding coefficient
Xfloodplain deposits, vertical
Channel-deposit proportion

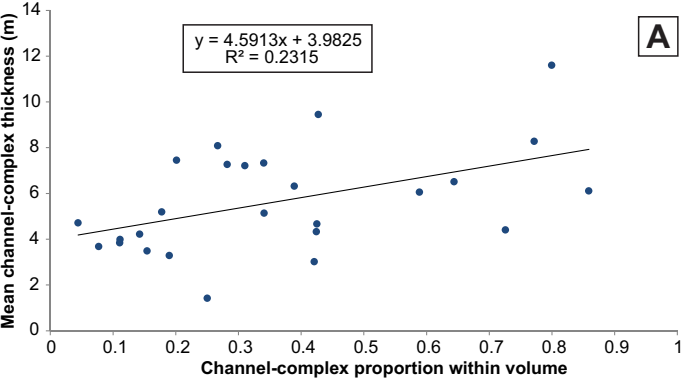
A
y = 4.5913x + 3.9825
R² = 0.2315
Mean channel-complex thickness (m)
Channel-complex proportion within volume

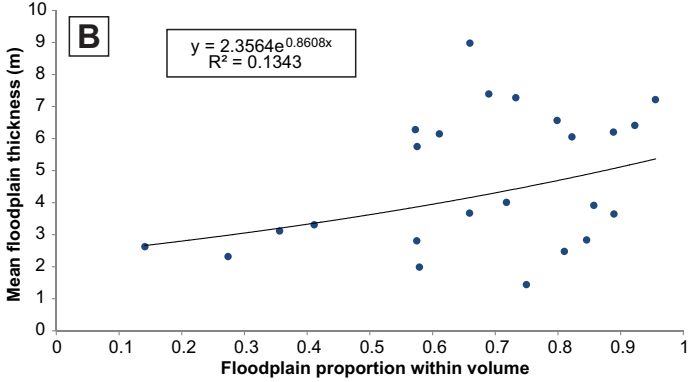
B
y = 2.3564e^0.8608x
R² = 0.1343
Mean floodplain thickness (m)
Floodplain proportion within volume

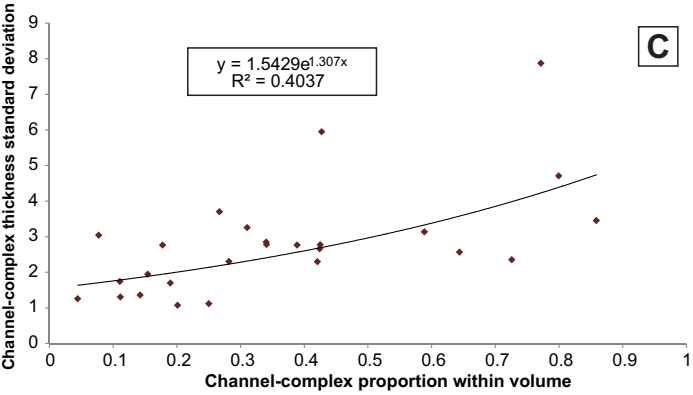
C
y = 1.5429e^1.307x
R² = 0.4037
Channel-complex thickness standard deviation
Channel-complex proportion within volume

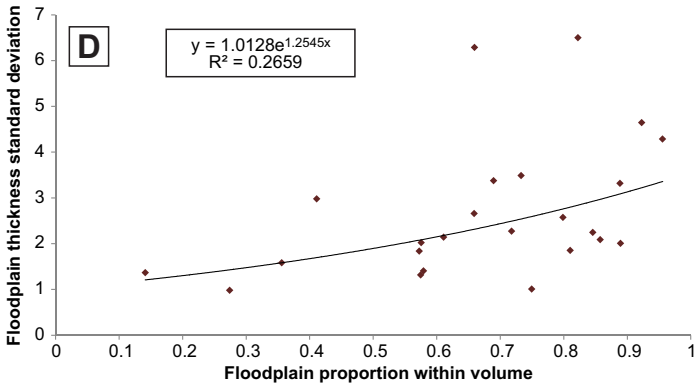
D
y = 1.0128e^1.2545x
R² = 0.2659
Floodplain thickness standard deviation
Floodplain proportion within volume

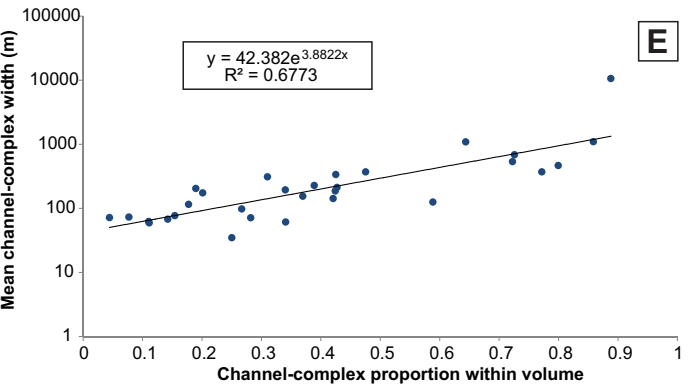
E
y = 42.382e^3.8822x
R² = 0.6773
Mean channel-complex width (m)
Channel-complex proportion within volume

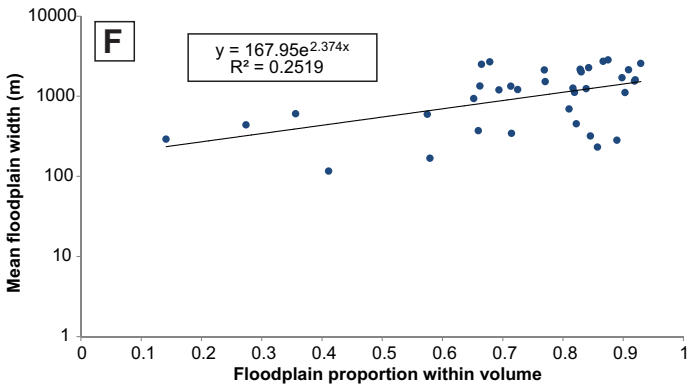
F
y = 167.95e^2.374x
R² = 0.2519
Mean floodplain width (m)
Floodplain proportion within volume

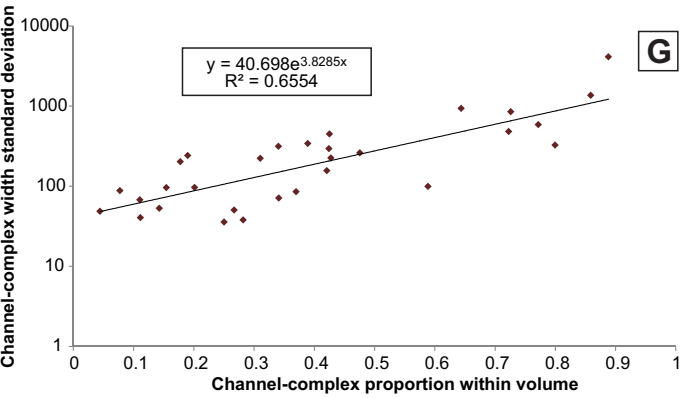
G
y = 40.698e^3.8285x
R² = 0.6554
Channel-complex width standard deviation
Channel-complex proportion within volume

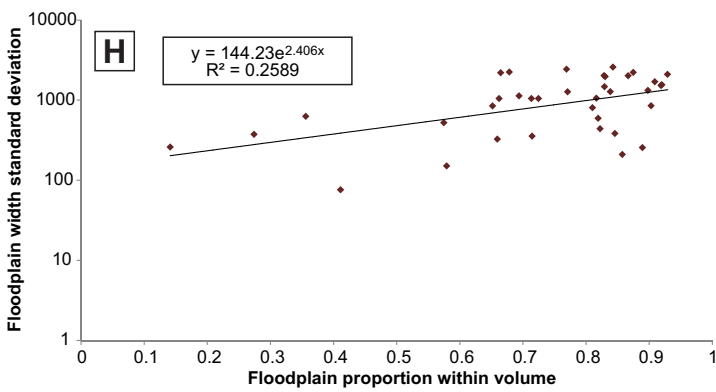
H
y = 144.23e^2.406x
R² = 0.2589
Floodplain width standard deviation
Floodplain proportion within volume

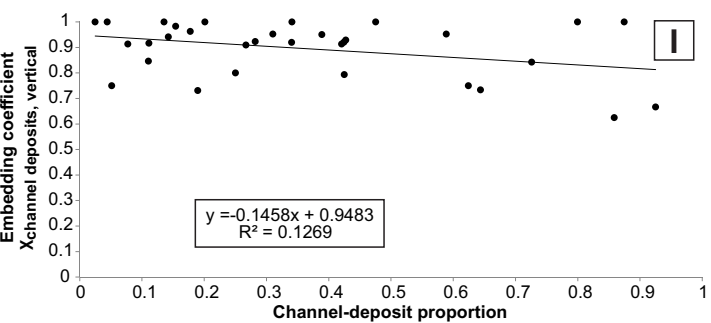
I
y =-0.1458x + 0.9483
R² = 0.1269
Embedding coefficient
Xchannel deposits, vertical
Channel-deposit proportion

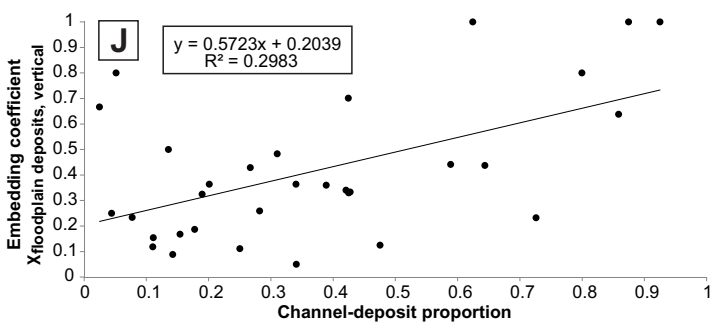
J
y = 0.5723x + 0.2039
R² = 0.2983
Embedding coefficient
Xfloodplain deposits, vertical
Channel-deposit proportion

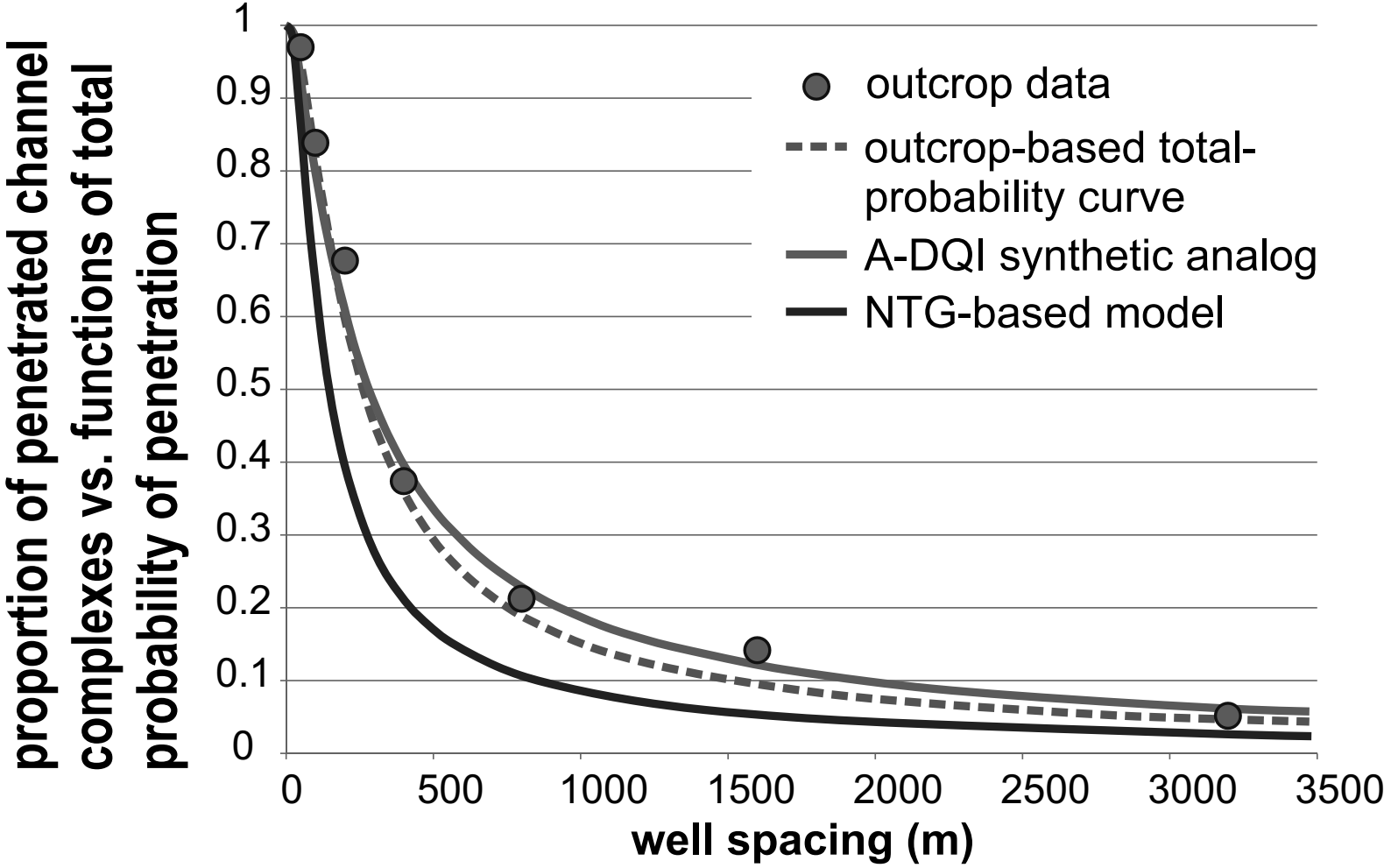
proportion of penetrated channel complexes vs. functions of total probability of penetration
1
0.9
0.8
0.7
0.6
0.5
0.4
0.3
0.2
0.1
0
0
500
1000
1500
2000
2500
3000
3500
well spacing (m)
outcrop data
outcrop-based total-probability curve
A-DQI synthetic analog
NTG-based model

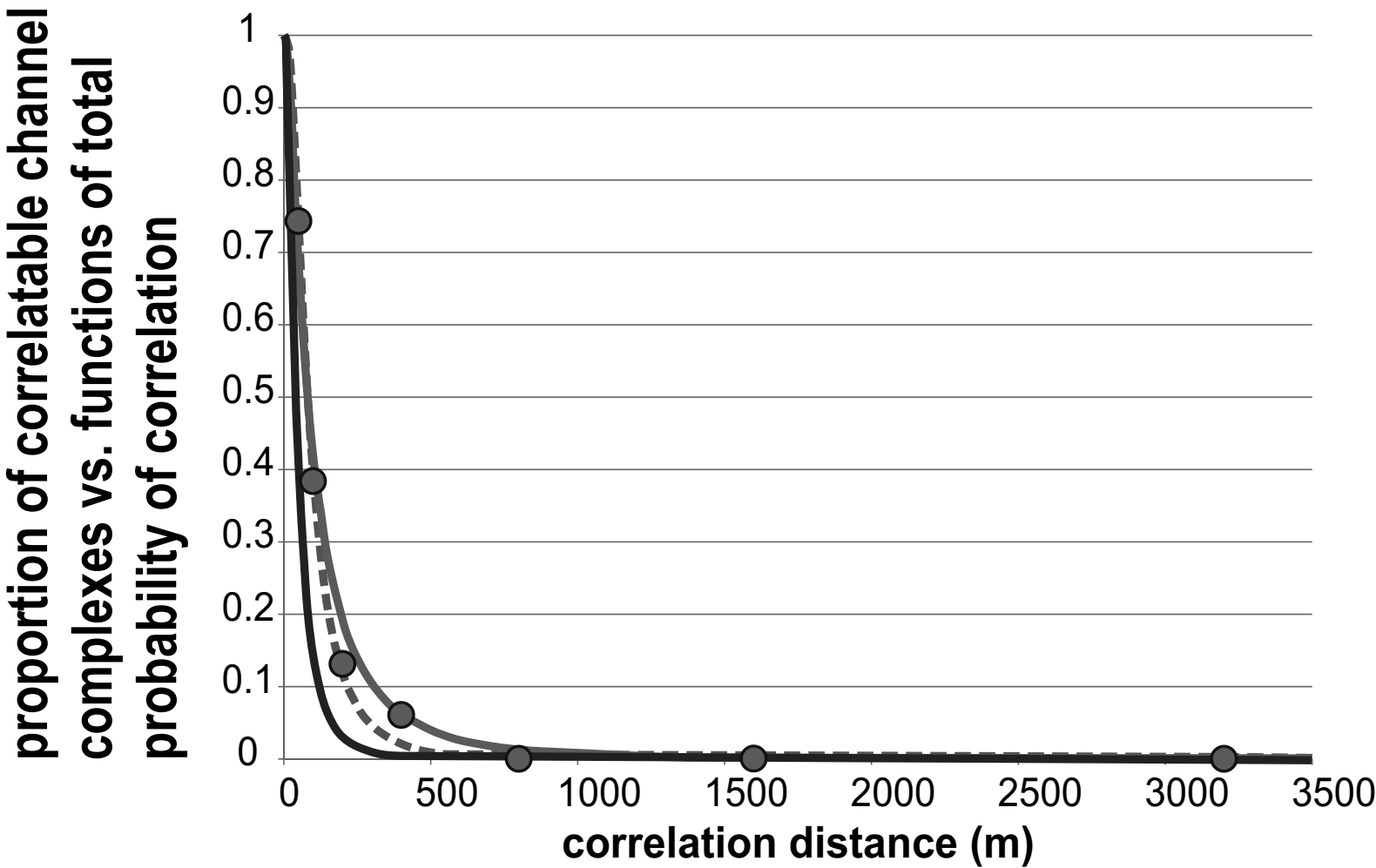
proportion of correlatable channel complexes vs. functions of total probability of correlation
1
0.9
0.8
0.7
0.6
0.5
0.4
0.3
0.2
0.1
0
0
500
1000
1500
2000
2500
3000
3500
correlation distance (m)

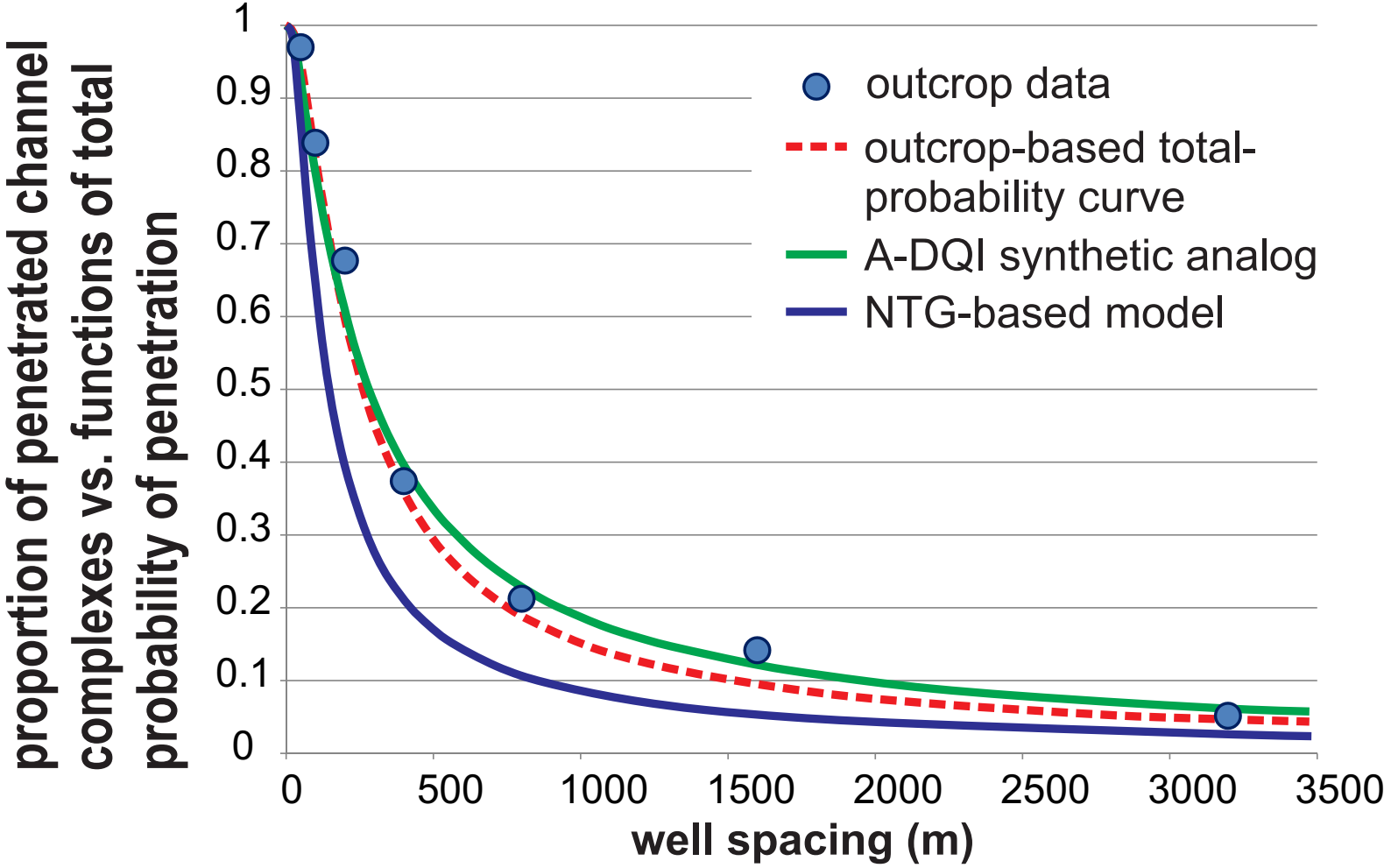
proportion of penetrated channel complexes vs. functions of total probability of penetration
1
0.9
0.8
0.7
0.6
0.5
0.4
0.3
0.2
0.1
0
outcrop data
outcrop-based total-probability curve
A-DQI synthetic analog
NTG-based model
0
500
1000
1500
2000
2500
3000
3500
well spacing (m)

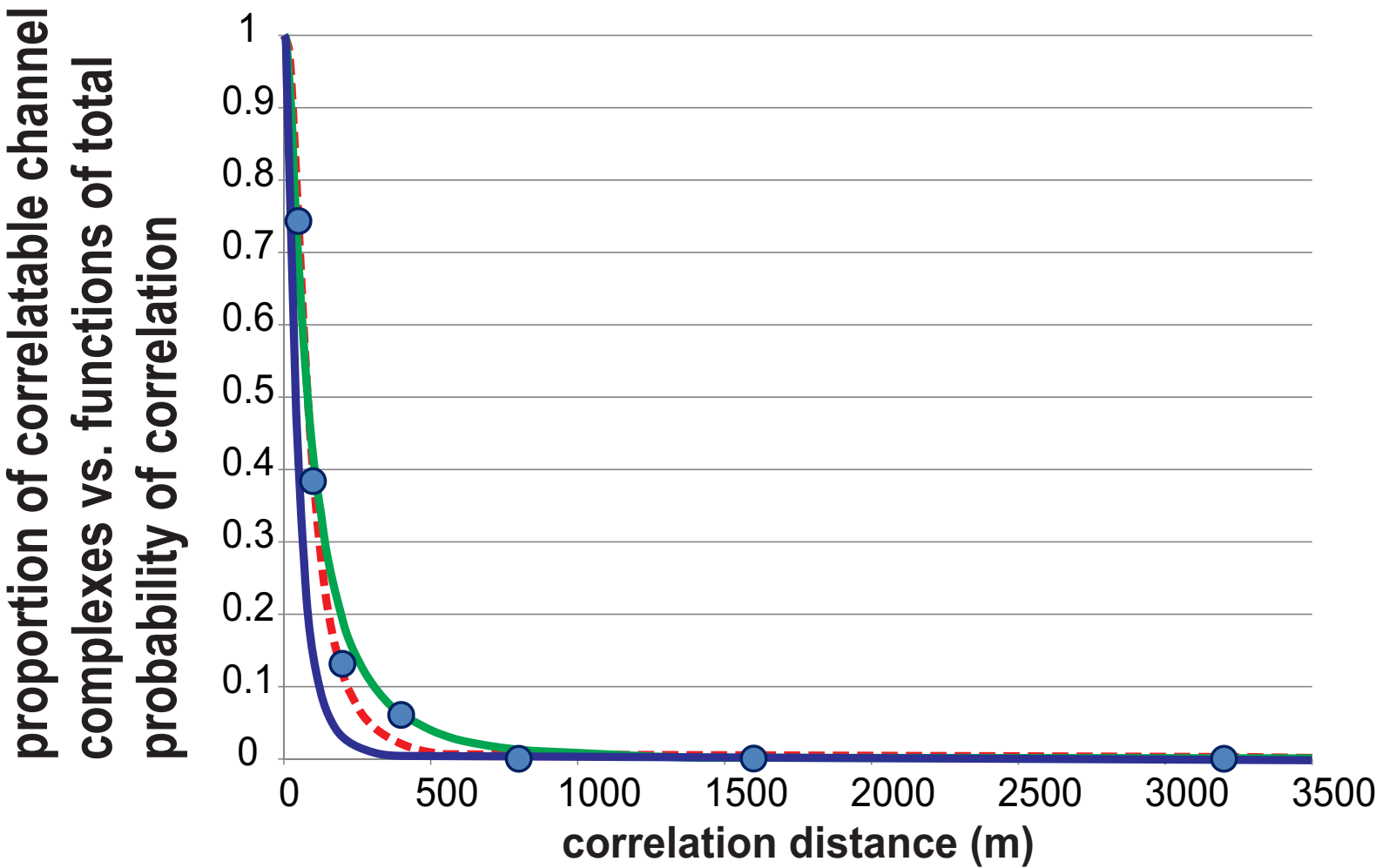
proportion of correlatable channel complexes vs. functions of total probability of correlation
1
0.9
0.8
0.7
0.6
0.5
0.4
0.3
0.2
0.1
0
0
500
1000
1500
2000
2500
3000
3500
correlation distance (m)

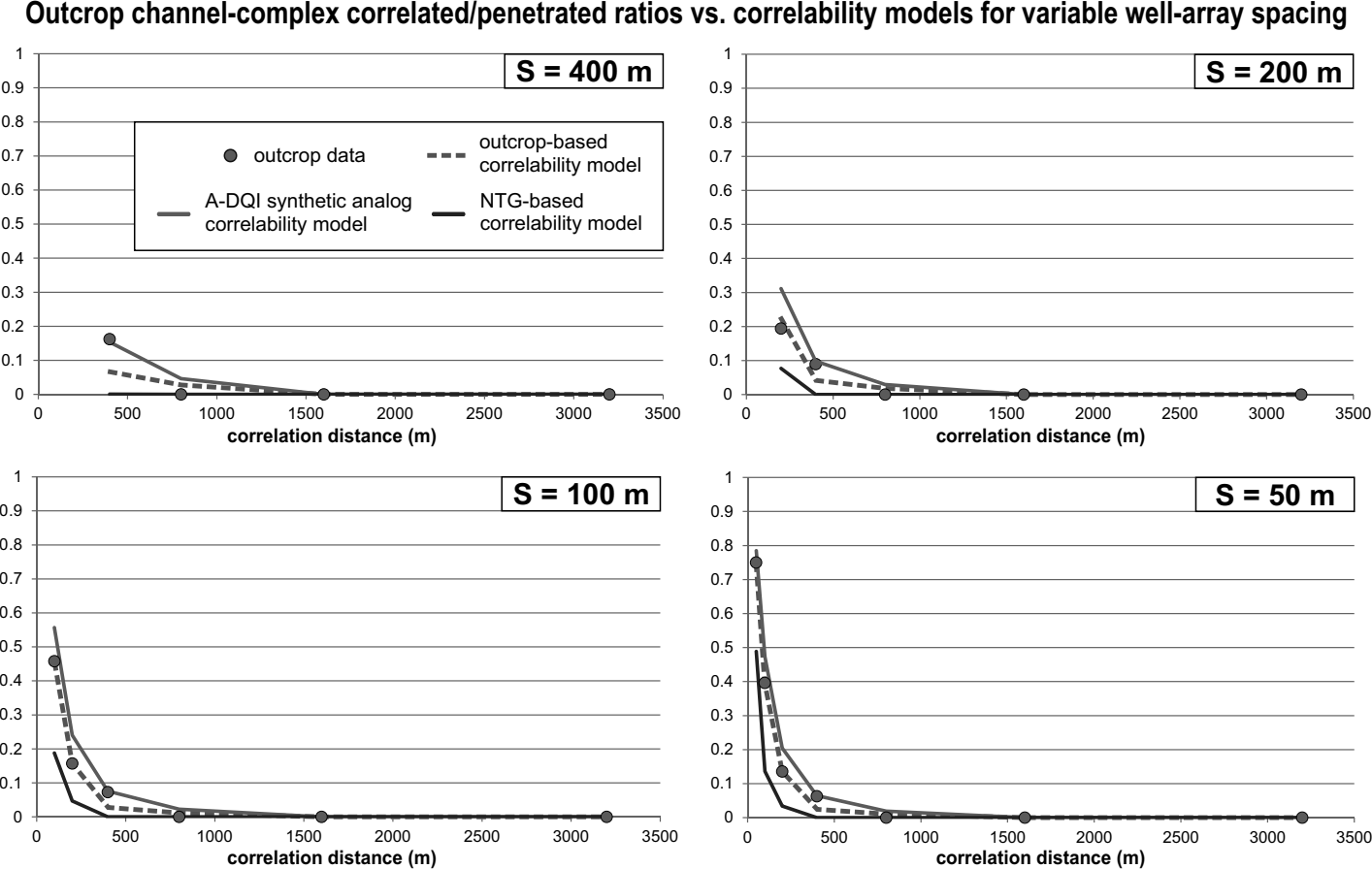
Outcrop channel-complex correlated/penetrated ratios vs. correlability models for variable well-array spacing
S = 400 m
S = 200 m
S = 100 m
S = 50 m
outcrop data
outcrop-based correlability model
A-DQI synthetic analog correlability model
NTG-based correlability model
correlation distance (m)
0
0.1
0.2
0.3
0.4
0.5
0.6
0.7
0.8
0.9
1
500
1000
1500
2000
2500
3000
3500

Outcrop channel-complex correlated/penetrated ratios vs. correlability models for variable well-array spacing

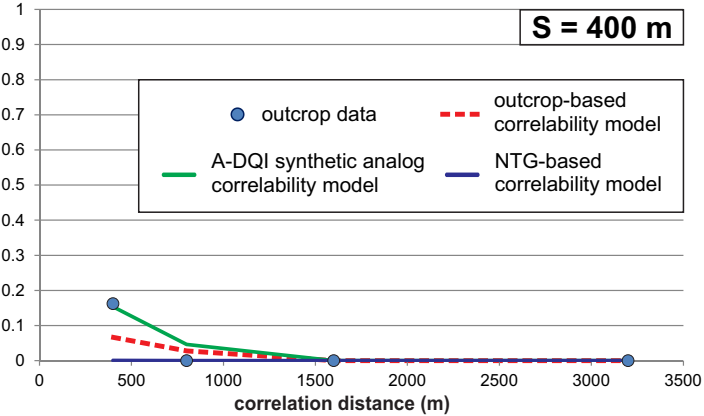

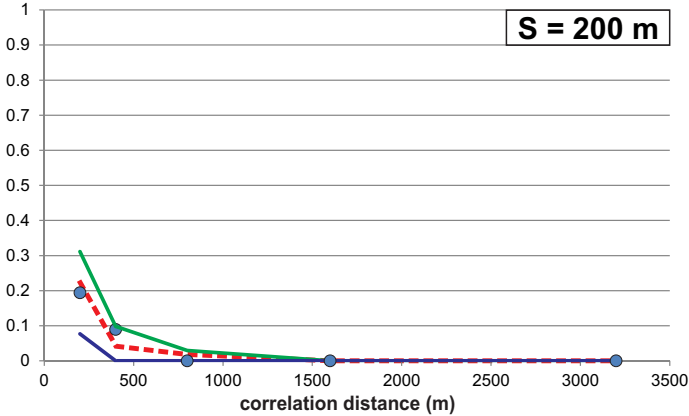

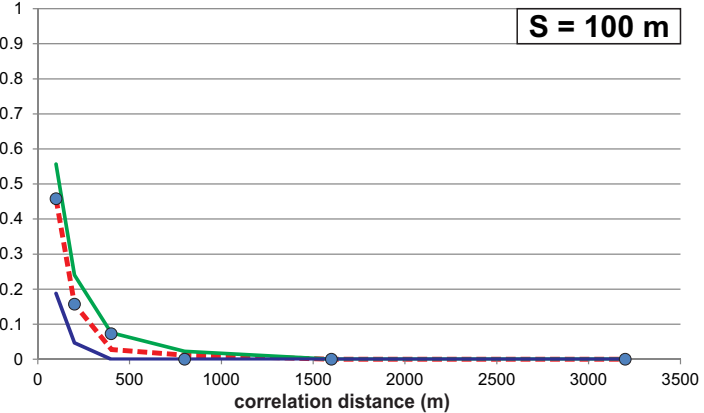

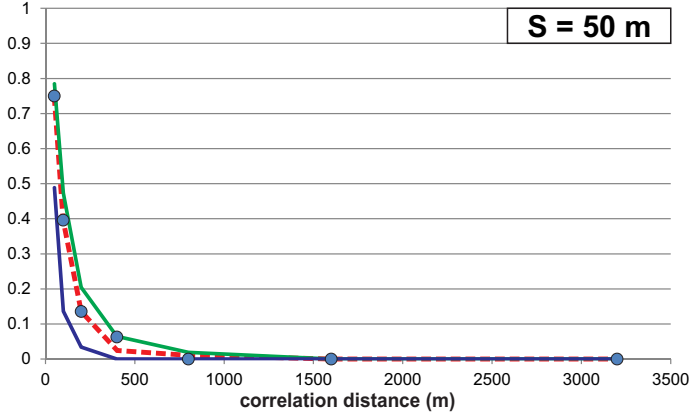

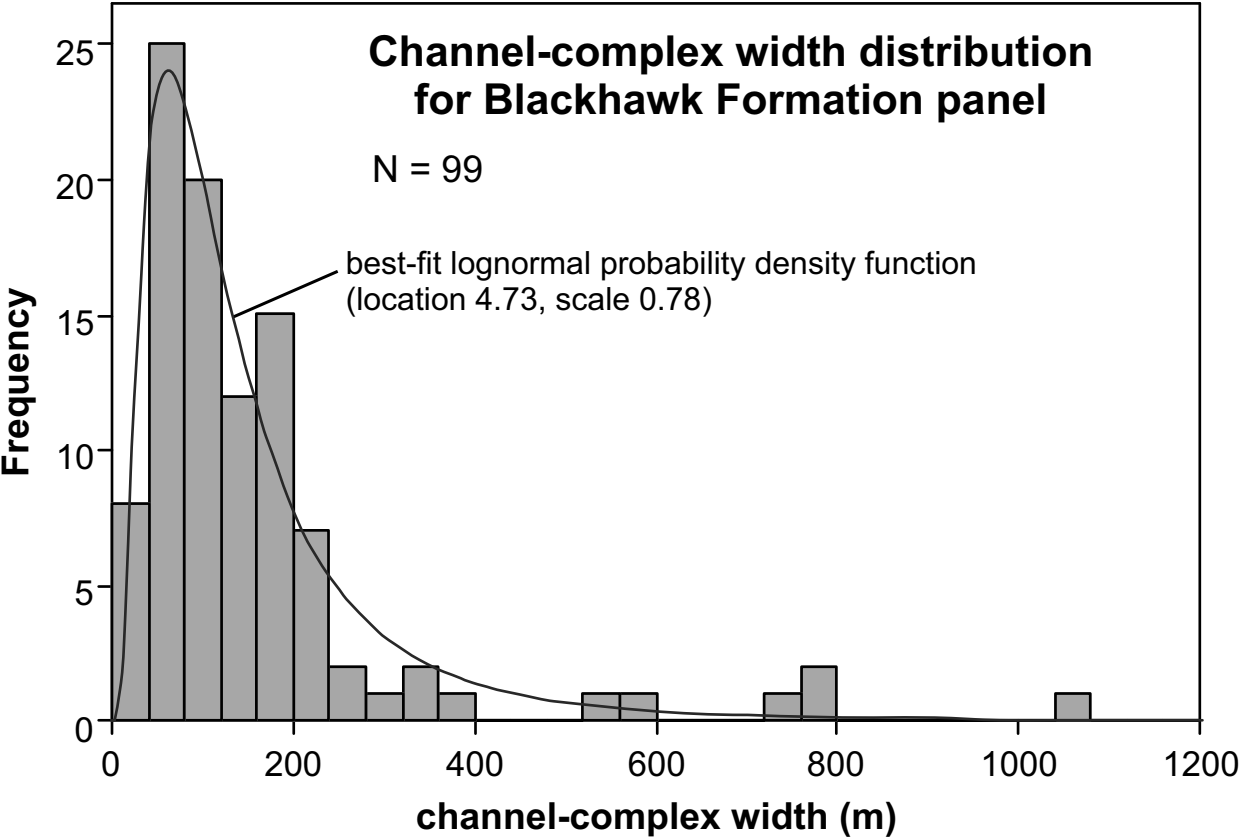
Channel-complex width distribution
for Blackhawk Formation panel
N = 99
best-fit lognormal probability density function
(location 4.73, scale 0.78)
Frequency
0
5
10
15
20
25
0
200
400
600
800
1000
1200
channel-complex width (m)

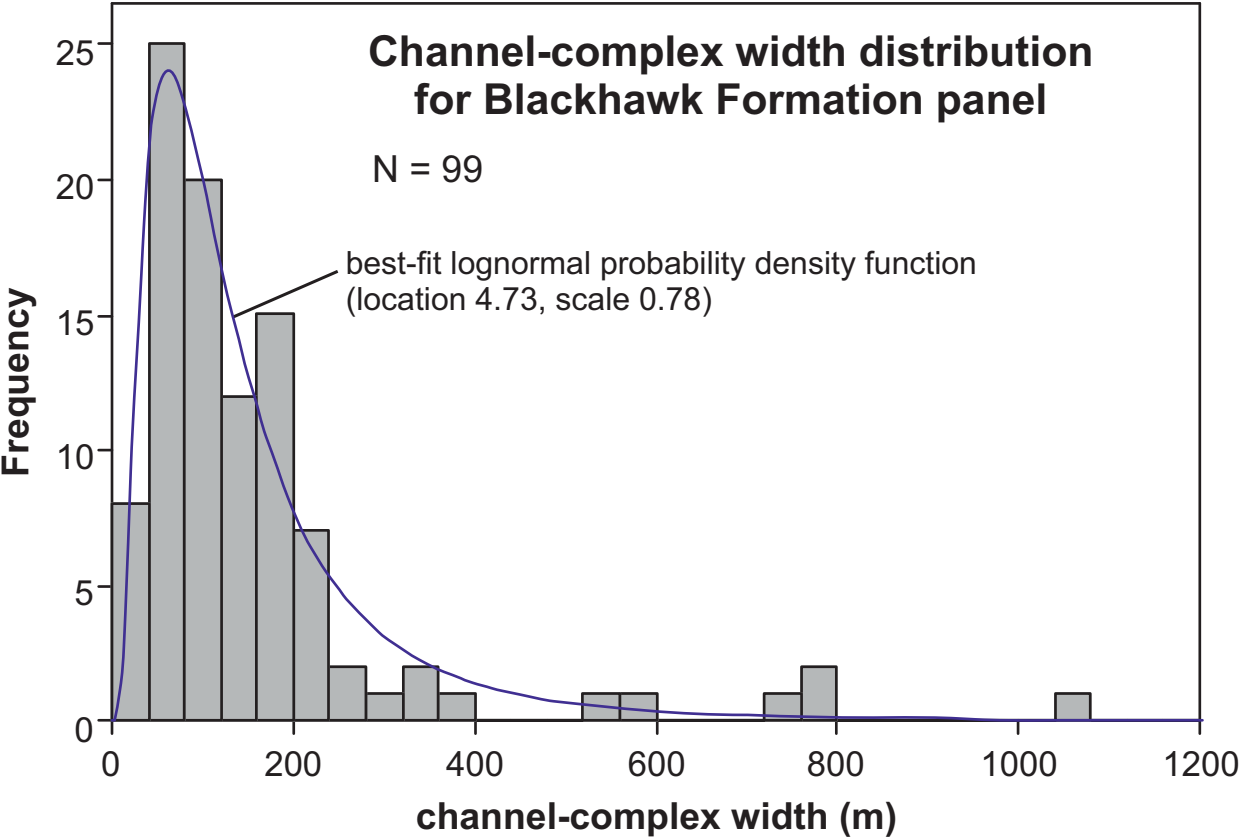
Channel-complex width distribution
for Blackhawk Formation panel
N = 99
best-fit lognormal probability density function
(location 4.73, scale 0.78)
Frequency
0
5
10
15
20
25
0
200
400
600
800
1000
1200
channel-complex width (m)

Outcrop vs. model cumulative-discrepancy values for variable well-array spacing

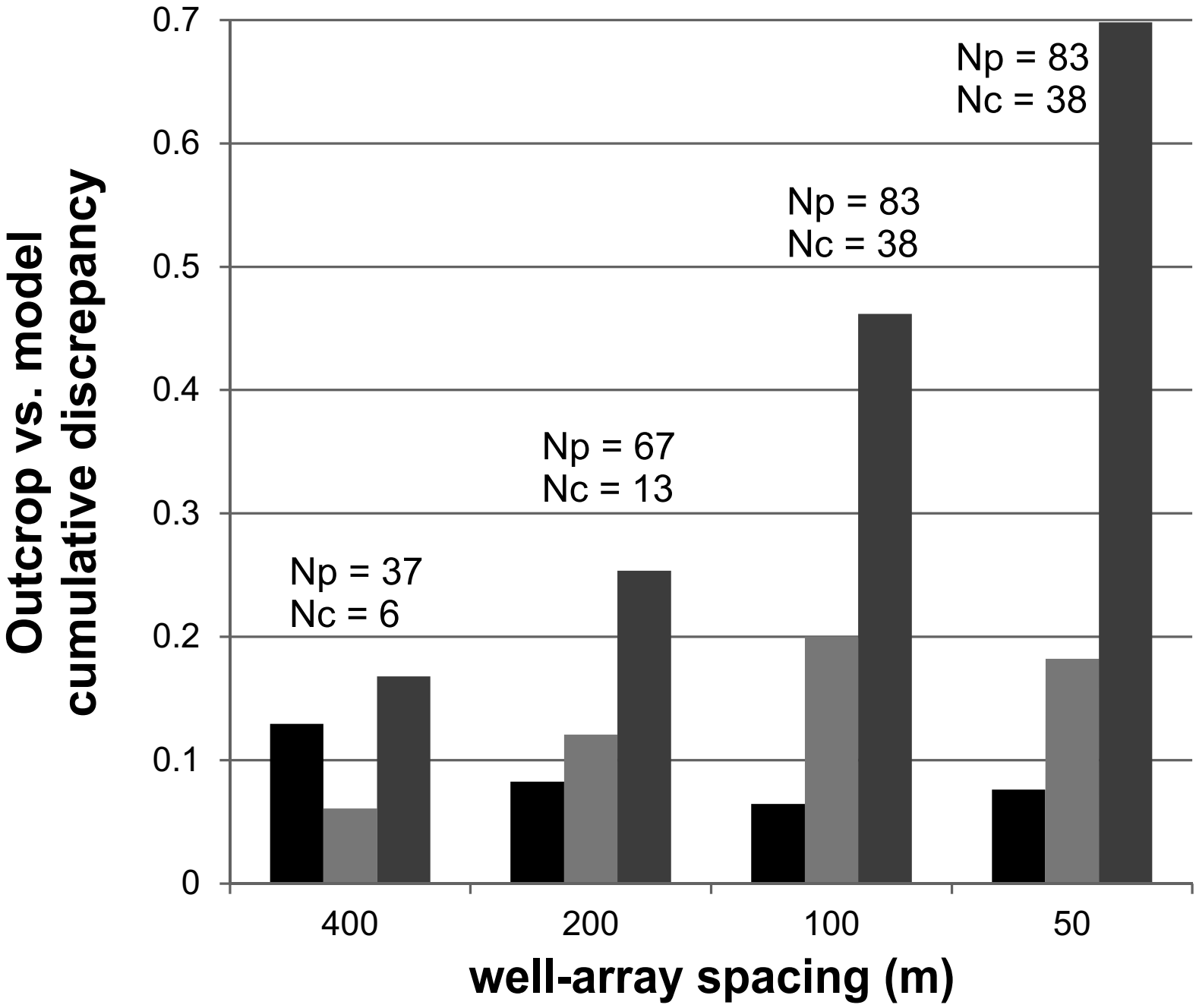

Outcrop vs. model cumulative-discrepancy values for variable well-array spacing

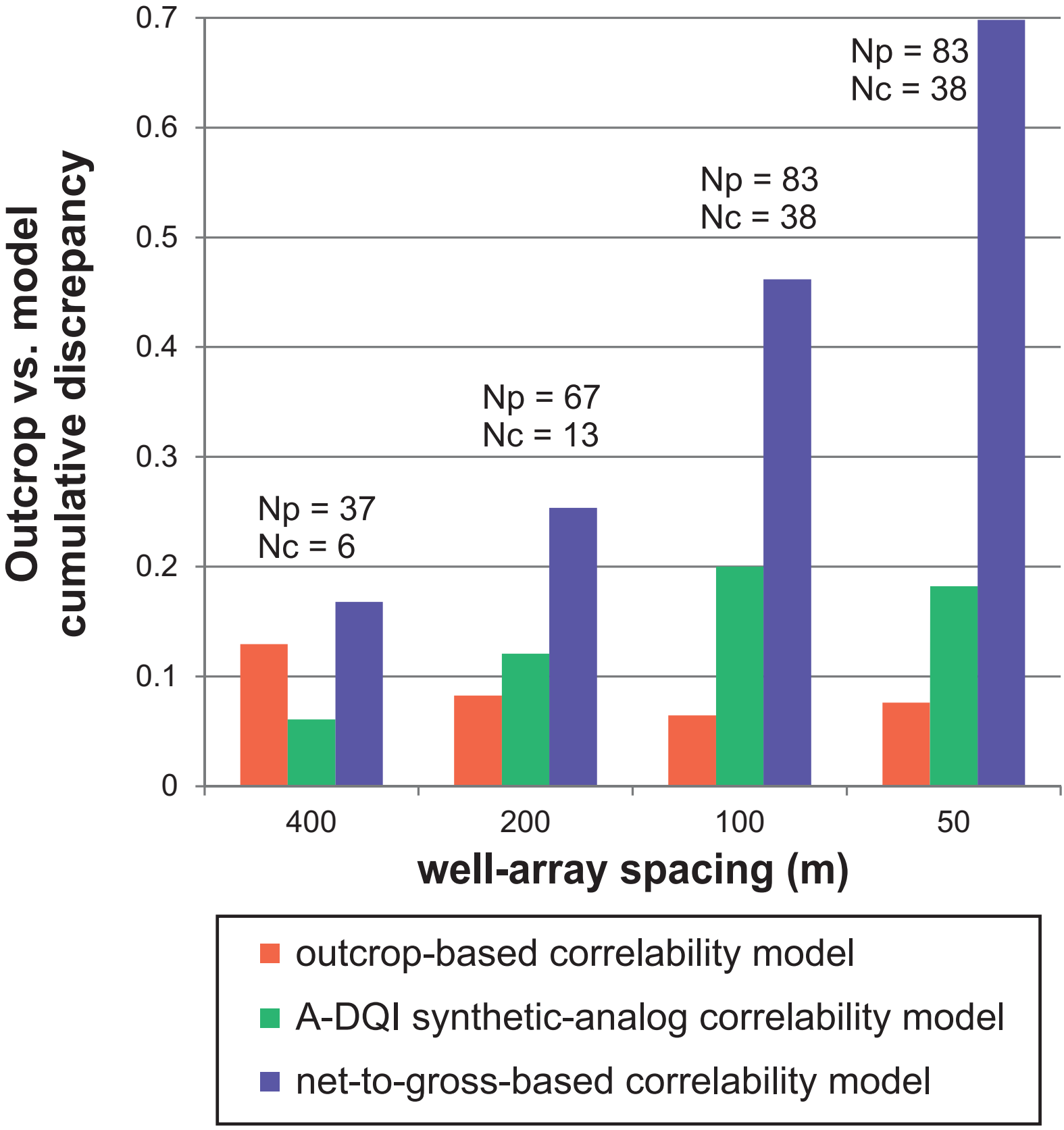

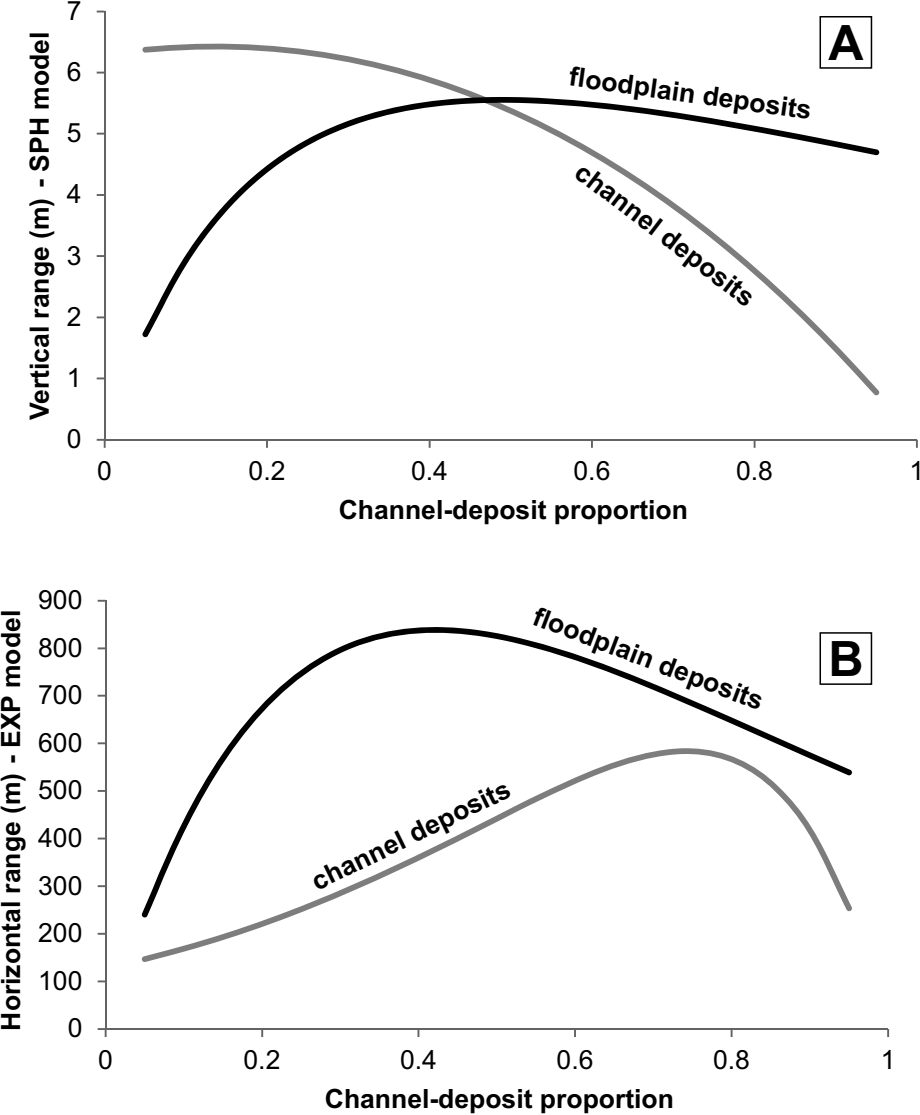
A
floodplain deposits
channel deposits
Vertical range (m) - SPH model
0
1
2
3
4
5
6
7
0
0.2
0.4
0.6
0.8
1
Channel-deposit proportion
B
floodplain deposits
channel deposits
Horizontal range (m) - EXP model
0
100
200
300
400
500
600
700
800
900
0
0.2
0.4
0.6
0.8
1
Channel-deposit proportion

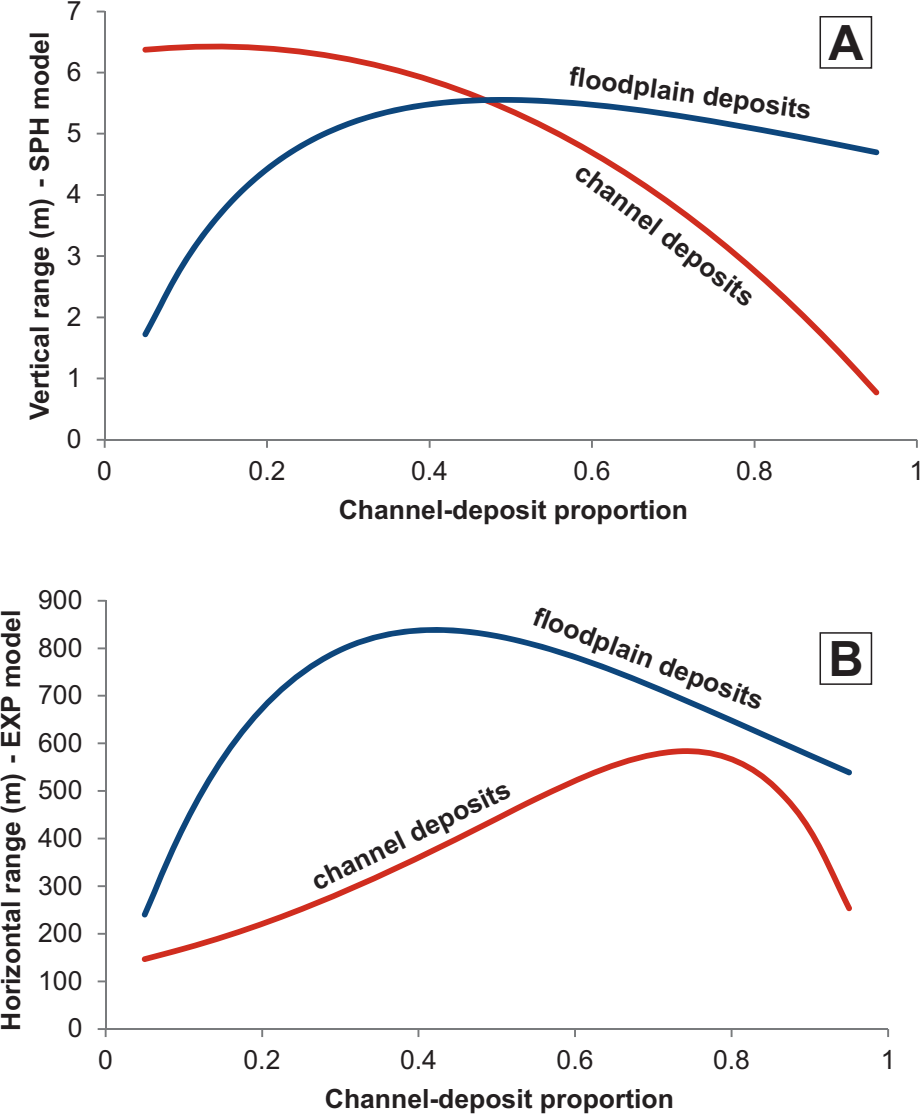
A
floodplain deposits
channel deposits
Vertical range (m) - SPH model
0
1
2
3
4
5
6
7
0
0.2
0.4
0.6
0.8
1
Channel-deposit proportion
B
floodplain deposits
channel deposits
Horizontal range (m) - EXP model
0
100
200
300
400
500
600
700
800
900
0
0.2
0.4
0.6
0.8
1
Channel-deposit proportion

grid size: X = 4000 m, Y = 200 m (vertical exaggeration x5) floodplain deposits channel deposits

Comparison of channel-complex geometries between SISIM simulation based on empirical constraints for 10% net:gross and FAKTS case studies with 8.5% to 11.5% net:gross

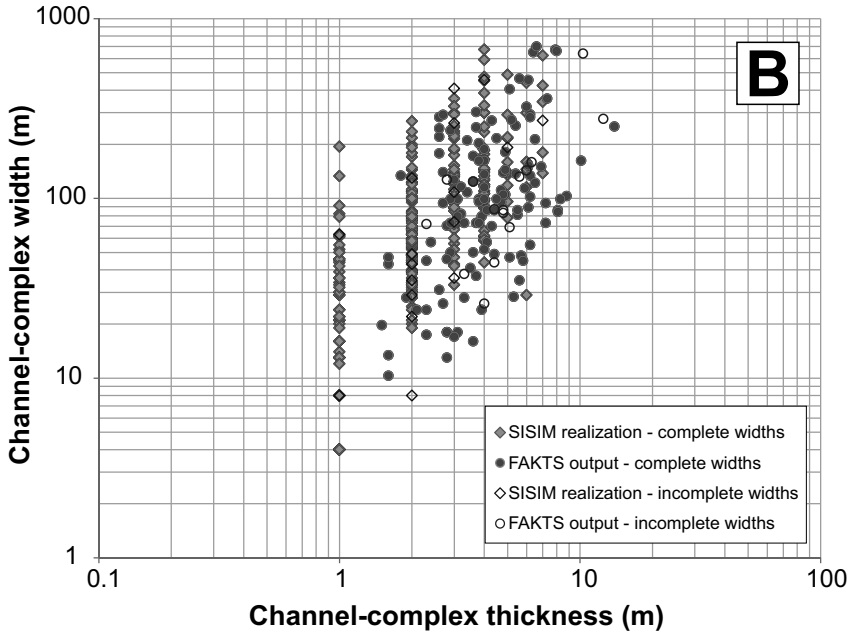

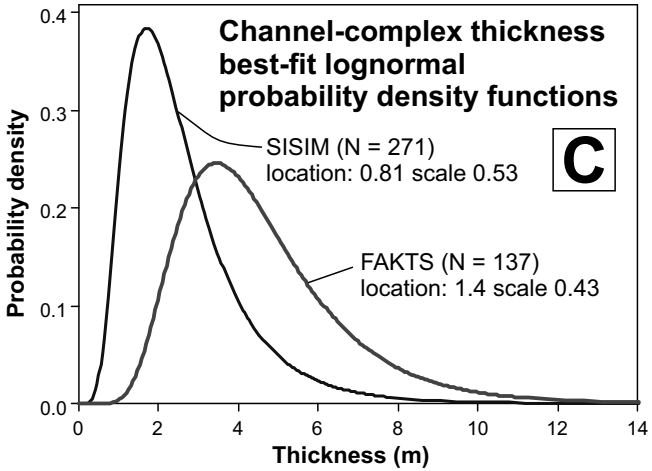

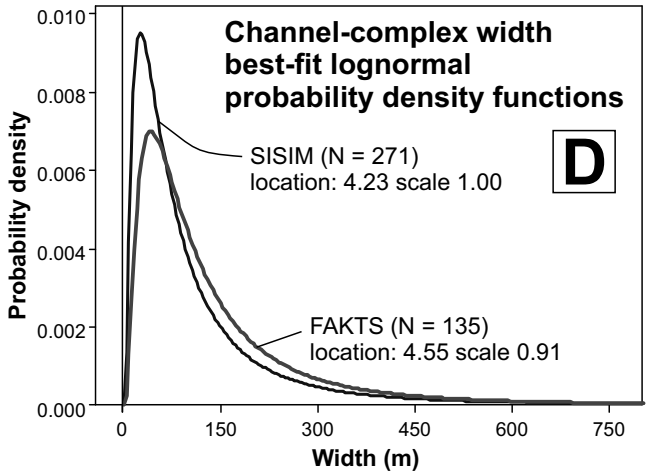

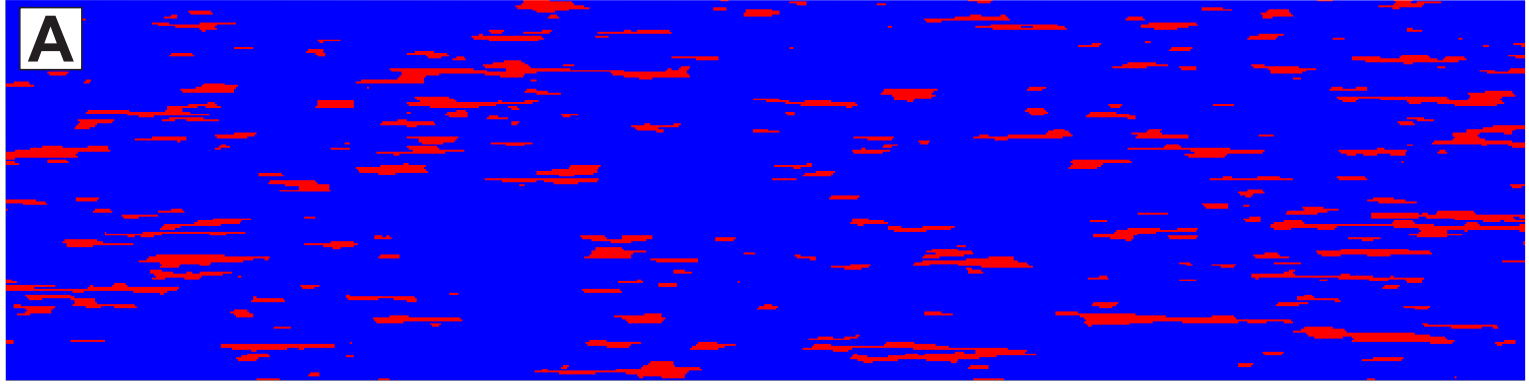

grid size: X = 4000 m, Y = 200 m (vertical exaggeration x5)

floodplain deposits

channel deposits

Comparison of channel-complex geometries between SISIM simulation based on empirical constraints for 10% net:gross and FAKTS case studies with 8.5% to 11.5% net:gross

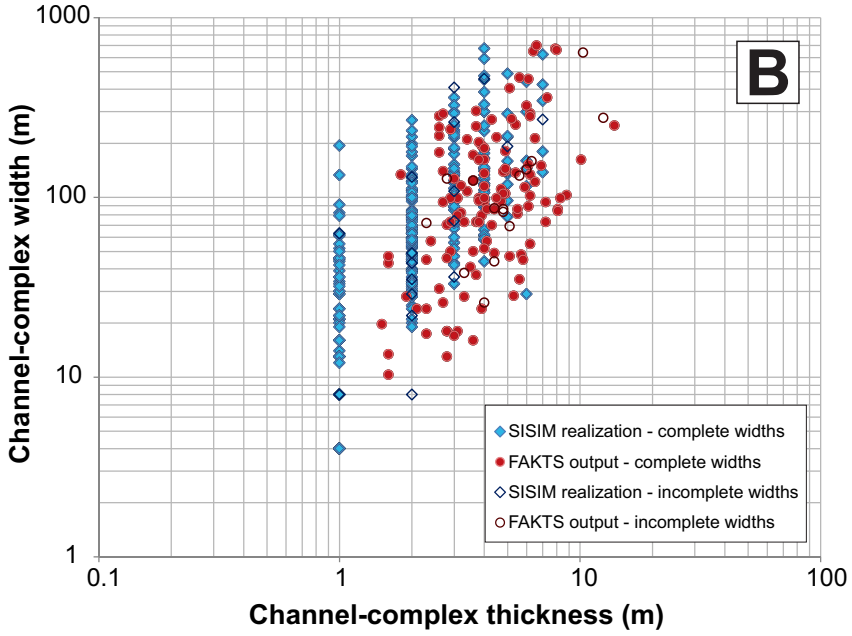

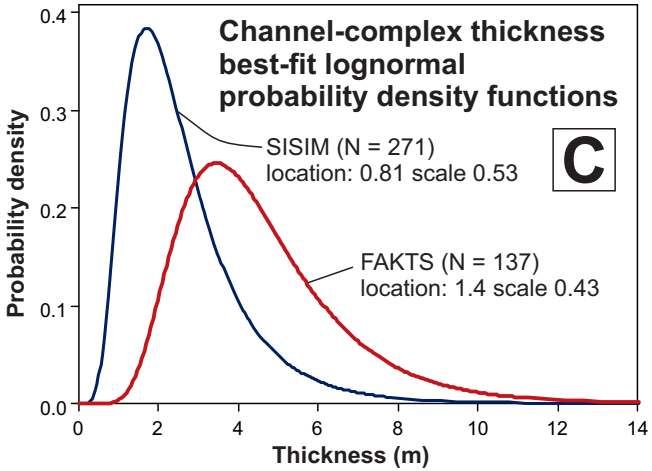

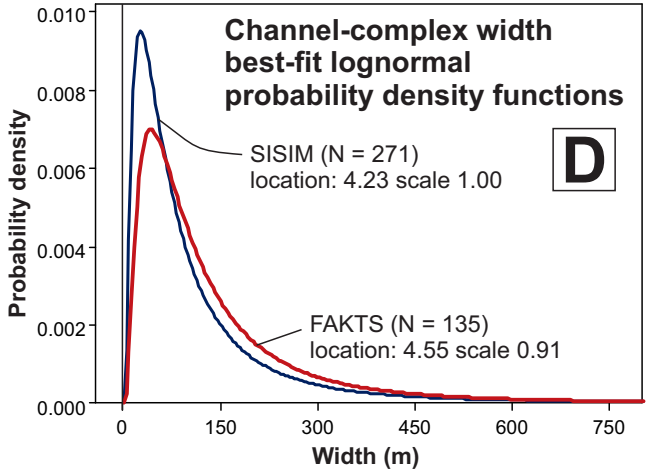

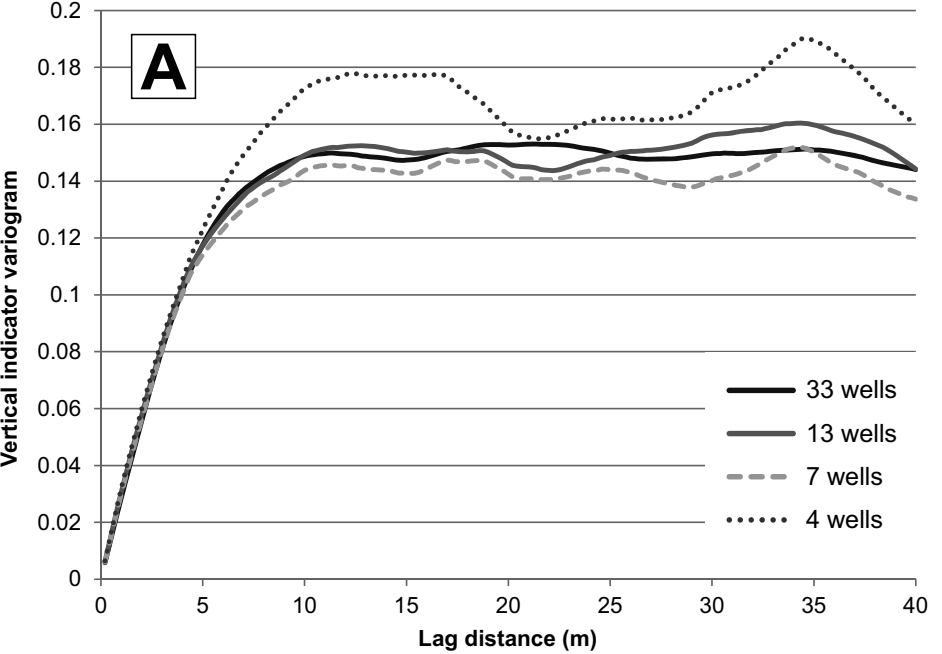
A
Vertical indicator variogram
0.2
0.18
0.16
0.14
0.12
0.1
0.08
0.06
0.04
0.02
0
0
5
10
15
20
25
30
35
40
Lag distance (m)
33 wells
13 wells
7 wells
4 wells

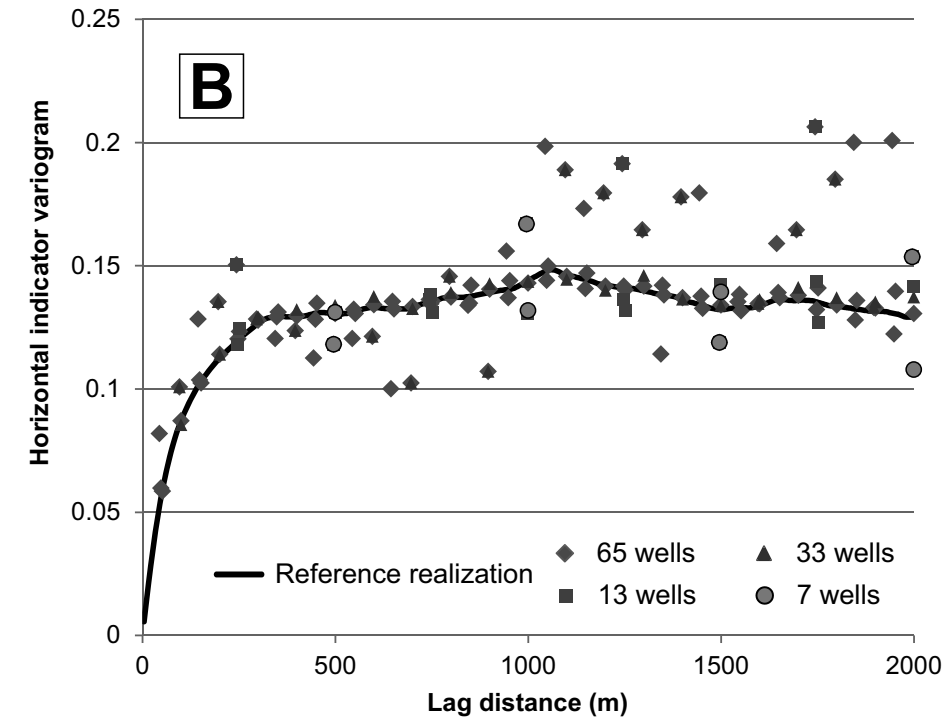
B
Horizontal indicator variogram
0.25
0.2
0.15
0.1
0.05
0
0
500
1000
1500
2000
Lag distance (m)
Reference realization
65 wells
33 wells
13 wells
7 wells

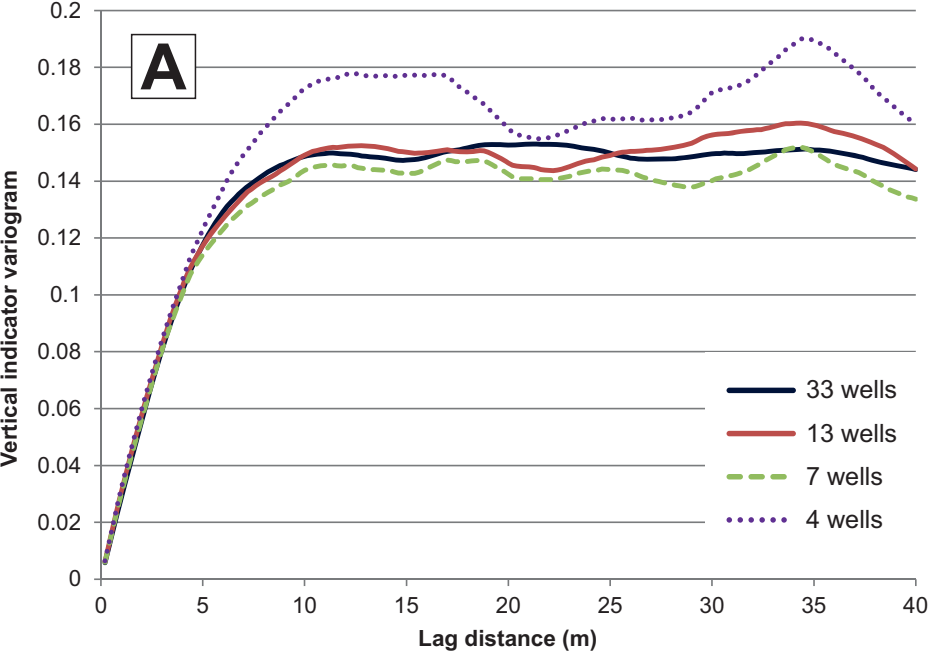
A
Vertical indicator variogram
0.2
0.18
0.16
0.14
0.12
0.1
0.08
0.06
0.04
0.02
0
0
5
10
15
20
25
30
35
40
Lag distance (m)
33 wells
13 wells
7 wells
4 wells

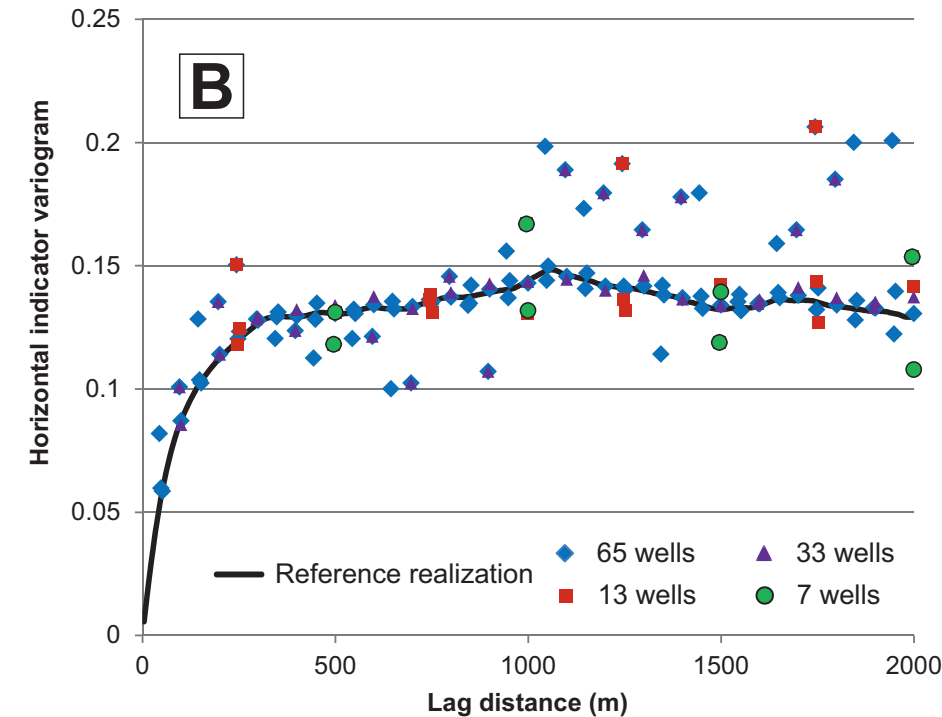
B
Horizontal indicator variogram
0.25
0.2
0.15
0.1
0.05
0
0
500
1000
1500
2000
Lag distance (m)
Reference realization
65 wells
33 wells
13 wells
7 wells

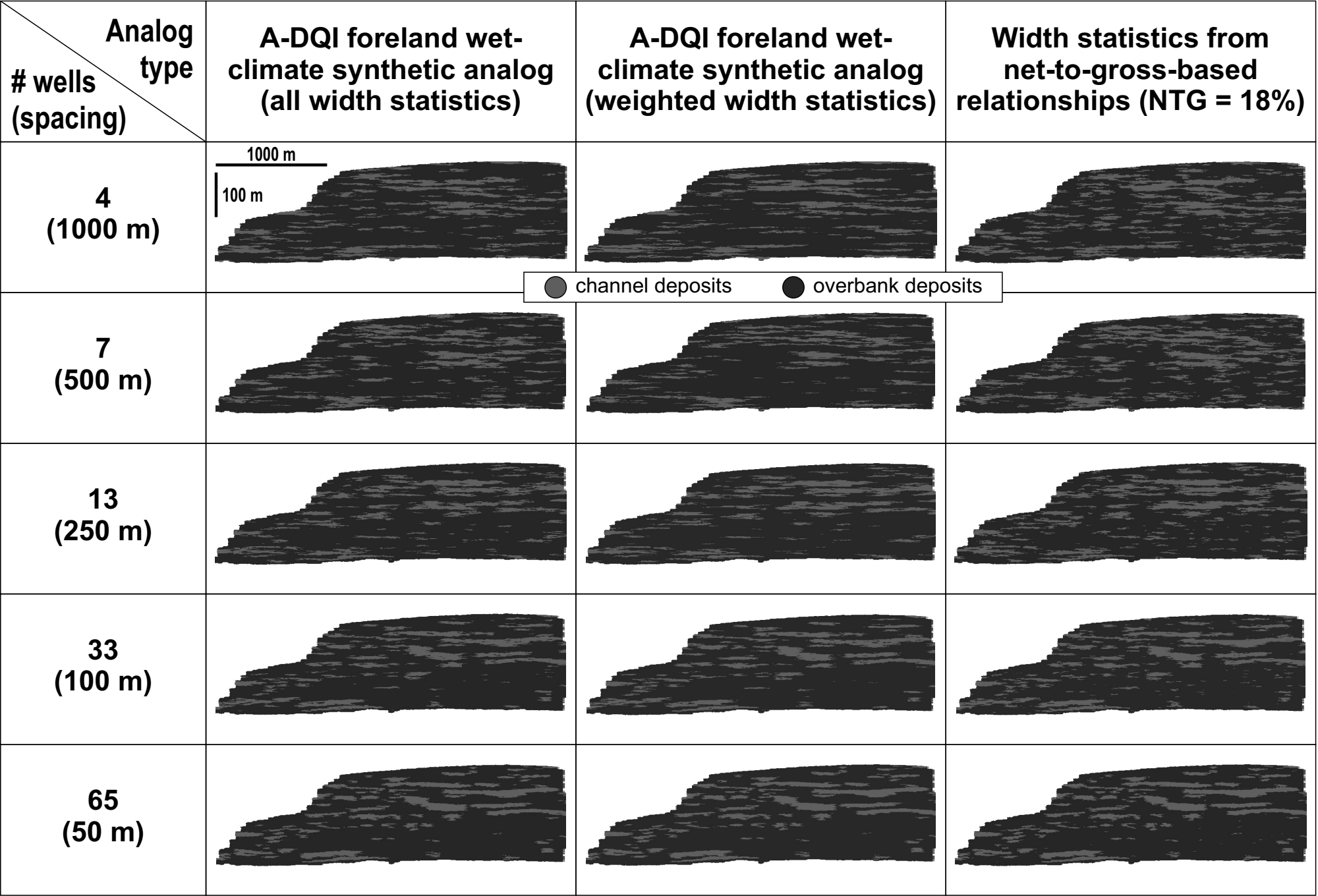
Analog type
wells (spacing)
A-DQI foreland wet-climate synthetic analog (all width statistics)
A-DQI foreland wet-climate synthetic analog (weighted width statistics)
Width statistics from net-to-gross-based relationships (NTG = 18%)
1000 m
100 m
channel deposits
overbank deposits
4 (1000 m)
7 (500 m)
13 (250 m)
33 (100 m)
65 (50 m)

# wells (spacing) \ Analog type	A-DQI foreland wet-climate synthetic analog (all width statistics)	A-DQI foreland wet-climate synthetic analog (weighted width statistics)	Width statistics from net-to-gross-based relationships (NTG = 18%)
4 (1000 m)	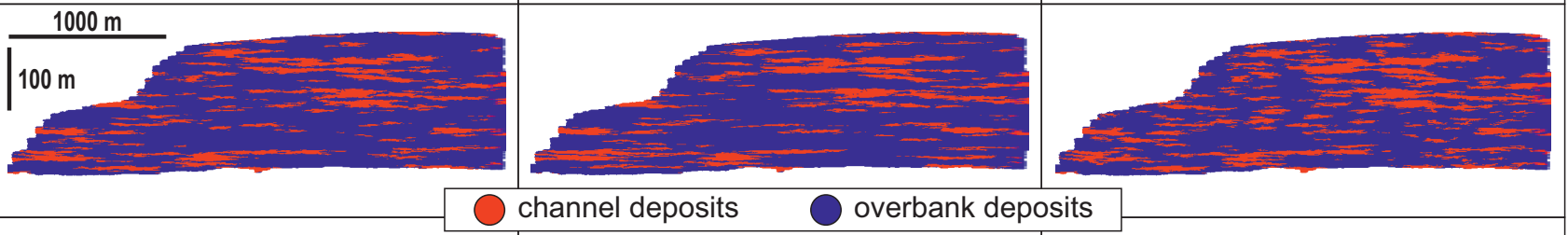		
7 (500 m)	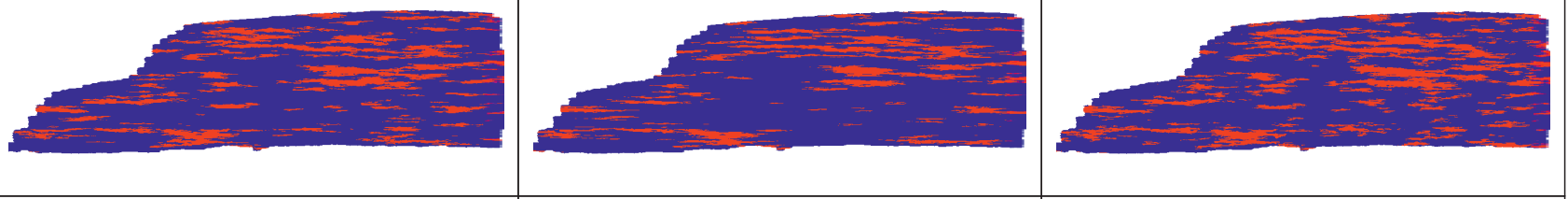		
13 (250 m)	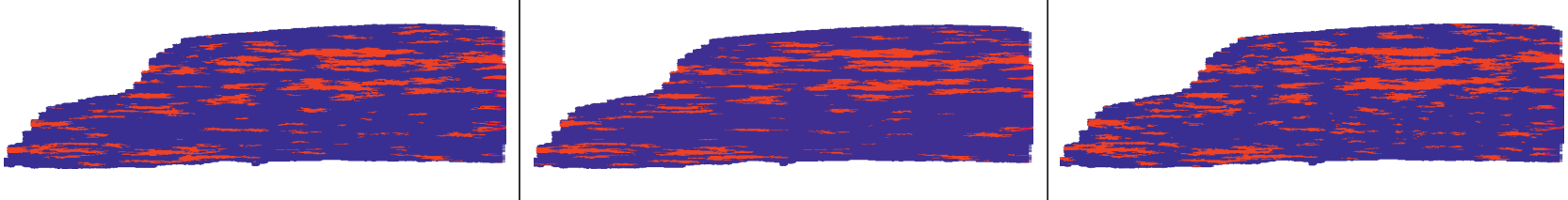		
33 (100 m)	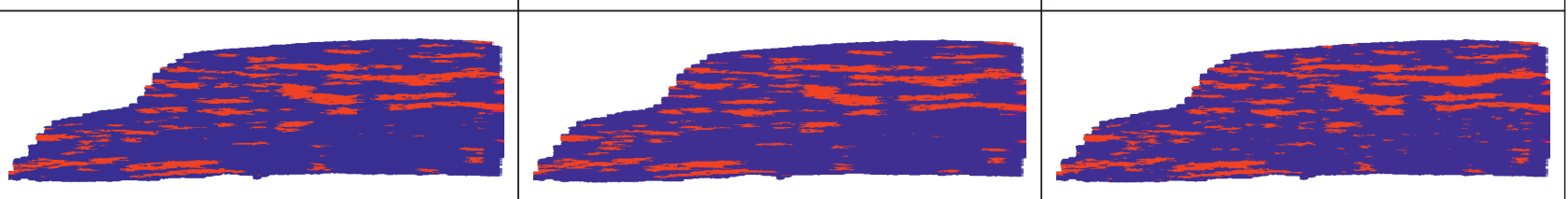		
65 (50 m)	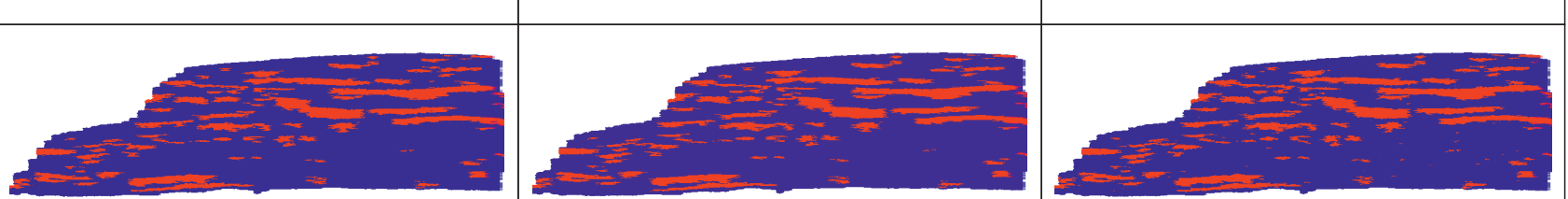		

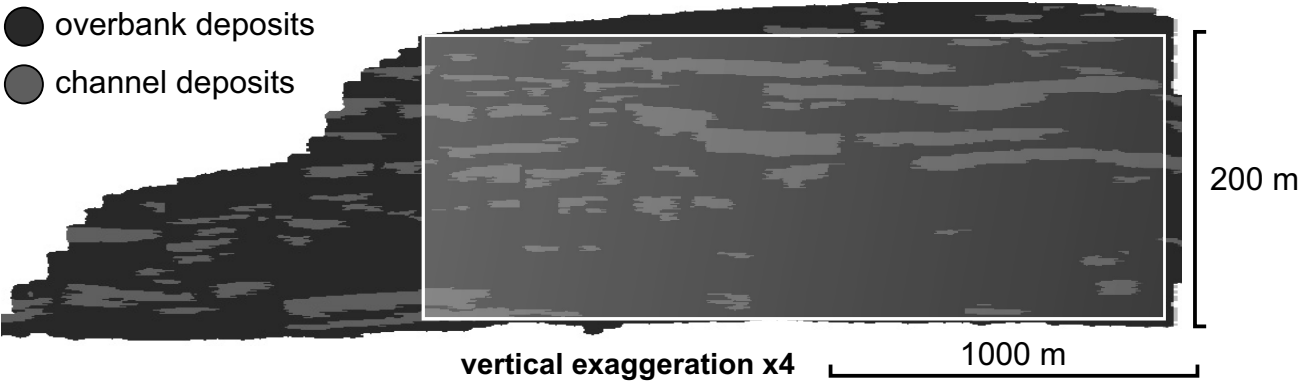
overbank deposits
channel deposits
200 m
vertical exaggeration x4
1000 m

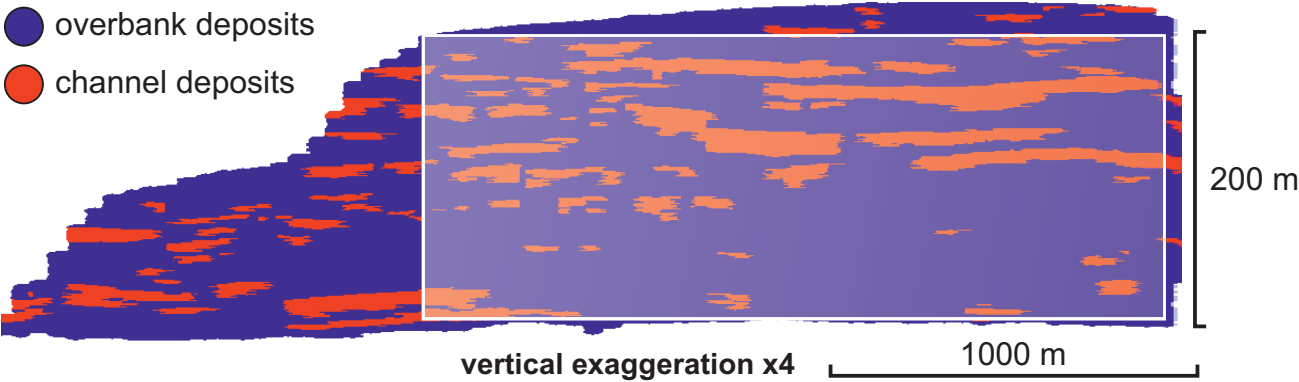
overbank deposits
channel deposits
200 m
vertical exaggeration x4
1000 m

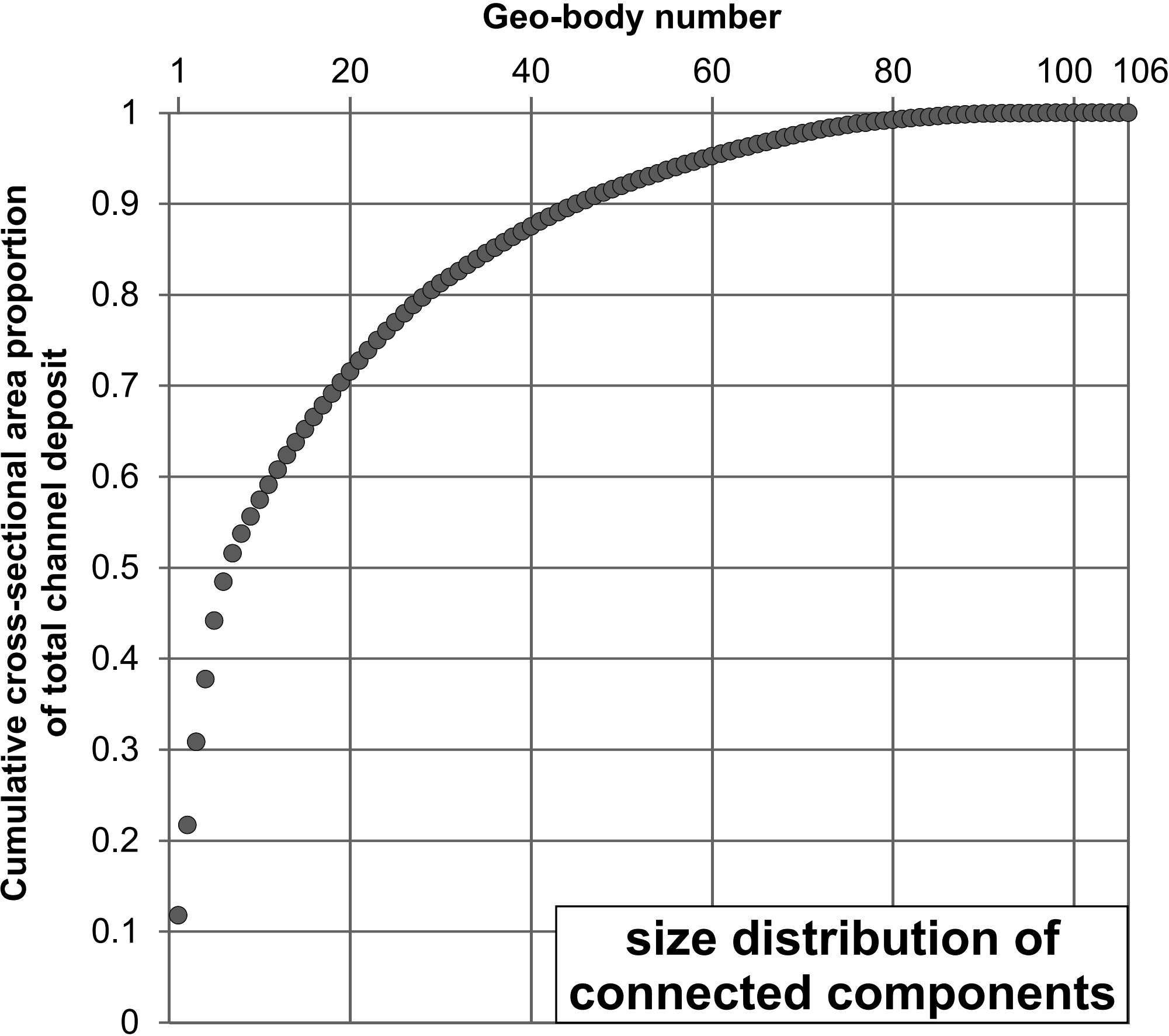
Geo-body number
1
20
40
60
80
100
106
Cumulative cross-sectional area proportion of total channel deposit
1
0.9
0.8
0.7
0.6
0.5
0.4
0.3
0.2
0.1
0
size distribution of connected components

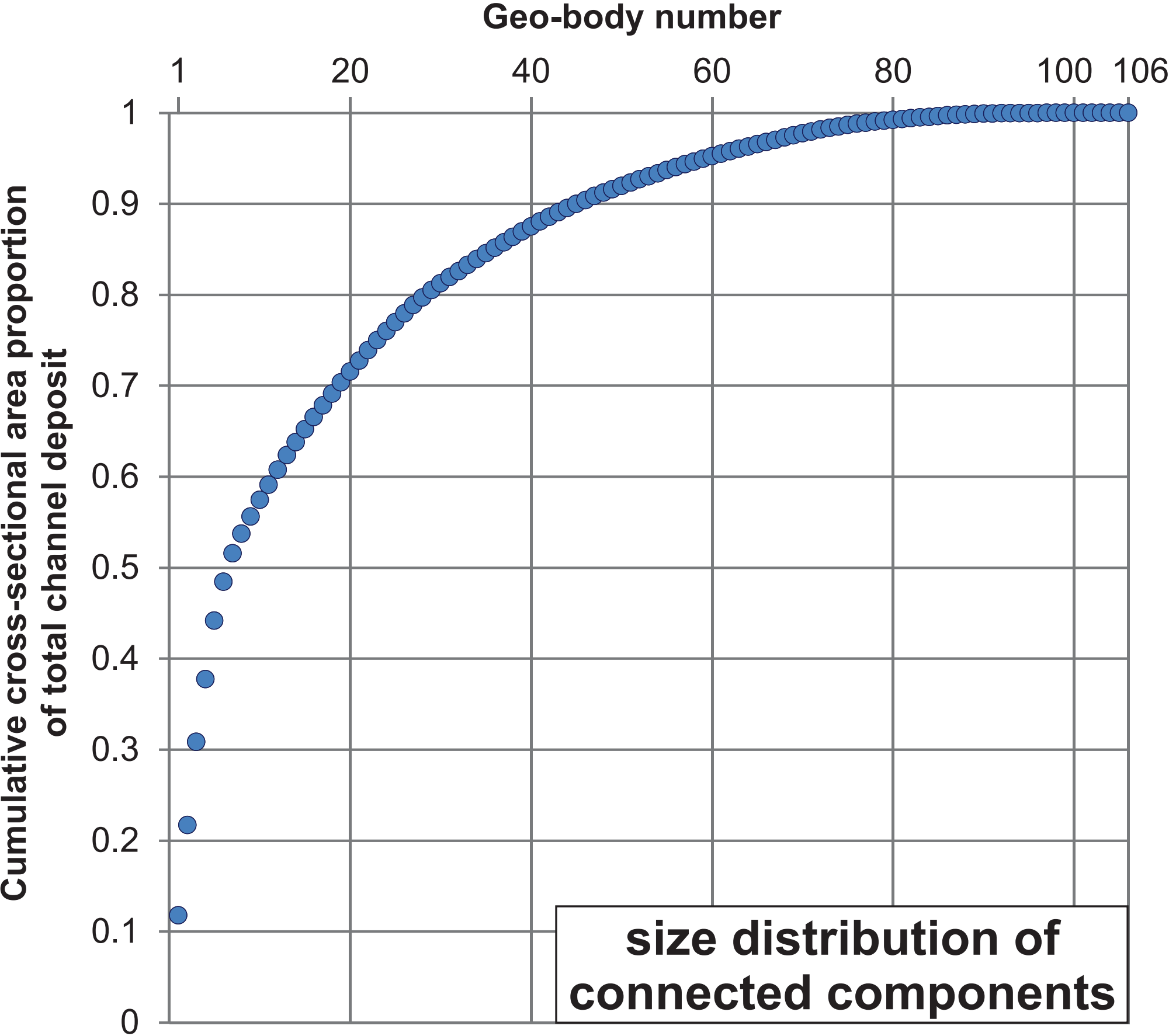
Geo-body number
1
20
40
60
80
100
106
Cumulative cross-sectional area proportion of total channel deposit
1
0.9
0.8
0.7
0.6
0.5
0.4
0.3
0.2
0.1
0
size distribution of connected components

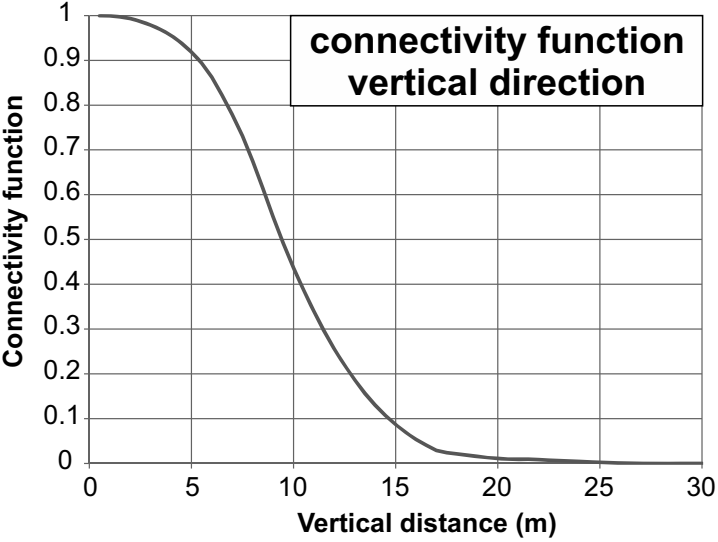
connectivity function
vertical direction
Connectivity function
1
0.9
0.8
0.7
0.6
0.5
0.4
0.3
0.2
0.1
0
0
5
10
15
20
25
30
Vertical distance (m)

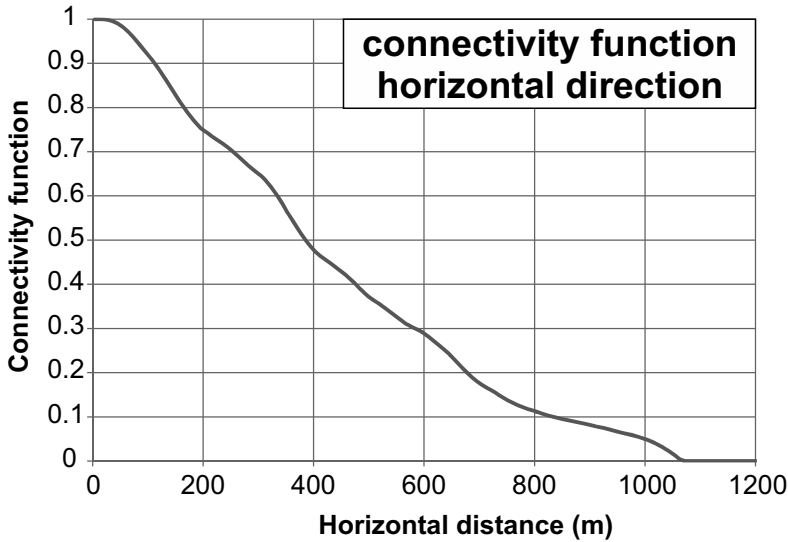
connectivity function
horizontal direction
Connectivity function
1
0.9
0.8
0.7
0.6
0.5
0.4
0.3
0.2
0.1
0
0
200
400
600
800
1000
1200
Horizontal distance (m)

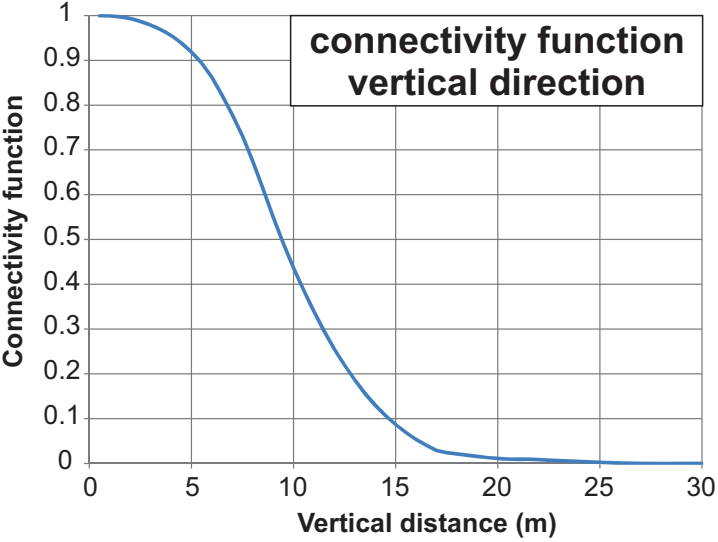
connectivity function
vertical direction
Connectivity function
1
0.9
0.8
0.7
0.6
0.5
0.4
0.3
0.2
0.1
0
0
5
10
15
20
25
30
Vertical distance (m)

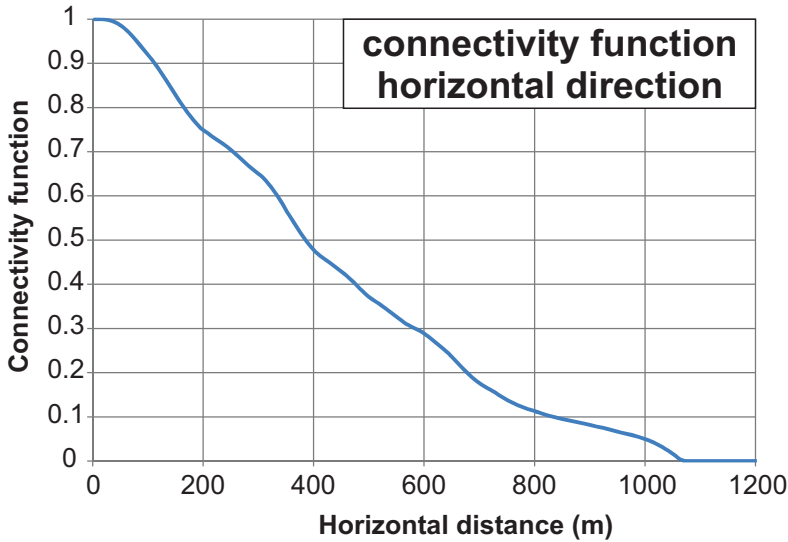
connectivity function
horizontal direction
Connectivity function
1
0.9
0.8
0.7
0.6
0.5
0.4
0.3
0.2
0.1
0
0
200
400
600
800
1000
1200
Horizontal distance (m)

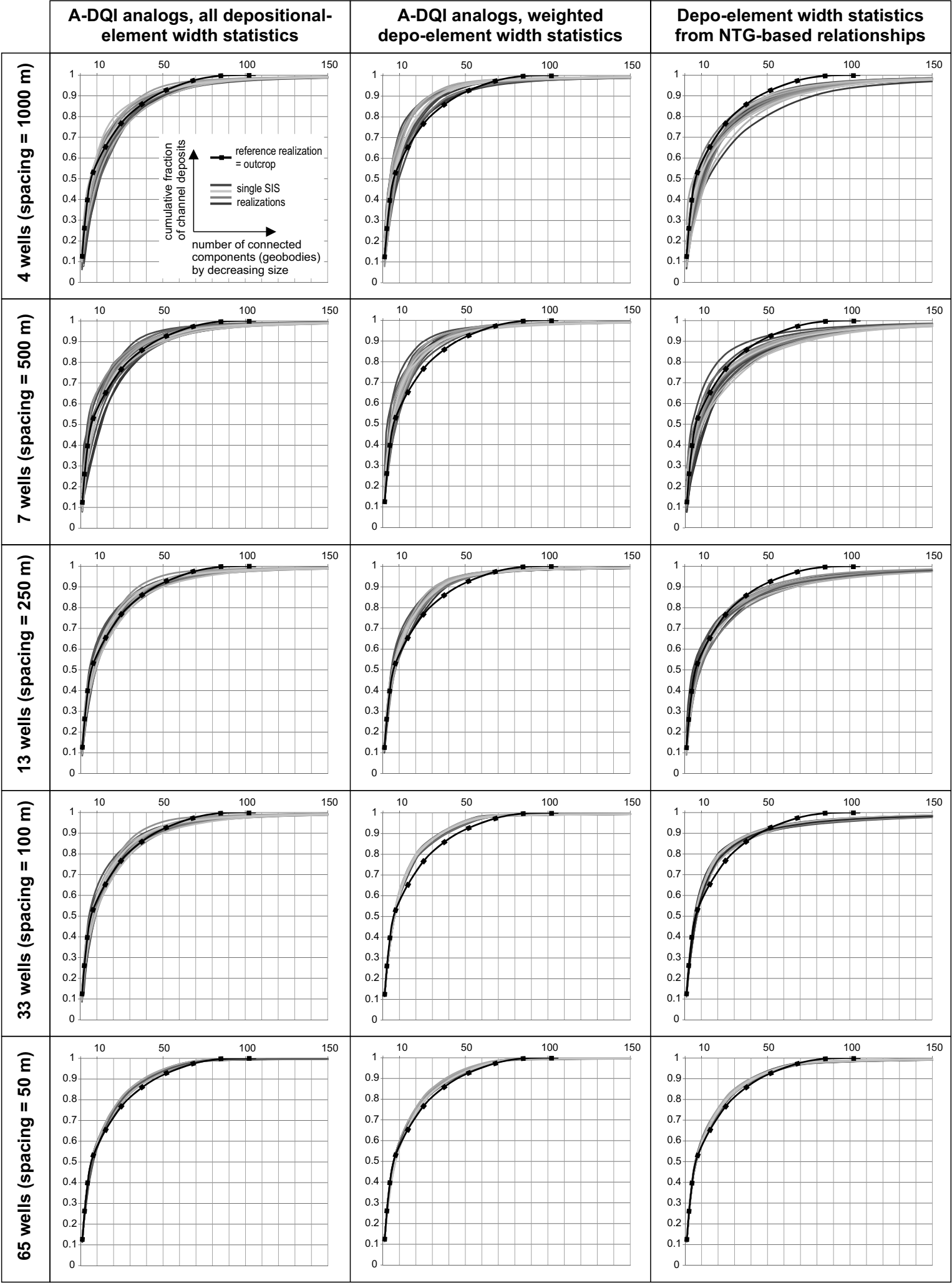
A-DQI analogs, all depositional-element width statistics
A-DQI analogs, weighted depo-element width statistics
Depo-element width statistics from NTG-based relationships
4 wells (spacing = 1000 m)
7 wells (spacing = 500 m)
13 wells (spacing = 250 m)
33 wells (spacing = 100 m)
65 wells (spacing = 50 m)
cumulative fraction of channel deposits
reference realization = outcrop
single SIS realizations
number of connected components (geobodies) by decreasing size
10
50
100
150
0
0.1
0.2
0.3
0.4
0.5
0.6
0.7
0.8
0.9
1

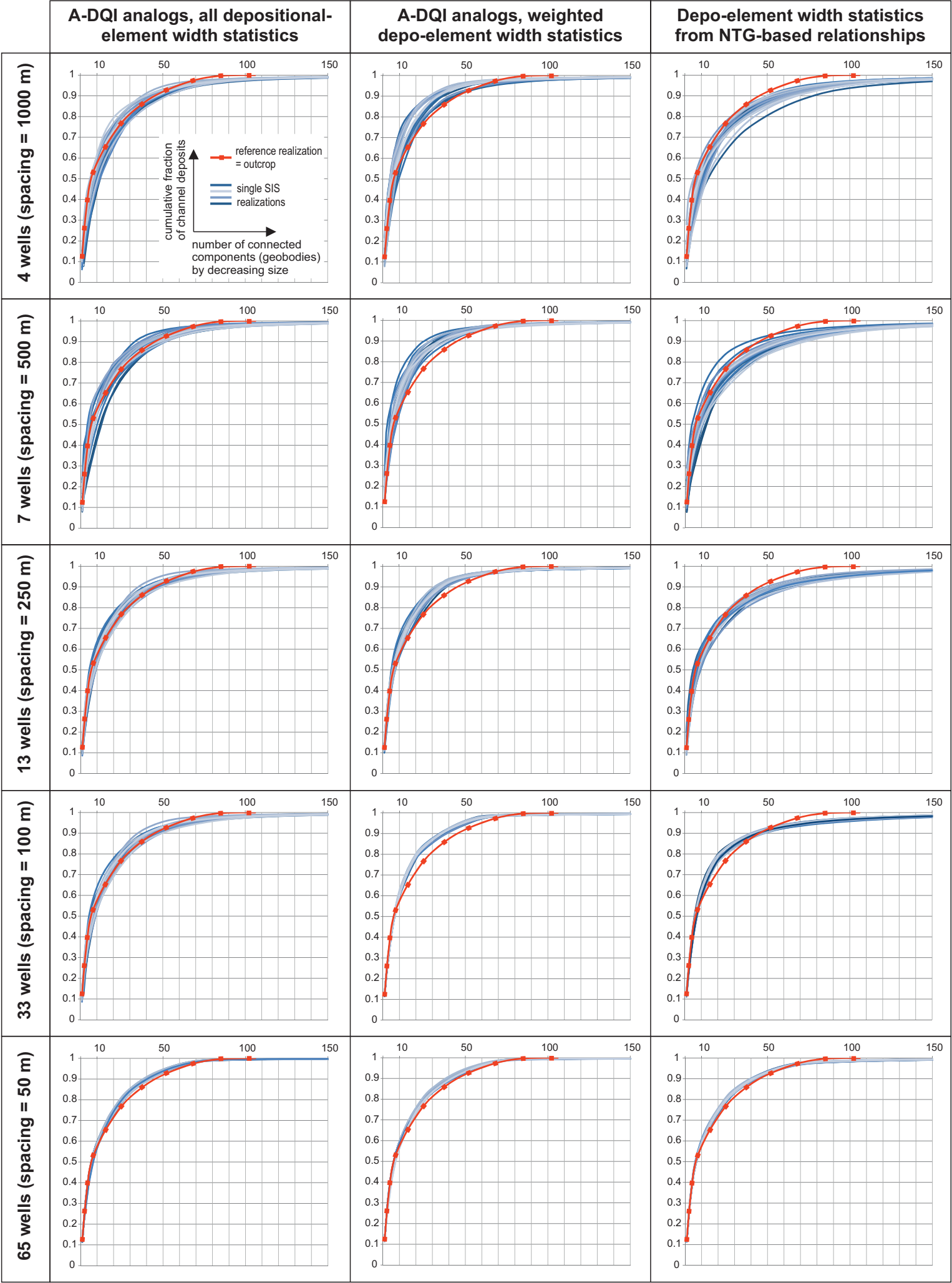
A-DQI analogs, all depositional-element width statistics
A-DQI analogs, weighted depo-element width statistics
Depo-element width statistics from NTG-based relationships
4 wells (spacing = 1000 m)
7 wells (spacing = 500 m)
13 wells (spacing = 250 m)
33 wells (spacing = 100 m)
65 wells (spacing = 50 m)
cumulative fraction of channel deposits
reference realization = outcrop
single SIS realizations
number of connected components (geobodies) by decreasing size
10
50
100
150
0
0.1
0.2
0.3
0.4
0.5
0.6
0.7
0.8
0.9
1

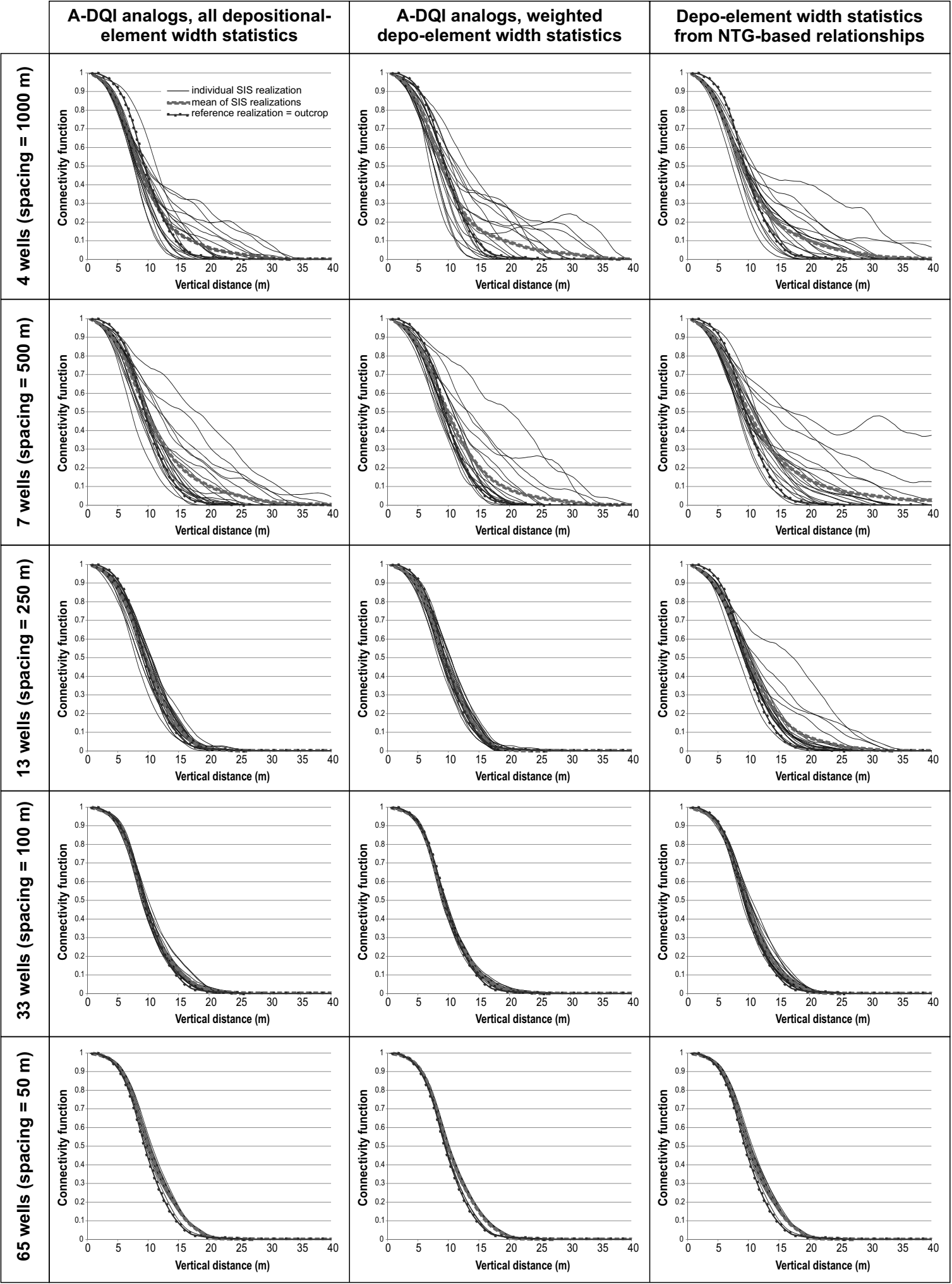
A-DQI analogs, all depositional-element width statistics
A-DQI analogs, weighted depo-element width statistics
Depo-element width statistics from NTG-based relationships
4 wells (spacing = 1000 m)
7 wells (spacing = 500 m)
13 wells (spacing = 250 m)
33 wells (spacing = 100 m)
65 wells (spacing = 50 m)
individual SIS realization
mean of SIS realizations
reference realization = outcrop
Connectivity function
Vertical distance (m)

	A-DQI analogs, all depositional-element width statistics	A-DQI analogs, weighted depo-element width statistics	Depo-element width statistics from NTG-based relationships
4 wells (spacing = 1000 m)	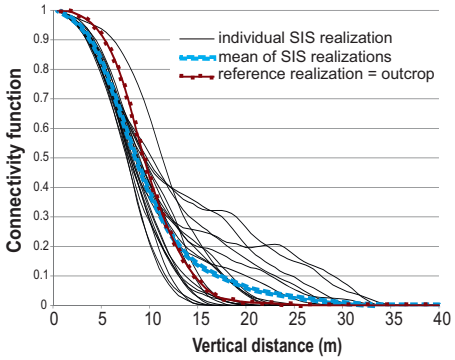	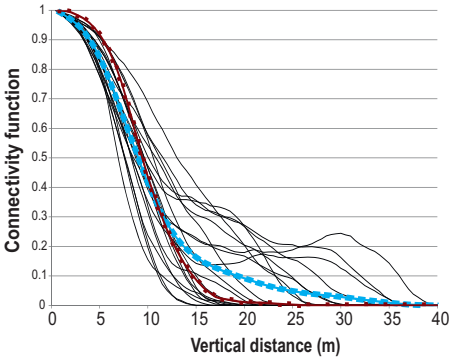	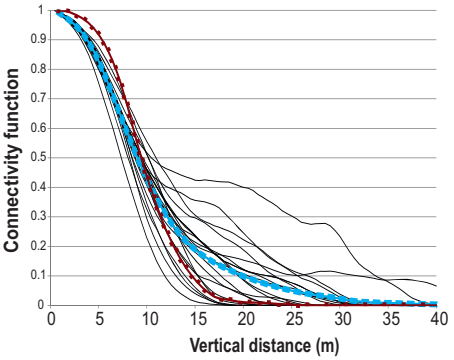
7 wells (spacing = 500 m)	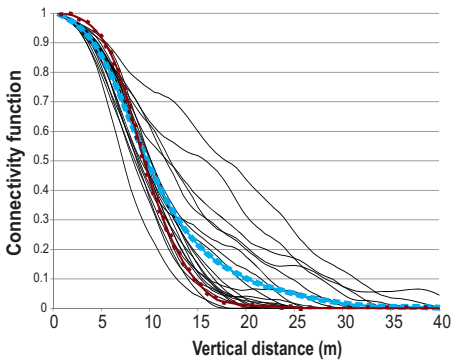	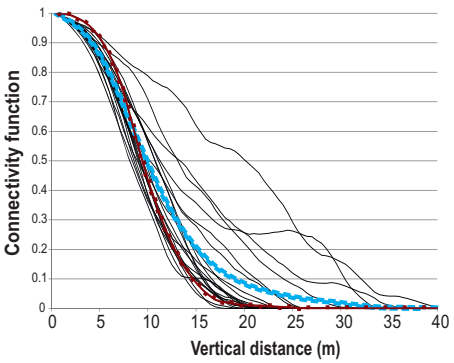	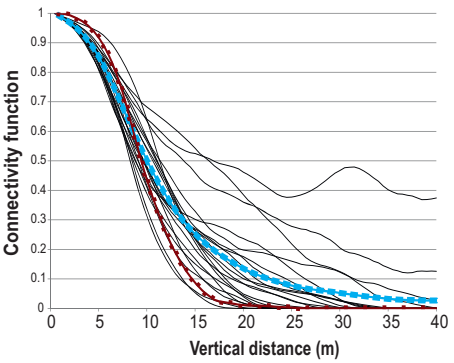
13 wells (spacing = 250 m)	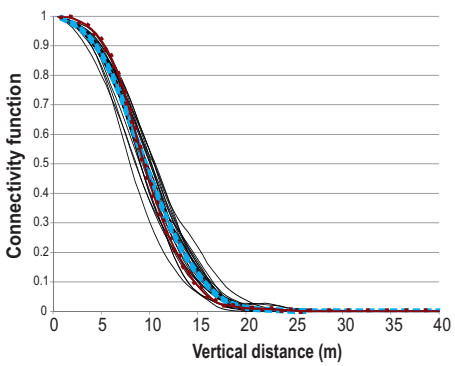	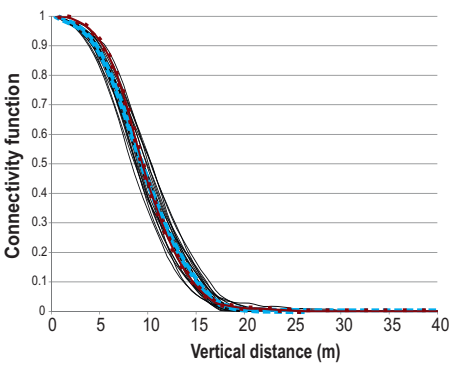	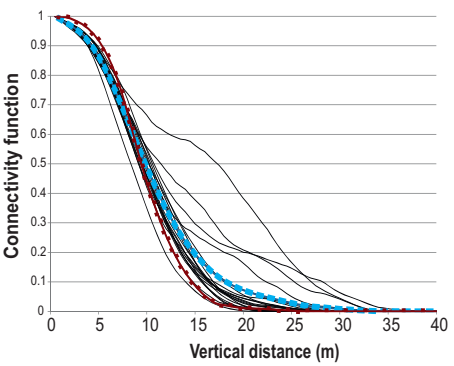
33 wells (spacing = 100 m)	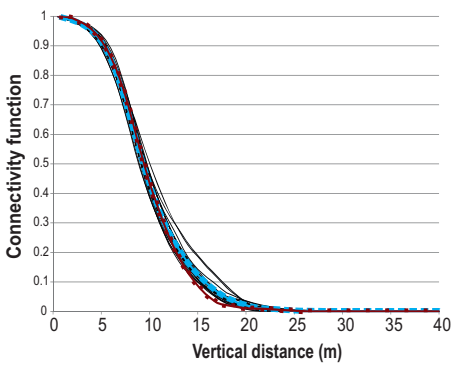	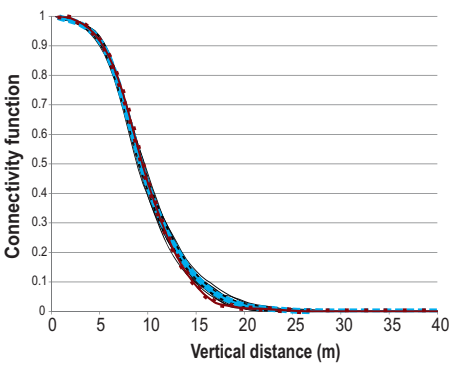	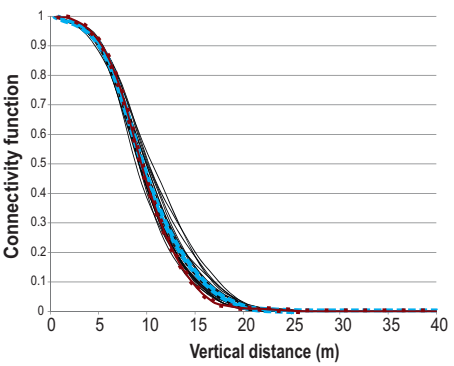
65 wells (spacing = 50 m)	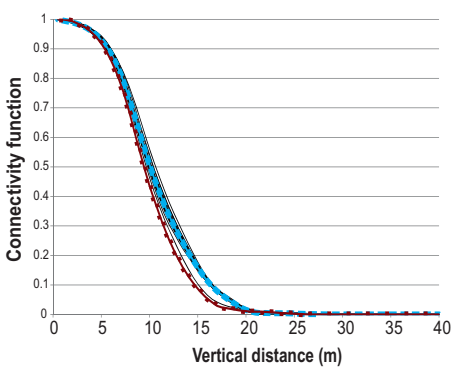	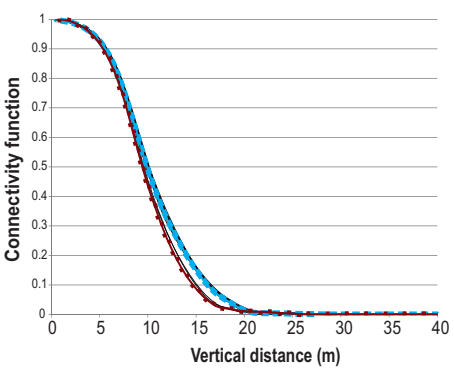	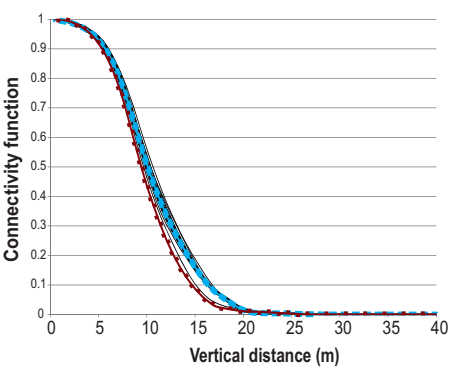

	A-DQI analogs, all depositional-element width statistics	A-DQI analogs, weighted depo-element width statistics	Depo-element width statistics from NTG-based relationships
4 wells (spacing = 1000 m)	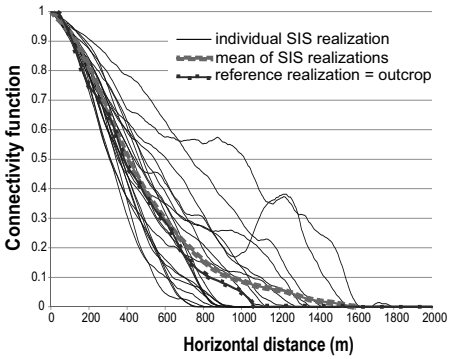	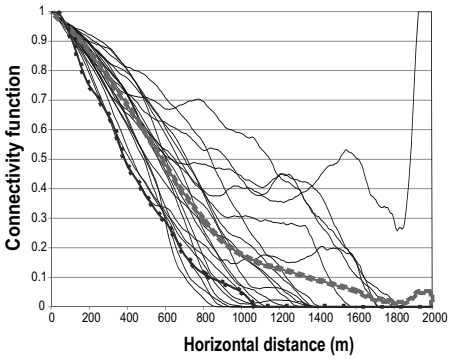	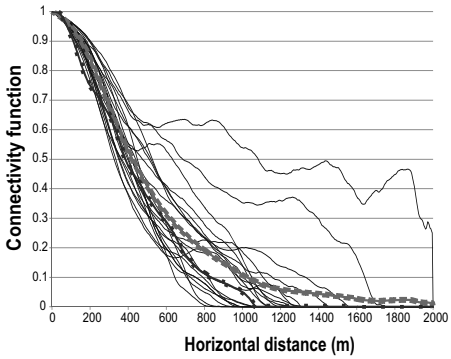
7 wells (spacing = 500 m)	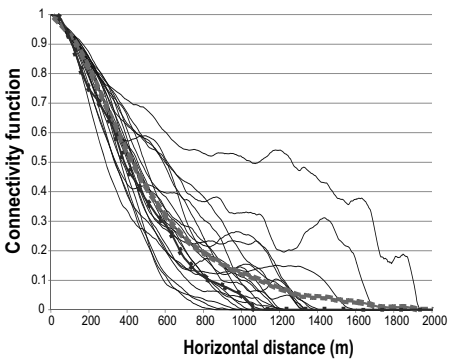	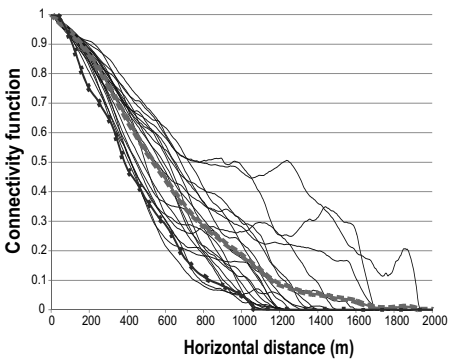	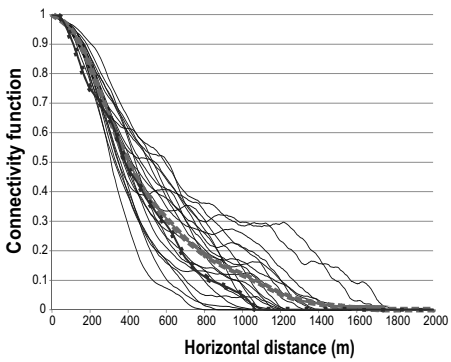
13 wells (spacing = 250 m)	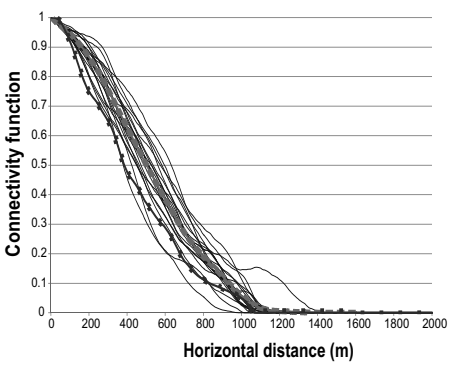	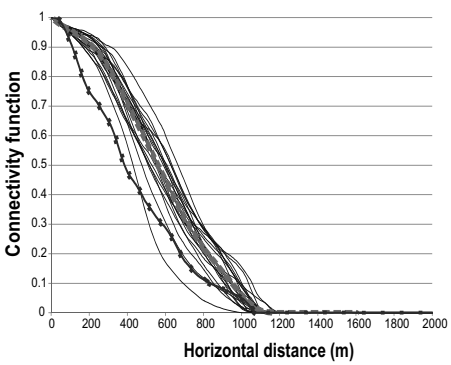	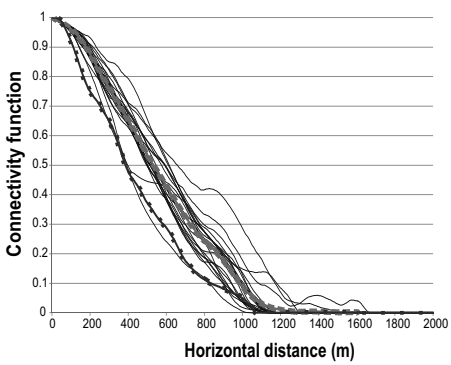
33 wells (spacing = 100 m)	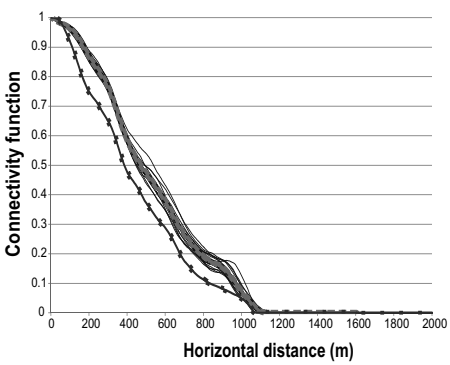	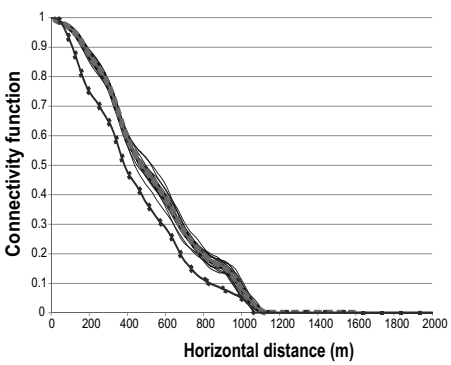	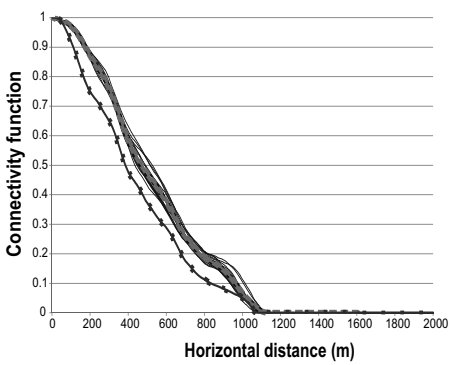
65 wells (spacing = 50 m)	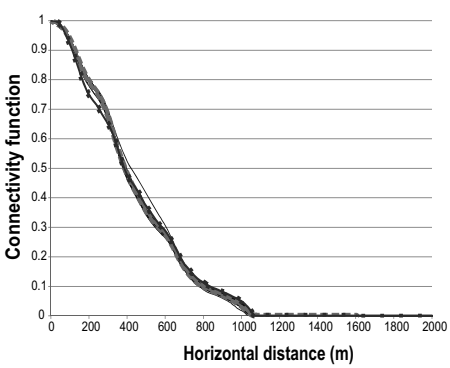	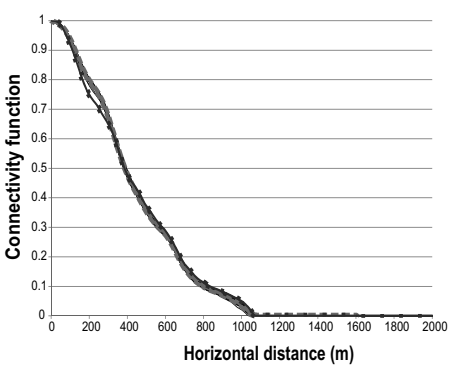	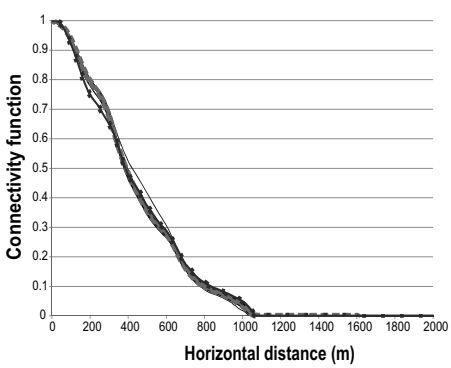

	A-DQI analogs, all depositional-element width statistics	A-DQI analogs, weighted depo-element width statistics	Depo-element width statistics from NTG-based relationships
4 wells (spacing = 1000 m)	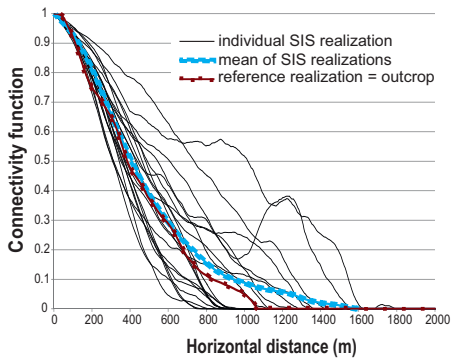	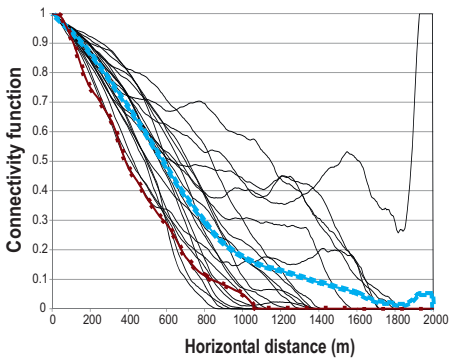	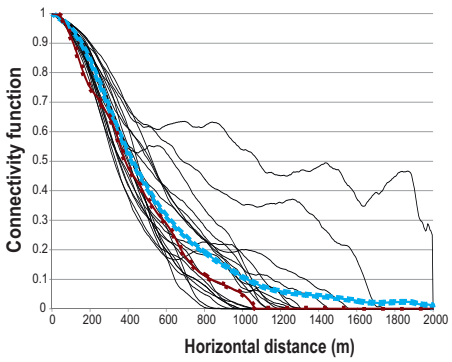
7 wells (spacing = 500 m)	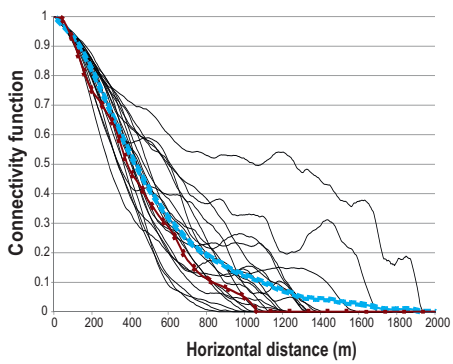	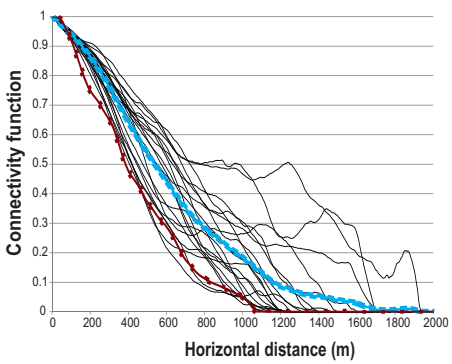	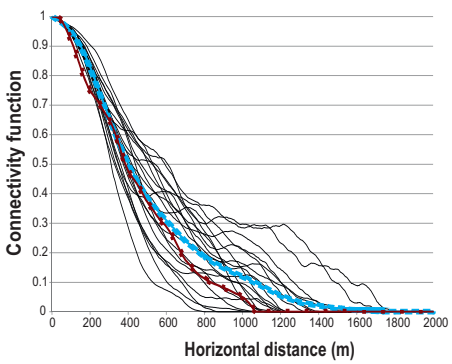
13 wells (spacing = 250 m)	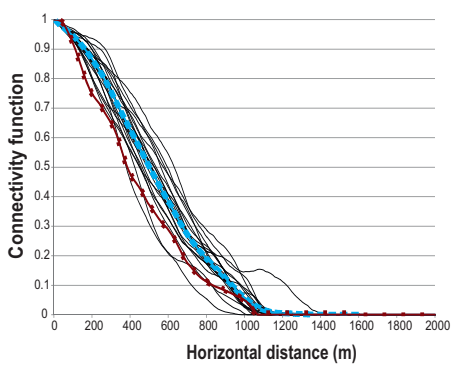	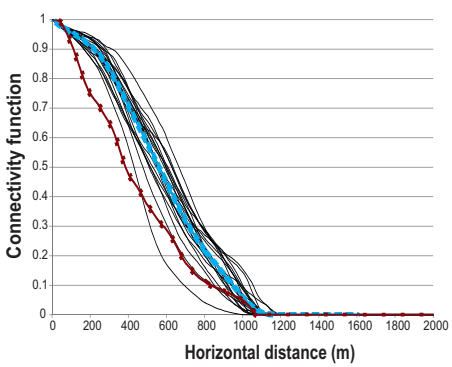	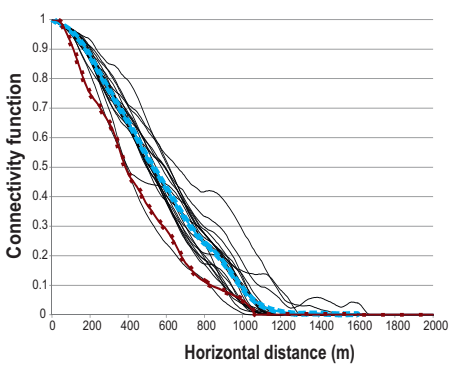
33 wells (spacing = 100 m)	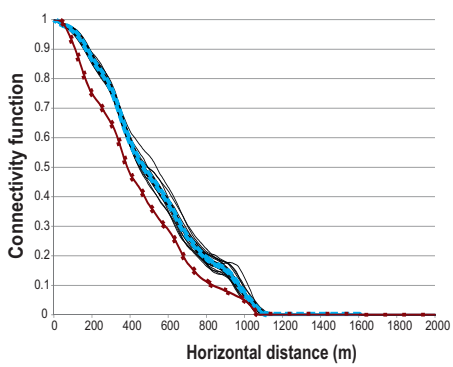	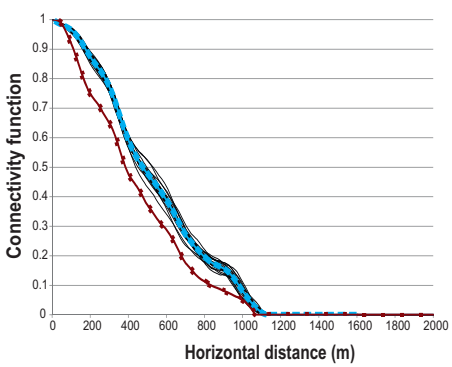	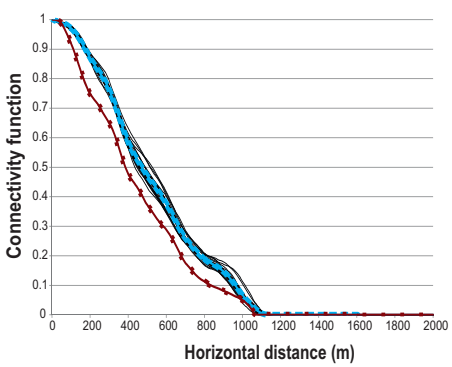
65 wells (spacing = 50 m)	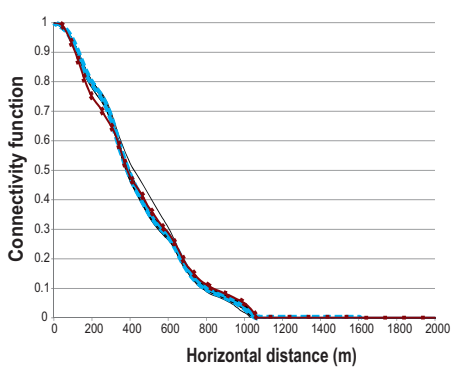	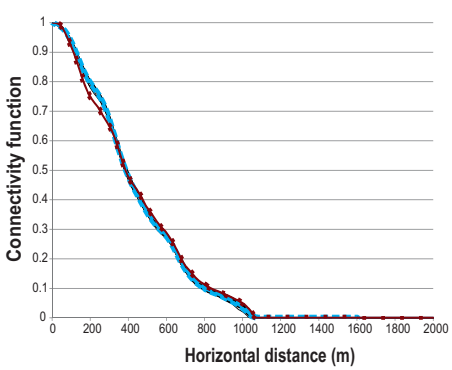	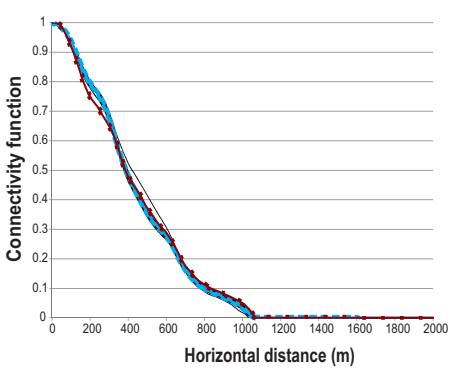

A-DQI analogs, all depositional-element width statistics

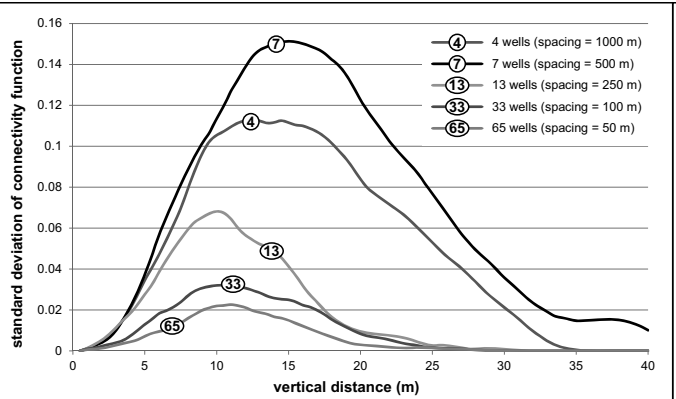

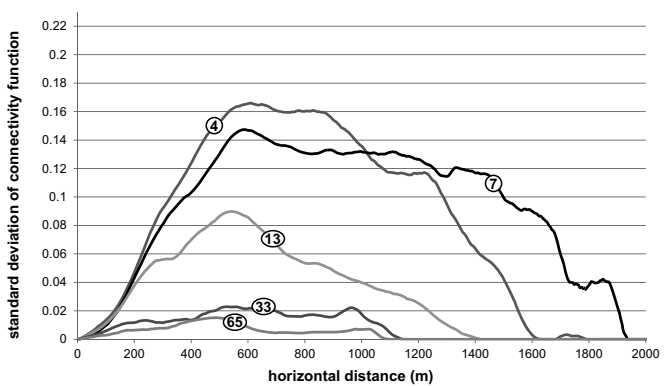

A-DQI analogs, weighted depo-element width statistics

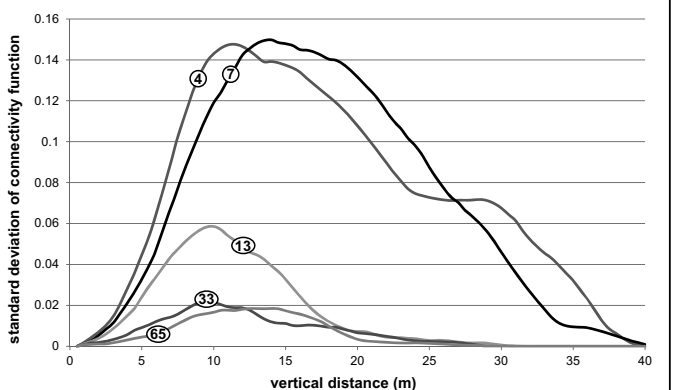

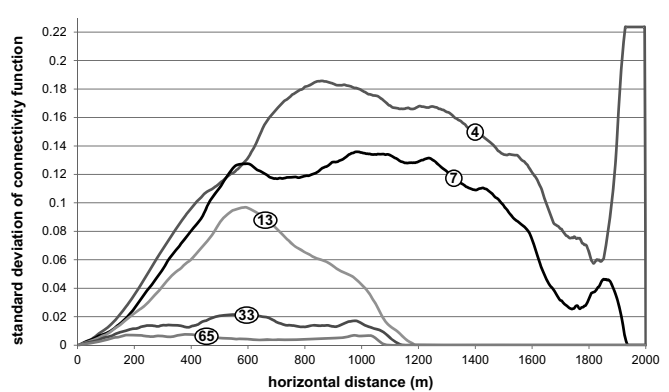

Depo-element width statistics from NTG-based relationships

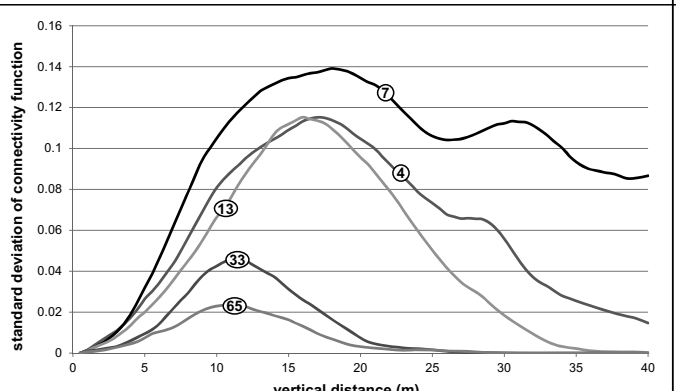

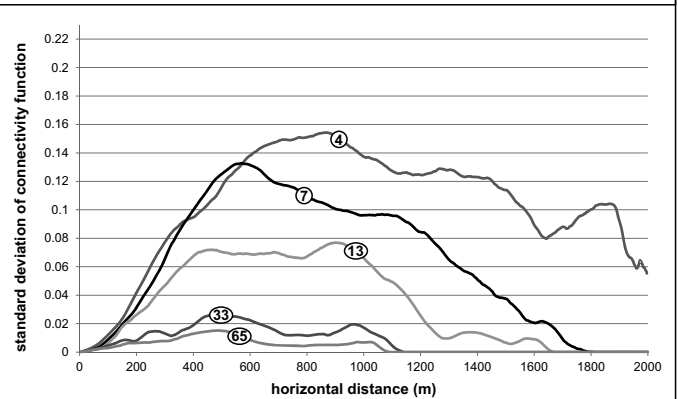

A-DQl analogs, all depositional-element width statistics

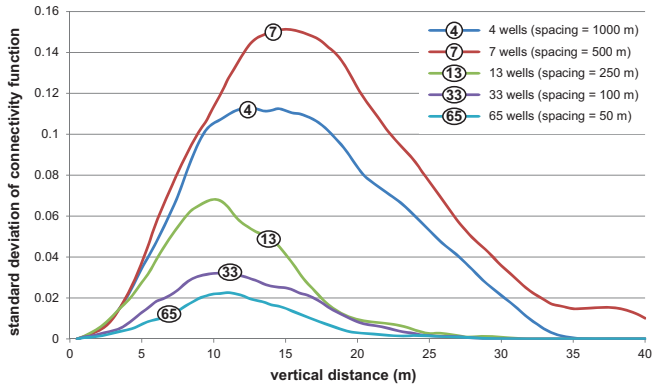

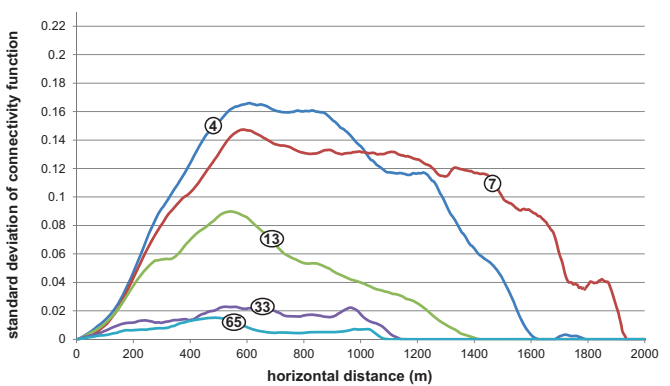

A-DQl analogs, weighted depo-element width statistics

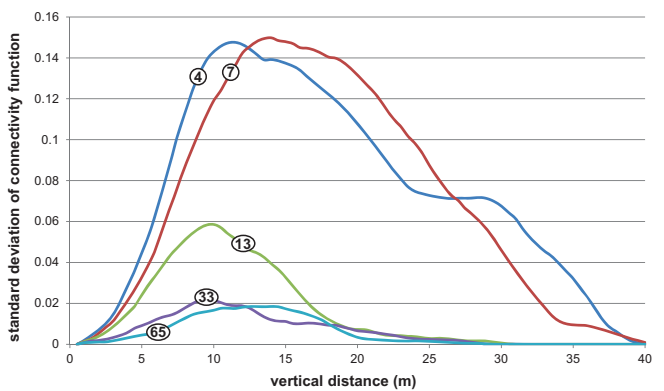

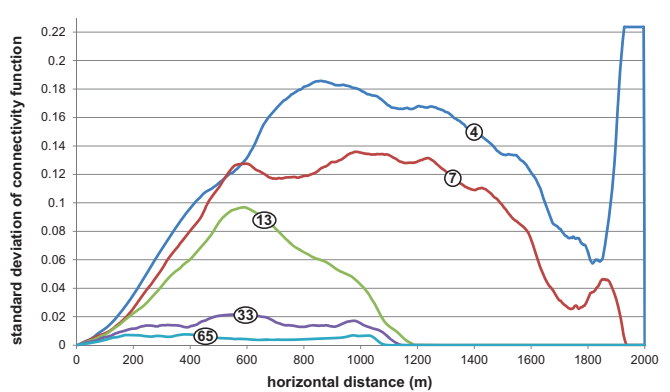

Depo-element width statistics from NTG-based relationships

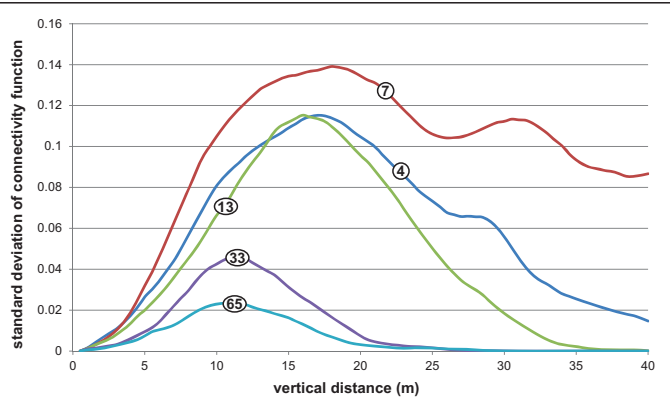

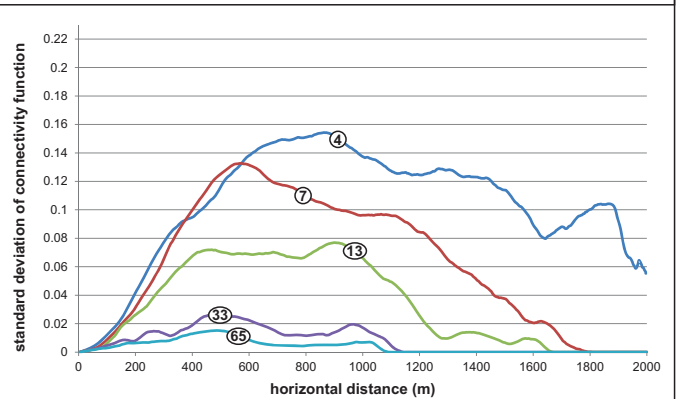

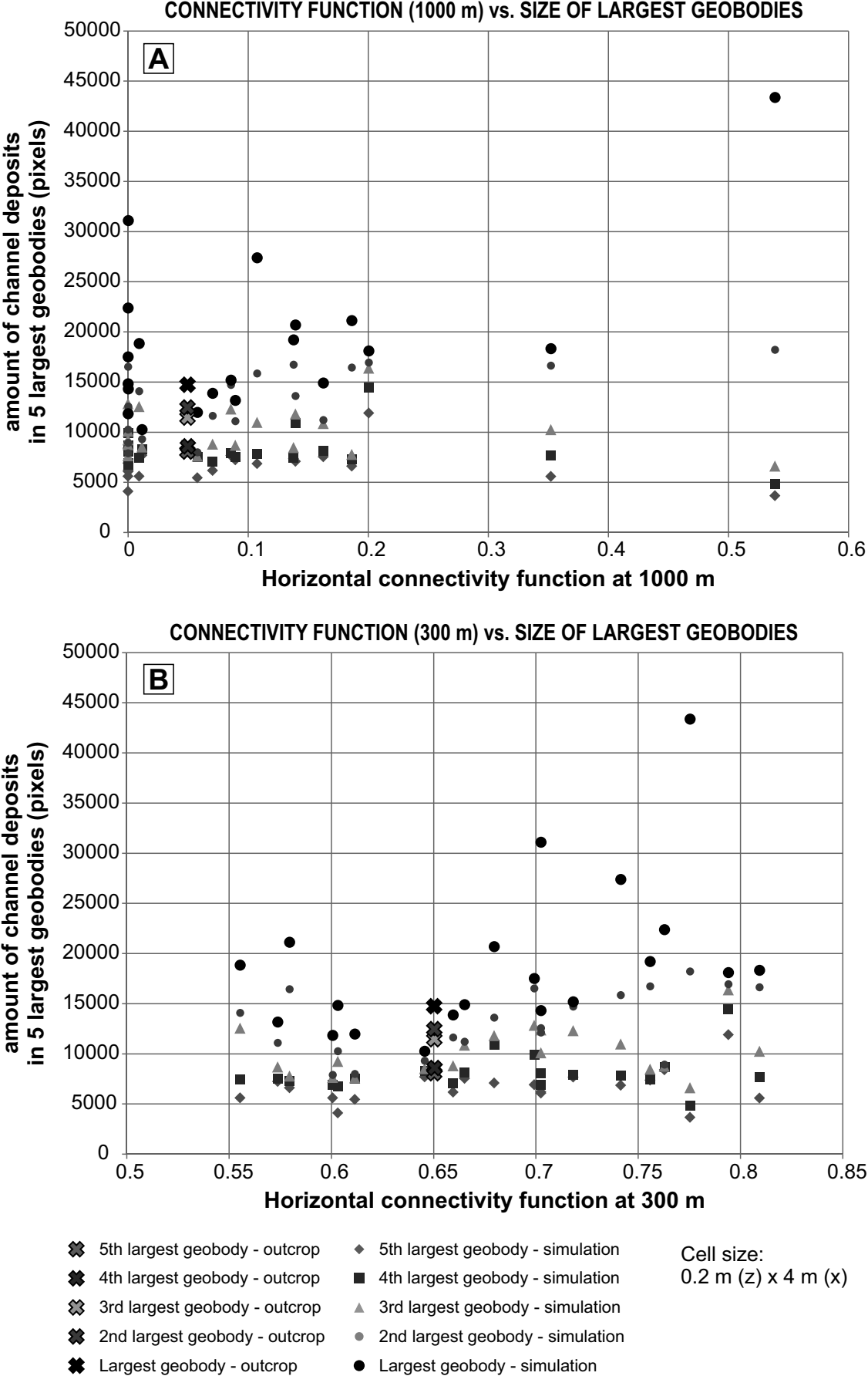
CONNECTIVITY FUNCTION (1000 m) vs. SIZE OF LARGEST GEOBODIES
A
amount of channel deposits in 5 largest geobodies (pixels)
50000
45000
40000
35000
30000
25000
20000
15000
10000
5000
0
0
0.1
0.2
0.3
0.4
0.5
0.6
Horizontal connectivity function at 1000 m
CONNECTIVITY FUNCTION (300 m) vs. SIZE OF LARGEST GEOBODIES
B
amount of channel deposits in 5 largest geobodies (pixels)
50000
45000
40000
35000
30000
25000
20000
15000
10000
5000
0
0.5
0.55
0.6
0.65
0.7
0.75
0.8
0.85
Horizontal connectivity function at 300 m
5th largest geobody - outcrop
4th largest geobody - outcrop
3rd largest geobody - outcrop
2nd largest geobody - outcrop
Largest geobody - outcrop
5th largest geobody - simulation
4th largest geobody - simulation
3rd largest geobody - simulation
2nd largest geobody - simulation
Largest geobody - simulation
Cell size:
0.2 m (z) x 4 m (x)

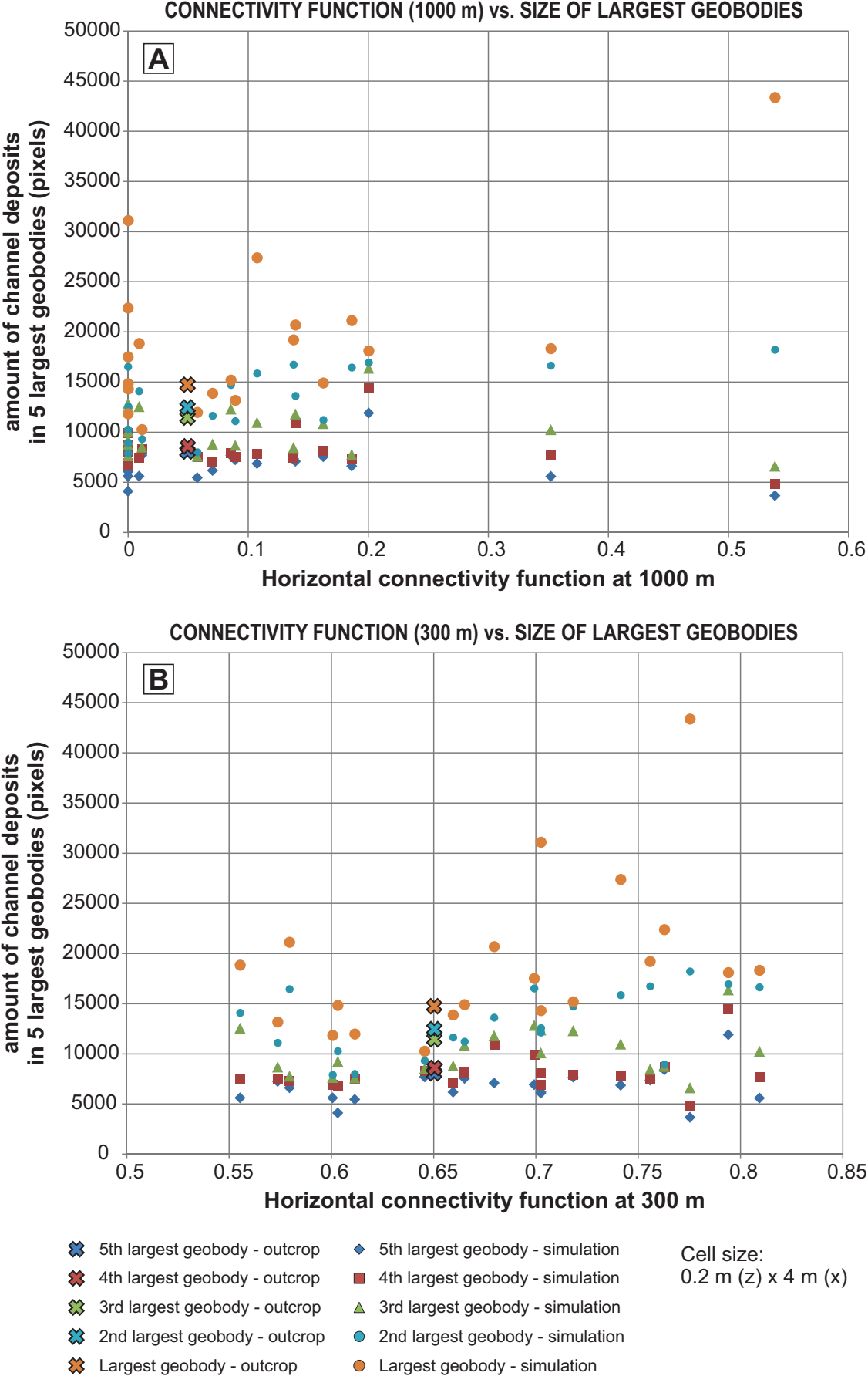
CONNECTIVITY FUNCTION (1000 m) vs. SIZE OF LARGEST GEOBODIES
A
amount of channel deposits in 5 largest geobodies (pixels)
50000
45000
40000
35000
30000
25000
20000
15000
10000
5000
0
0
0.1
0.2
0.3
0.4
0.5
0.6
Horizontal connectivity function at 1000 m
CONNECTIVITY FUNCTION (300 m) vs. SIZE OF LARGEST GEOBODIES
B
amount of channel deposits in 5 largest geobodies (pixels)
50000
45000
40000
35000
30000
25000
20000
15000
10000
5000
0
0.5
0.55
0.6
0.65
0.7
0.75
0.8
0.85
Horizontal connectivity function at 300 m
5th largest geobody - outcrop
4th largest geobody - outcrop
3rd largest geobody - outcrop
2nd largest geobody - outcrop
Largest geobody - outcrop
5th largest geobody - simulation
4th largest geobody - simulation
3rd largest geobody - simulation
2nd largest geobody - simulation
Largest geobody - simulation
Cell size:
0.2 m (z) x 4 m (x)

	A-DQI analogs, all depo-element width and thickness statistics	Blackhawk Fm. outcrop depo-element width statistics	Blackhawk Fm. outcrop experimental indicator variograms
4 wells (spacing = 1000 m)	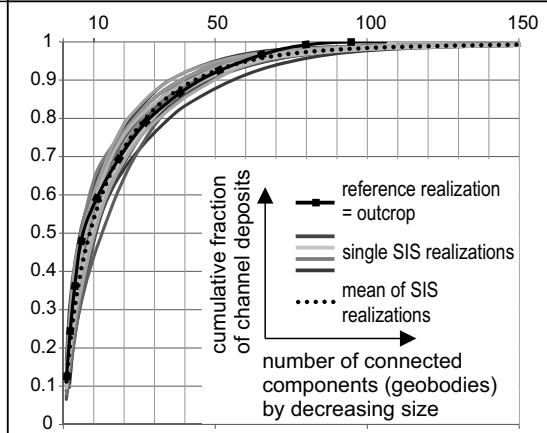	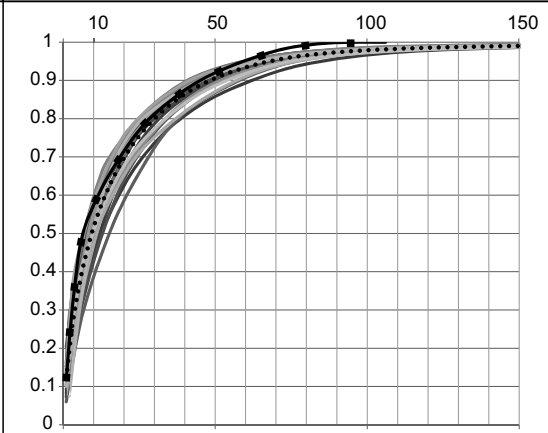	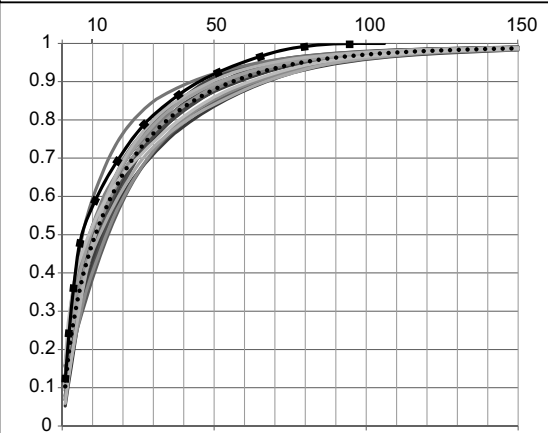

	A-DQI analogs, all depo-element width and thickness statistics	Blackhawk Fm. outcrop depo-element width statistics	Blackhawk Fm. outcrop experimental indicator variograms
4 wells (spacing = 1000 m)	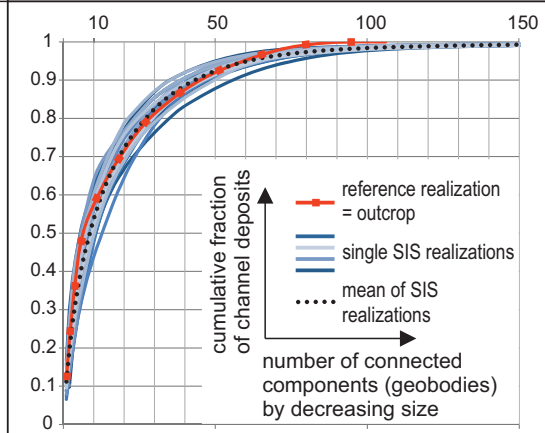	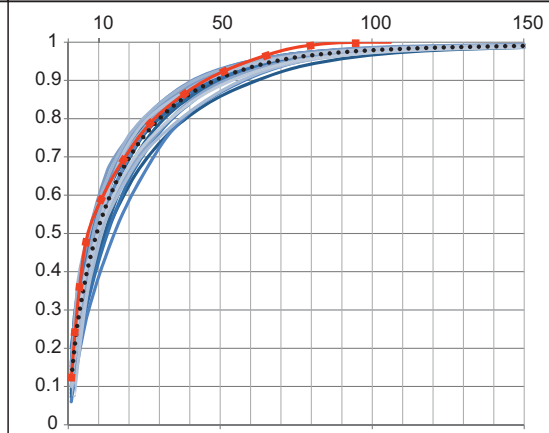	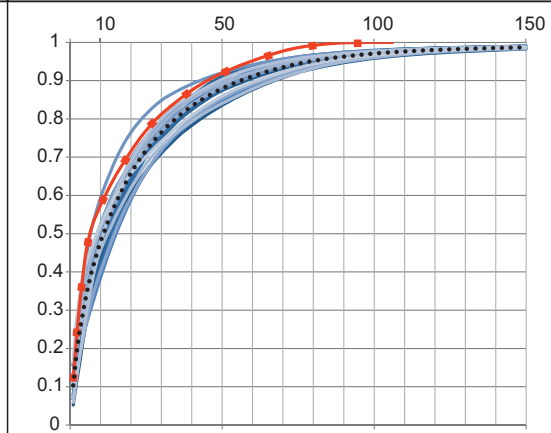

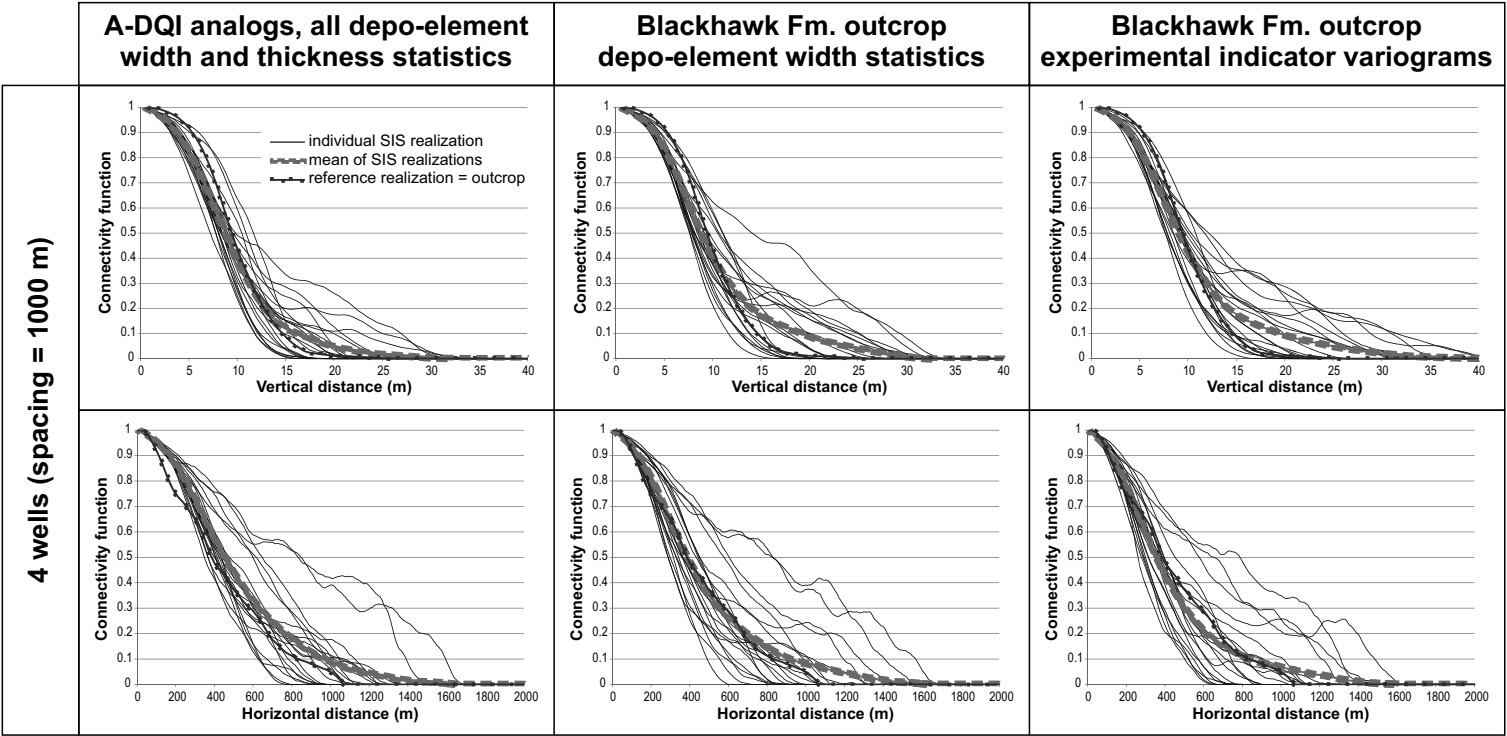
A-DQI analogs, all depo-element width and thickness statistics
Blackhawk Fm. outcrop depo-element width statistics
Blackhawk Fm. outcrop experimental indicator variograms
4 wells (spacing = 1000 m)
individual SIS realization
mean of SIS realizations
reference realization = outcrop
Connectivity function
Vertical distance (m)
Horizontal distance (m)

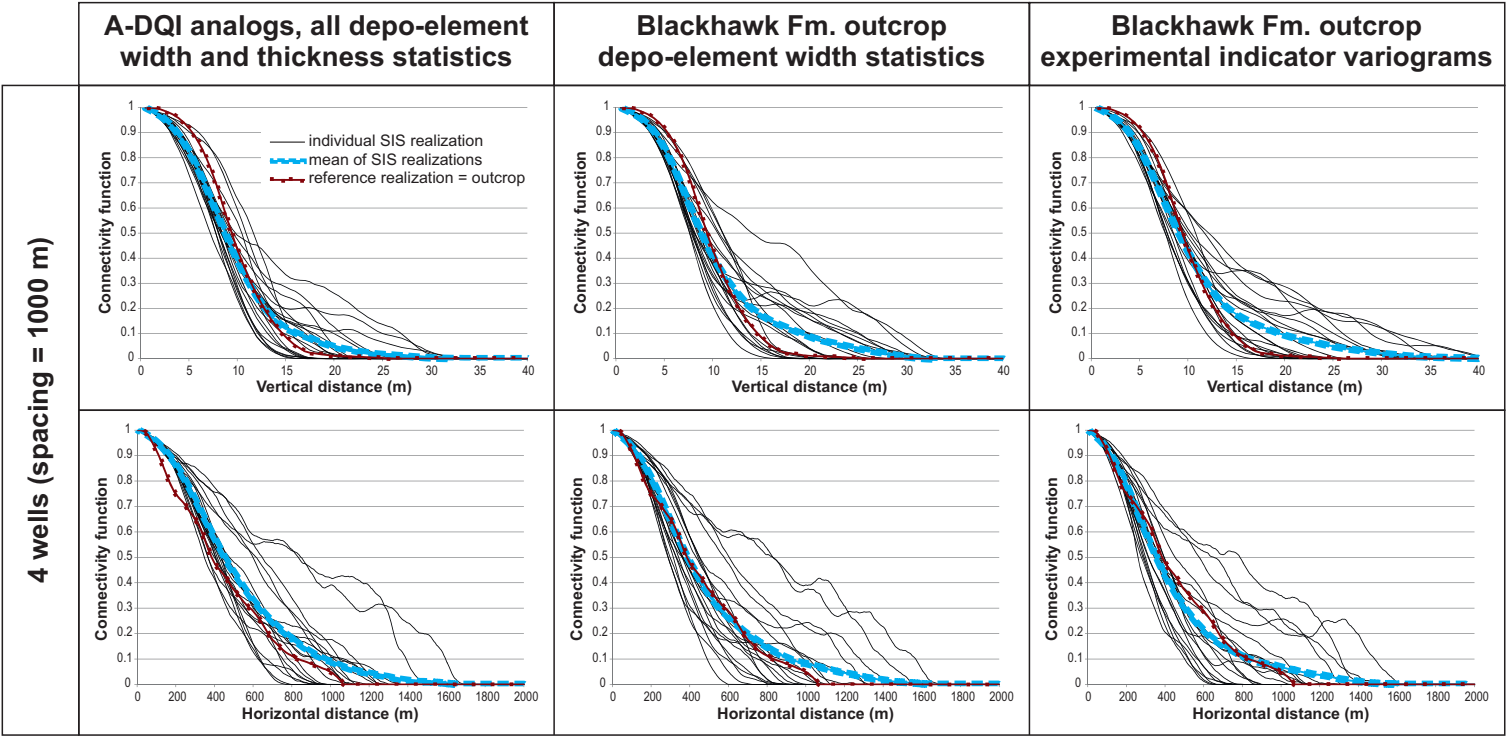
A-DQI analogs, all depo-element width and thickness statistics
Blackhawk Fm. outcrop depo-element width statistics
Blackhawk Fm. outcrop experimental indicator variograms
4 wells (spacing = 1000 m)
individual SIS realization
mean of SIS realizations
reference realization = outcrop
Connectivity function
Vertical distance (m)
Horizontal distance (m)